2019-04-28

# Carbon Dots: from Lab Synthesis to Unique Applications

Yiqun Zhou
*University of Miami*, yxz431@gmail.com

UNIVERSITY OF MIAMI

# CARBON DOTS: FROM LAB SYNTHESIS TO UNIQUE APPLICATIONS

By

Yiqun Zhou

A DISSERTATION

Submitted to the Faculty
of the University of Miami
in partial fulfillment of the requirements for
the degree of Doctor of Philosophy

Coral Gables, Florida

May 2019

UNIVERSITY OF MIAMI

A dissertation submitted in partial fulfillment of
the requirements for the degree of
Doctor of Philosophy

# CARBON DOTS: FROM LAB SYNTHESIS TO UNIQUE APPLICATIONS

Yiqun Zhou

Approved:

| | |
|---|---|
| _____<br>Roger M. Leblanc, Ph.D.<br>Professor of Chemistry | _____<br>Burjor Captain, Ph.D.<br>Associate Professor of Chemistry |
| _____<br>Orlando Acevedo, Ph.D.<br>Associate Professor of Chemistry | _____<br>Guillermo Prado, Ph.D.<br>Dean of the Graduate School |
| _____<br>Isaac Skromne, Ph.D.<br>Assistant Professor of Biology<br>University of Richmond | |

ZHOU, YIQUN (Ph.D., Chemistry)
Carbon Dots: from Lab Synthesis to Unique Applications (May 2019)

Abstract of a dissertation at the University of Miami.

Dissertation supervised by Professor Roger M. Leblanc.
No. of pages in text. (103)

Carbon dots (CDs) have joined the research of carbon-based nanoparticles since 2004. Upon the discovery of carbon dots, CDs were observed to be photoluminescent and small in size (1-10 m). The subsequent broad studies gradually reveal the potential values of CDs. Firstly, CDs have been synthesized with numerous carbon-based precursors including both classic and novel starting materials by various techniques. In this thesis, I will mainly introduce the development of three types of CDs (black CDs, gel-like CDs and orange CDs). Then, considering the lack of careful discussion of purification procedure in many present literatures, I have systematically studied the purification effect of different methods and observed that the selection of purification method should reply on the difference of size, molecular weight, and polarity between precursors and resulting CDs. Besides, the separation of gel-like CDs by TLC or orange CDs by SEC indicates CDs separate fractions are heterogeneous in polarity, molecular weight or size. Characterizations of CDs are often performed with various instruments to reveal their optical, structural and morphological properties. And some other unique properties can be also observed in certain CDs species such as thermal effect in gel-like CDs or solvent effect in orange CDs. In addition, different CDs species *in vivo* exhibit different properties. Using zebrafish as a model, black CDs species are observed to specially target the bones of zebrafish, which inspires the drug conjugation and delivery of biotin, retinoic acid and gel-like CDs. Furthermore, blood-

brain barrier (BBB) is as obstacle for drug delivery to the central nervous system (CNS). Considering the controllable size, charge, hydrophobicity and surface moiety, different CDs species have been explored for crossing the BBB and have shown the ability to overcome the BBB of zebrafish with different cellular mechanisms. For example, orange CDs have shown the ability to cross the BBB via passive diffusion while CDs prepared from tryptophan cross the BBB by carrier-mediated transport. Additionally, CDs have been widely studied regarding the cytotoxicity with different cell lines and it turned out that CDs are nontoxic regardless of different preparations. Moreover, due to the high photoluminescence, CDs have the potential and have been successfully applied in 2D, 3D printings and cosmetics such as fluorescent hair colorant and nail polish. Among them, 3D printing was first achieved by taking use of the special property of superabsorbent polymer to absorb water to embed orange CDs into superabsorbent polymer. In conclusion, in this thesis, the development of CDs will be illustrated in terms of versatile synthesis, purification, separation, characterization, drug delivery toward bones or across the BBB, printing and cosmetics. However, as a new family member of carbon-based nanoparticles, the studies of CDs have not reached the peak and there are still many properties to be characterized such as photocatalysis and thermoelectricity. Among them, photocatalysis and drug delivery by the conjugation between two CDs species are the focus of my future work.

**Acknowledgements**

In the journey toward acquiring the Ph.D. degree, I met many excellent people who gave me a lot of help and support. I would like to take this opportunity to say "Thank you" to them.

First of all, I would like to say "Thank you" to my Ph.D. supervisor, Dr. Roger M. Leblanc. He gave me the most support whenever I got a crazy research idea and he encouraged me to explore those bold ideas. When the idea worked, he was even happier than me and said he was very proud of me. In addition, when I got frustrated or upset, he was always ready to share my sorrows, so I was able to quickly get rid of those negative emotions and gain strength back. Dr. Leblanc teaches his students the importance of discipline, which has been a great influence on the way I think, speak and behave. He cares about the life of students and constantly reminds us to communicate, which makes me feel at home in the lab. Additionally, I thank him for his trust and confidence in my work. Besides, I like his sense of humor and talent for language, which makes our lab so international and lively despite the tedious work. All in all, I am so lucky to have Dr. Roger M. Leblanc as my 5-year Ph.D. supervisor and I hope in the future I can also become as great a person as him.

Secondly, I would like to say "Thank you" to my great parents and family for their understanding and support, especially when I was exhausted, sick or met financial problems. Also, there is another group of people I consider to be my "family", who are my dear lab mates: Dr. Shanghao Li, Dr. Zhili Peng, Dr. Shiv K. Sharma, Sajini D. Hettiarachchi, Piumi Y. Liyanage, Elif S. Seven, Keenan J. Mintz and Suraj Paudyal. I

especially appreciate their encouragement, caring and help so that I could always move on. We are more than lab mates; we are like family. At work, I enjoy brainstorming with them to generate research ideas and publishing papers. After work, we frequently gathered for a casual lunch or dinner. I believe we made the best team ever, and I wish them all success in the future.

Thirdly, I appreciate the help I received from Dr. Tegan Eve, Dr. Eduardo Veliz, Dr. Julia Dallman, Dr. Elsayed M. Zahran, Dr. Charles C. Chusuei, Dr. Emrah Celik, Dr. Ajeet Kaushik, Dr. Burjor Captain, Dr. Orlando Acevedo and Dr. Isaac Skromne. For Dr. Eve, I really appreciate his trust, good comments and great help to become the best T.A. and to join the T.A. evaluation committee. Dr. Veliz was always around when I needed help for unfamiliar knowledge points, chemical ordering and collaboration with undergraduate students. In addition, I really appreciate the guidance and help from Dr. Dallman, Dr. Zahran, Dr. Chusuei, Dr. Celik and Dr. Kaushik for the completion of various research projects. Firstly, I appreciate Dr. Captain's class in my first year. Then I appreciate both Dr. Captain and Dr. Acevedo for their willingness to be my committee members and their valuable suggestions to perfect each of my exams. Also, I thank Dr. Isaac Skromne for being my external committee member for my Ph.D. defense and I appreciate all the good results coming from our collaboration.

Fourthly, I'd like to thank my friends such as Atul D. Parab, Abhishek Thakur, Alexandra Desserre, Francesca Cardano, Dr. Mehdi R. Avei, Leonardo F. Serafim and Guillaume Mercado for their support and help in research and life. Also, I appreciate my undergraduate students such as Bruno Quiroga, Jennifer Perez, Daniel Ferras, Ling Cheng, and Dylan Morisson for their help with achieving such great results.

In the end, I would like to say thank you to all the staff in the Chemistry Department, including Ana, Noel, Elizabeth and Juanita for their generous help in all aspects. I am grateful for all the convenient conditions and comfortable environment provided by University of Miami. I am so proud to be part of the “U”.

## TABLE OF CONTENTS

Page

## LIST OF FIGURES

## LIST OF TABLES

# Chapter 1 Introduction

## 1.1 History of the Development of Carbon Nanomaterials

Carbon-based nanomaterials have constantly popped up since 1963 when nanodiamonds were created by nuclear explosions triggered by carbon-based explosives.[1] 20 years later, fullerene was discovered and named after Richard Buckminster Fuller, a well-known architectural modeler who was credited with the U.S. popularization of the geodesic dome that is similar to the shape of fullerene. Shortly, multiwalled carbon nanotubes (MWCNTs) were brought into the awareness of the scientific community as a whole by a paper of Sumio Iijima of NEC published in 1991. However, as to the first discoverer of MWCNTs, it is a subject of controversy. Even though Iijima has been much credited for inspiring many scientists to study MWCNTs, the earliest literature about MWCNTs was reported by L. V. Radushkevich and V. M. Lukyanovich in 1952 with clear TEM images of MWCNTs (50 nm in diameter) published in the Soviet Journal of Physical Chemistry.[2] This discovery was largely unnoticed, as the article was published in Russian, and Western scientists' access to Soviet press was limited during the Cold War. Shortly, an increasing number of carbon-based nanomaterials with various shapes was developed which include carbon nano-onion (1992),[3] SWCNTs (1993),[4] carbon nanocones (1994),[5] and carbon nanohorns (1999).[6] In 2004, carbon dots (carbon nanodots or carbon quantum dots) (CDs) were serendipitously discovered by Xu et al. during the purification of SWCNTs,[7] which soon triggered extensive studies. And to date, CDs have become one hotspot topic. Figure 1.1 is a graphical illustration of the structures of these carbon-based nanomaterials.

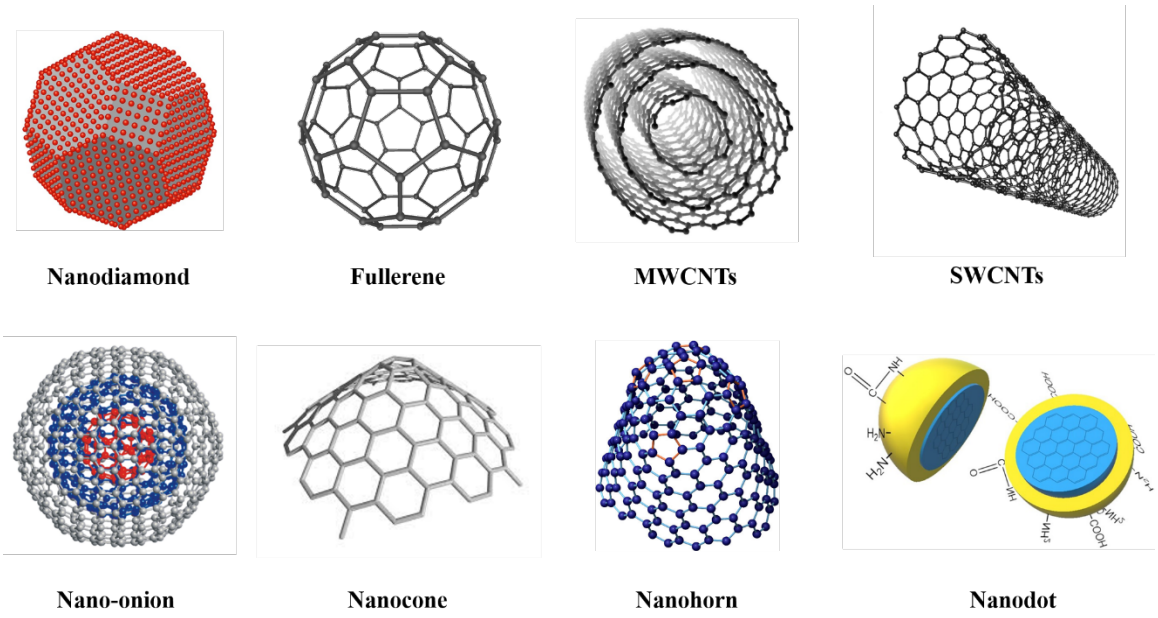


**Figure 1.1** The structures of various carbon-based nanomaterials.

## 1.2 Carbon Dots

CDs are a class of photoluminescent spherical nanoparticles (NPs) with less than 10 nm in diameter.[8] They are similar to traditional quantum dots (QDs) in terms of the core-shell structure but different in terms of elemental composition.[9] As to the elemental composition, CDs generally include hydrogen, carbon, nitrogen and oxygen.[10-11] Sometimes, other element such as sulfur, boron, silicon or phosphorus may be also involved, which depends on the species of their synthetic precursors or post-synthesis surface dopants.[12-15] However, most CDs don't contain metal elements, which is their most distinct feature from traditional QDs. Considering the presence of heavy metal elements such as mercury,[16] lead,[17] and cadmium,[18] traditional QDs bear much doubt and concern in the application of biomedical field.[19] In comparison, the absence of metal elements in CDs endows them with low toxicity but high compatibility which have been confirmed by numerous *in vitro* or *in vivo* studies.[20-21]

The most attractive property of CDs is photoluminescence (PL). And CDs typically display excitation-dependent PL.[22] In other words, the emission wavelength of CDs varies with the excitation. Nonetheless, not all CDs display excitation-dependent PL and a few CDs species have been reported for exhibiting excitation-independent PL.[23] Excitation-dependent PL is favor of bioimaging while excitation-independent PL is critical for making carbon-based solid-state laser devices.[24] Therefore, both PL behaviors are useful in combination of particular application. In fact, the excitation-dependency of PL has never become the focus of attention. Instead, scientists are more concerned about PL intensity and emission color.

As a measure of PL, fluorescence quantum yield (QY) is often calculated for each newly obtained CDs species. In the early development stage, the fluorescence QY of CDs was generally below 50%.[10] After years' endeavor, the fluorescence QY of CDs has been greatly improved and to date, the highest fluorescence QY is 93.3%, which was reported by Zheng et al.[25] So far, the PL of CDs has achieved a comparable level with traditional QDs and it is no longer a farseeing goal to continue enhancing the fluorescence QY of CDs. However, most CDs exhibit PL emission at short wavelengths, which is disadvantageous for bioimaging considering the interference of autofluorescence of some organs or tissues.[26] In addition, even though some CDs displaying long emission wavelengths have been developed, their fluorescence QY is always much lower than those CDs emitting at short wavelengths.[27] Therefore, the most urgent demand is the development of long-wavelength emissive CDs with high fluorescence QY. And even though the PL mechanism has been repeatedly illustrated in many researched, it is still under debate with several main theories which will be introduced in **Chapter 3: Characterization of Carbon Dots**.

CDs have been attracting considerable attention as a green substitute for traditional QDs in the applications where nontoxicity and biocompatibility are required.[28] In addition, due to the abundant hydrophilic functional groups on the surface, CDs have high water-dispersal ability.[29] And in some CDs, the lack of hydrophilic functional groups or abundance of hydrophobic moieties can make CDs amphiphilic and disperse in both water and non-polar organic solvents.[30] Furthermore, the presence of abundant functional groups makes it possible to conjugate CDs with compounds via covalent bonds. Thus, considering low toxicity, high compatibility, water-dispersal ability and PL emission intensity, CDs are a promising drug nanocarrier.

Furthermore, CDs have been applied in many fields. For example, since CDs are semiconductors and have definite conduction-valence band gaps, they have been applied to photocatalysis.[31] In addition, PL quenching induced by selective ions such as $Hg^{2+}$ and $Fe^{3+}$,[32-33] and molecules such as hydrogen peroxide,[34] suggests that CDs can be used as sensitive and selective biosensors. Moreover, the excellent PL property allows CDs to be applied to bioimaging, printing and cosmetics.

In conclusion, CDs are a class of photoluminescent NPs with less than 10 nm in diameter. They exhibit nontoxic and biocompatible chemical composition. They display unique PL behaviors. As a substitute of traditional QDs, CDs can be applied as a trustworthy drug nanocarrier. In addition, the excellent electrical and PL properties allow CDs to be used for photocatalysis, bioimaging, printing and cosmetics design.

**1.3 Summary**

As a new family member of carbon-based NPs, CDs were discovered in 2004 during the process of purification of SWCNTs. In the past 15 years, there was a tremendous

development of CDs regarding their theoretical studies such as PL mechanism, and varieties of promising applications such as drug delivery. In the thesis, in the first chapter, I will introduce all the characterizations and development of CDs from my work. Then, I will show my perspective of the future development of CDs. The content is illustrated as follows. In chapter 2, I will present my work on synthesis, purification and separation of CD, with an emphasis on critical key aspects of purification and separation techniques. In chapter 3, I will present the instrumentation used for the characterization of CDs as well as the unique properties of CDs resulting from their analyses. In chapters 4 and 5 I will illustrate the biomedical application of CDs for specifically targeting bones and crossing the blood-brain barrier (BBB), respectively. In chapter 6, some creative inventions such as text printing, 3D printing and cosmetics using CDs will be exhibited. And in the last chapter, I will highlight the future application of CDs in photocatalysis and drug delivery.

## Chapter 2 Synthesis, Purification and Separation of Carbon Dots

In this chapter, the synthesis of CDs will be illustrated in terms of synthetic approaches, techniques and precursors. The purification method will be analyzed by comparing the purification effect of CDs using dialysis, size exclusion chromatography (SEC) and solvent wash. As to the separation of CDs, both thin layer chromatography (TLC) and SEC are unusual but efficient separation strategies. All synthesis, purification and separation will be illustrated in combination with the CDs synthesized in my work.

### 2.1 Synthesis of Carbon Dots

The synthetic approaches of CDs can be generally categorized into top-down and bottom-up patterns.[8] Top-down and bottom-up methods are relatively opposite concepts regarding the size change from precursors to final CDs. To be specific, top-down method indicates that precursors after surface modification such as oxidation or ablation will turn into smaller-size CDs. On the other hand, bottom-up approach usually consists of a series of reaction steps including ionization, polymerization and carbonization to build up CDs from the small basic compounds such as citric acid.[35] Therefore, the synthetic approach is closely related to the size or molecular weight change during the reaction. However, there is a common misunderstanding that the definition of synthetic approach relies on the technique applied.

The techniques that have been applied to synthesize CDs have evolved from the laser ablation,[7] hydrothermal/solvothermal,[36] to microwave and ultrasonication.[37-38] Among them, laser ablation was the technique used to discover CDs for the first time. Hydrothermal/solvothermal is a conventional technique to drive organic synthesis and the energy input is in the form of heat. Due to a higher-energy input compared with other

techniques, microwave becomes a fast and popular way to acquire CDs with the help of microwave energy.[39] In the end, ultrasonication, even though was reported, has been much less used to prepare CDs due to the lower sonic energy that will require much longer reaction time.[30] Based on the description of these synthesis techniques, the difference only exists in the different forms of energy while the way how size or molecular weight changes is not focused. Therefore, synthetic approach has nothing to do with synthesis techniques.

The precursors of CDs have a wide range from small basic molecules to large polymeric compounds and from lab synthesized chemicals to daily used natural products. For example, black CDs are prepared from carbon nanopowder,[19] gel-like CDs are synthesized from citric acid and 1,2-ethylenediamine (EDA),[35] while orange CDs are fabricated with citric acid and 1,2-phenylenediamine (OPD).[30] In addition, commercial egg yolk, ham, cheese, milk, orange juice, tea, coffee and wines have all been used to generate CDs.[40-45] Moreover, CDs have been discovered in honeycomb, which showed the first case of CDs present in nature.[46] In conclusion, CDs can be synthesized from various precursors, which reveals the ease of preparation and availability of CDs. Figure 2.1 is a summary of all the precursors used to synthesize CDs in my work.

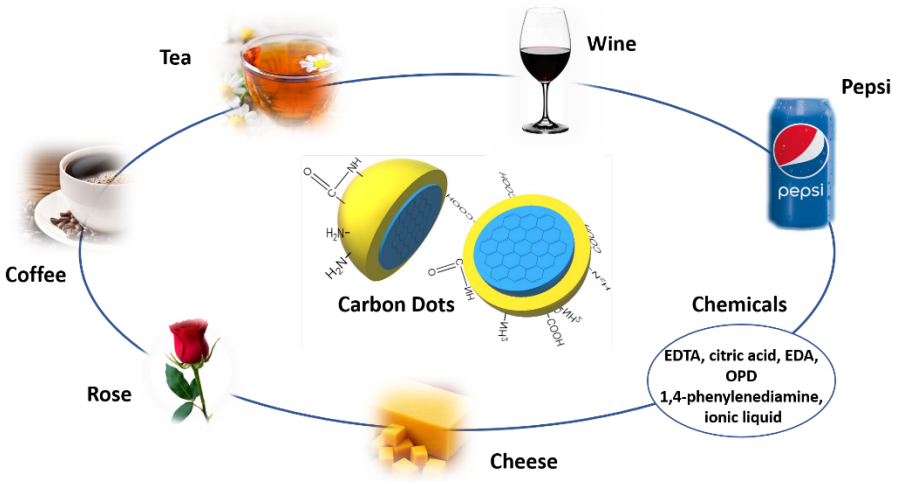


**Figure 2.1** A graphical illustration of all precursors used to synthesize CDs in my work.

The preparations of gel-like CDs and orange CDs are presented as examples for CDs synthesis. To synthesize gel-like CDs, in the beginning, argon gas was used to drive $O_2$ from solvothermal system for 5 min. Then, EDA (5 mL) was transferred into a 50 mL, round-bottomed flask and was heated with constant stirring in an oil bath on a hotplate (Chemglass, Opti Mag-st). When the temperature reached 160 °C, citric acid (1 g) was quickly added with vigorous stirring, and the reaction proceeded for 50 min until citric acid had completely reacted with EDA. After cooling the system for 15 min to room temperature, gel-like CDs were deposited at the bottom of the flask. The remaining supernatant EDA was then rinsed out with acetone. Then, gel-like CDs (0.8 g) were dissolved in water (1 mL) and heated by using a rotary evaporator (Bechi, R-114) to completely evaporate water at a constant temperature of 70 to 80 °C with reduced pressure. The gel-like CDs would then reform in this fashion.

The synthesis of orange CDs involved the use of 0.02 g citric acid as the carbon source and 0.28 g OPD as the N-dopant with a molar ratio of 1:25 dissolved in 10 mL deionized $H_2O$. In an ultrasonication bath the mixture was then sonicated for 1 h at a frequency of 42 kHz under the protection of argon gas. An orange solution was obtained showing yellow emission under a UV lamp (365 nm). After filtration of the unreacted OPD in the ice bath and removal of small fluorophores by SEC, orange CDs remained in aqueous solution. After evaporation of water, orange CDs were obtained as a brown powder.

However, with different techniques, the same precursors yielded different result. Instead of ultrasonication bath, when 0.02 g citric acid and 0.28 g OPD with a molar ratio of 1:25 dissolved in 10 mL deionized $H_2O$ were heated in a microwave oven (700 W) for 7 min.

The resulting CDs were obtained in black powder. After the purification by SEC, they were separated into three fractions.

Table 1 records some CDs prepared from my group from various precursors, reaction conditions, techniques, and synthetic approaches. It confirms the universality to synthesize CDs but also exhibits the diverse CDs behaviors resulting from different synthesis details. For example, gel-like CDs behave like gel due to the presence of EDA in the obtained CDs functioning as surface N-dopant. However, after the synthesis of gel-like CDs, EDA is hard to purify and will remain in the CDs forming a gel network. The similar case occurs in the synthesis of tryptophan CDs using tryptophan and EDA,[21] which indicates the importance of EDA on the formation of gel network.

**Table 1.** A summary of various CDs prepared from our group with different precursors by different synthetic approaches, techniques and reaction conditions.

| CDs species | Synthetic Approaches | Precursors | Reaction Conditions |
|---|---|---|---|
| Black CDs | Top-down, Hydrothermal | Raw carbon powder | $H_2SO_4/HNO_3$, 110 °C for 15 h |
| Gel-like CDs | Bottom-up, Solvothermal | Citric acid & EDA Molar ratio: 1:14 | Temperature: 160 °C Time: 50 min Protective gas: argon |
| Orange CDs | Bottom-up, Ultrasonication | Citric acid & OPD Molar ratio: 1:25 Solvent: water | Sonication bath Frequency: 42 kHz Time: 1 hour |
| Tea, coffee, wine, pepsi, cheese-based CDs | Bottom-up Microwave | Tea, coffee, wine, pepsi, cheese | Power: 700 W Time: 7 min |

## 2.2 Purification/Separation of Carbon Dots

### 2.2.1 Purification of Carbon Dots

As was mentioned in the synthesis section, purification is a hard but critical step following synthesis to remove the precursors. It helps reveal the true CDs behaviors, properties and

potential applications regardless of the interference of impurities including unreacted precursors or low-molecular-weight intermediates. As to the purification of CDs, the most common and effective purification technique is dialysis and its purification principle is based on the size or molecular weight difference between CDs and dialysis membrane. In other words, if the size or molecular weight of CDs is rather small, most CDs also can pass the dialysis membrane and disperse into water, which will cause the loss of CDs and low purification efficiency. On the contrary, when the size or molecular weight of CDs are larger than the dialysis membrane whose pore size or molecular weight is larger than impurities, CDs can maintain in the dialysis tubing. The application of dialysis is simple, and experimentalist only needs to regularly change water to imbalance the concentration of precursors in and out of the dialysis tubing to constantly reduce the precursors in the dialysis tubing. However, in many CDs studies, the purification step was either ignored or performed without considering the size of CDs.[47] Consequently, the obtained CDs may still mix with impurities.

In addition to dialysis, other purification techniques including solvent wash and SEC have all been tried to remove the impurities in CDs.[48] Compared with dialysis, they are unusual methodologies for the purification of CDs but in some case, they are more efficient than dialysis. For example, when gel-like CDs were purified to remove excessive EDA, given their small molecular weight (319 g/mol) revealed by mass spectroscopy,[35] most gel-like CDs leaked out of dialysis tubing (100-500 Da). Then in comparison, size exclusion chromatography (SEC) was applied for the purification of gel-like CDs. The purification step with SEC is according to different sizes or molecular weights between gel-like CDs and impurities. Since smaller impurities are likely to be trapped in the pores of stationary

phase while larger CDs can't enter but will pass by the pores, gel-like CDs were supposed to be the first eluent. With water as the developing solvent, gel-like CDs mixed with impurities were eluted with UV lamp (365 nm) irradiated for tracking the flow of gel-like CDs. However, since the impurities don't have PL, the purification was roughly processed until the blue PL of CDs could no longer be observed and there was no evidence of the reduction of impurities. Thus, no matter with dialysis or SEC, the purification of gel-like CDs was questionable. Therefore, a simple solvent (acetone) wash was performed in the room temperature considering that EDA can dissolve in acetone while CDs can't. The -$NH_2$ content of gel-like CDs was analyzed using a fluoroscopic analysis with fluorescamine and it decreased by 20% from 0.1050 to 0.0847 mmol/mg. It suggests at least 20% of the previous -$NH_2$ are free amine groups, which indicates EDA. After acetone wash, these EDA have been removed from the gel-like CDs.

Figure 2.2a shows gel-like CDs, gel-like CDs purified by acetone, SEC and dialysis on an analytical reversed-phased thin layer chromatography (TLC) plate from left to right, respectively. As to the developing agent, acetonitrile/water with different volume ratios (8:2, 7:3, 6:4 and 5:5) was previously tried to develop fractions of gel-like CDs on a TLC plate (Figure 2.2b). In comparison, the optimal volume ratio was $v_w$:$v_a$, 3/7 and four major CDs fractions were clearly observed. In addition, in comparison, it clearly illustrates the loss of CDs fractions caused by dialysis. Therefore, the use of dialysis as a purification technique needs to be confirmed with the molecular weight or size of CDs. And the purification techniques should vary according to the difference of polarity, molecular weight, size or charge between precursors and as-obtained CDs.

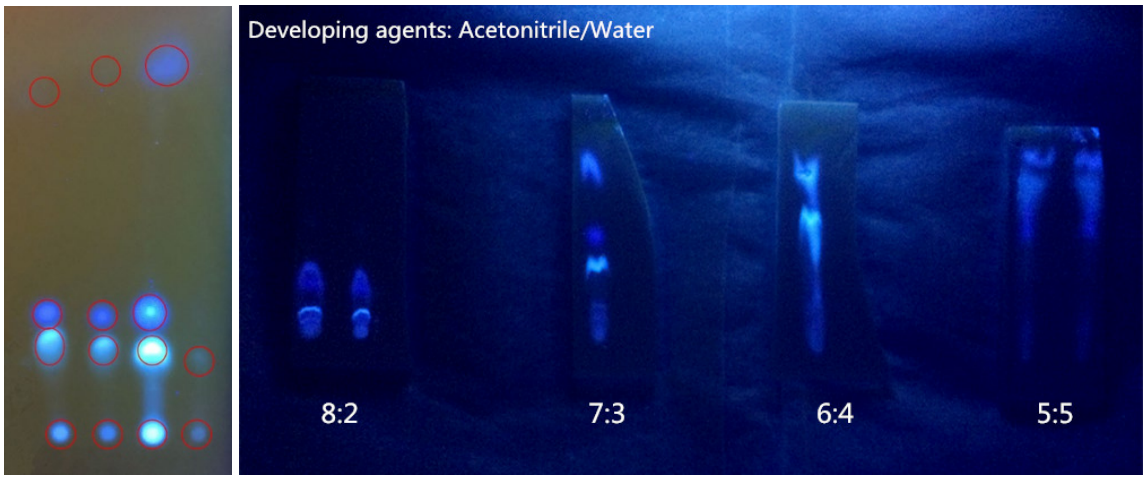


**(a)** **(b)**

**Figure 2.2** (a) Gel-like CDs, gel-like CDs purified by acetone, SEC and dialysis on a reversed-phase TLC plate from left to right, respectively, with acetonitrile/water as the developing solvent; (b) The study of acetonitrile/water with different volume ratios (8:2, 7:3, 6:4 and 5:5) to analyze the optimal developing agent of gel-like CDs on a reversed-phase TLC plate.

2.2.2 Separation of Carbon Dots

As is reported, CDs may not be homogeneous.[48] It is significant to unveil the constituent, which contributes another perspective to explaining the general behaviors and PL mechanism of CDs. Universally, the separation techniques mainly indicate chromatography. To date, the chromatography species used for CDs separation that have been reported include column chromatography (CC),[10] high-performance liquid chromatography (HPLC),[49] TLC,[48] and SEC.[44] All these techniques, except SEC, separate molecules or particles based on differences in polarity. However, since CDs are typically hydrophilic, the stationary phase of all three chromatography techniques must be hydrophobic as $C_{18}$-based materials. Moreover, the developing solvents ought to be polar solvents such as water or mixture of polar and nonpolar solvents. However, the use of polar solvents restricts the use of CC in the separation of CDs due to the long time involved. In addition, HPLC is a costly technique and not easy to access. In comparison, TLC is easy to access and operate with less time spent and efficient separation. Nonetheless, the

importance of TLC in the separation field is gradually overlooked with the development of new chromatography techniques such as HPLC and solid-phase extraction. Therefore, to demonstrate that TLC has the same separation effect as HPLC, TLC was applied in my group to separate gel-like CDs. With water/acetonitrile ($v_w$:$v_a$, 3/7) as the developing solvent, gel-like CDs were separated into four photoluminescent fractions on a reversed-phase TLC plate, which is presented in Figure 2.3a. To confirm the separation efficiency of TLC, TLC was also employed to separate carbon nitride dots prepared from citric acid and urea. With water as the developing solvent, we obtained five major fractions from the reversed TLC plate as shown in Figure 2.3b, which suggests the heterogeneity of CDs and carbon nitride dots and shows the excellent separation efficiency of TLC. In addition, all the CDs separate fractions were characterized by AFM with TEM (Figure 2.4) and the morphological study revealed that they were all spherical CDs in nature with an average size at around 3 nm.

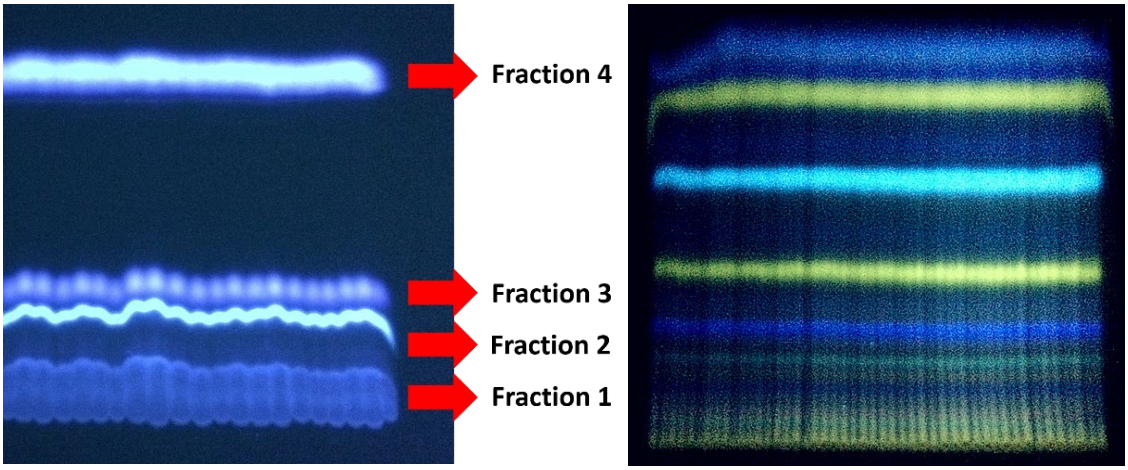


**Figure 2.3** (a) Four bright bands on a preparative $C_{18}$ reversed-phased TLC plate, labeled from bottom to top as fraction 1, 2, 3 and 4 of gel-like CDs; (b) Bright bands on a preparative $C_{18}$ reversed-phased TLC plate, which indicate many fractions of carbon nitride dots with different PL behaviors and polarities.

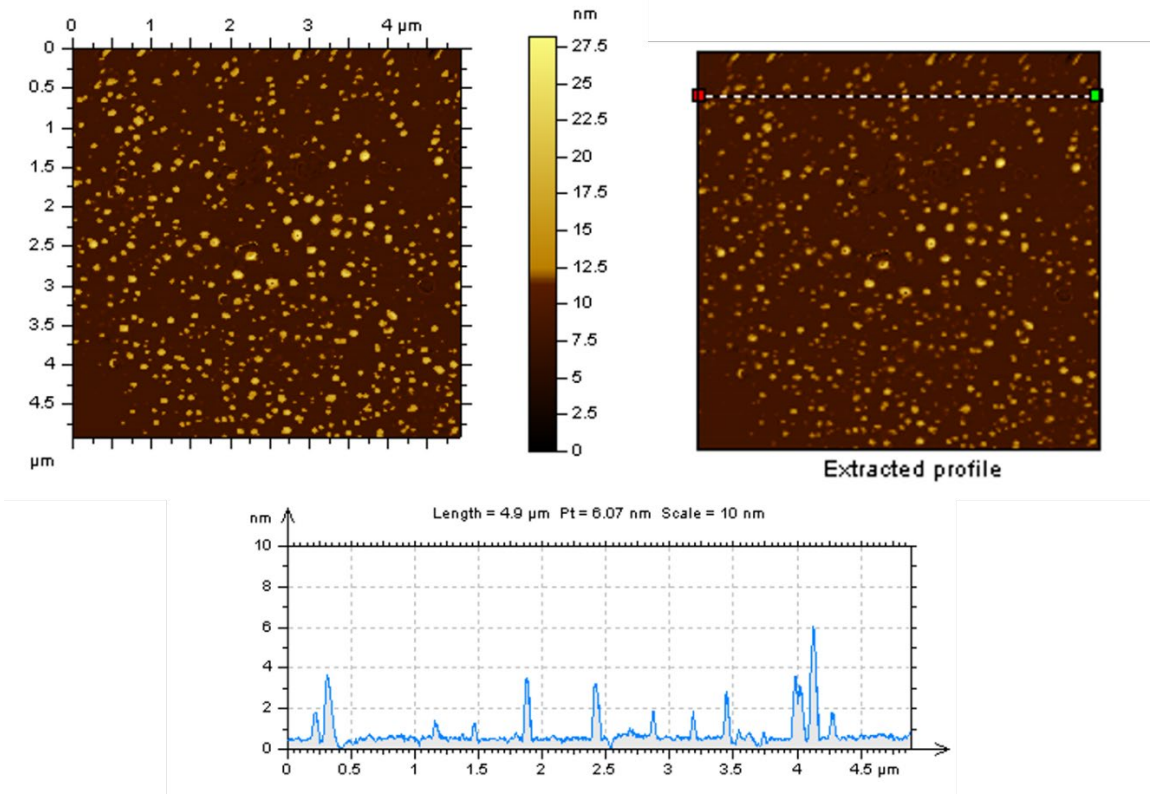
0 1 2 3 4 µm
µm
nm
27.5
25
22.5
20
17.5
15
12.5
10
7.5
5
2.5
0
Extracted profile
Length = 4.9 µm Pt = 6.07 nm Scale = 10 nm
nm
4.5 µm

**(a)**

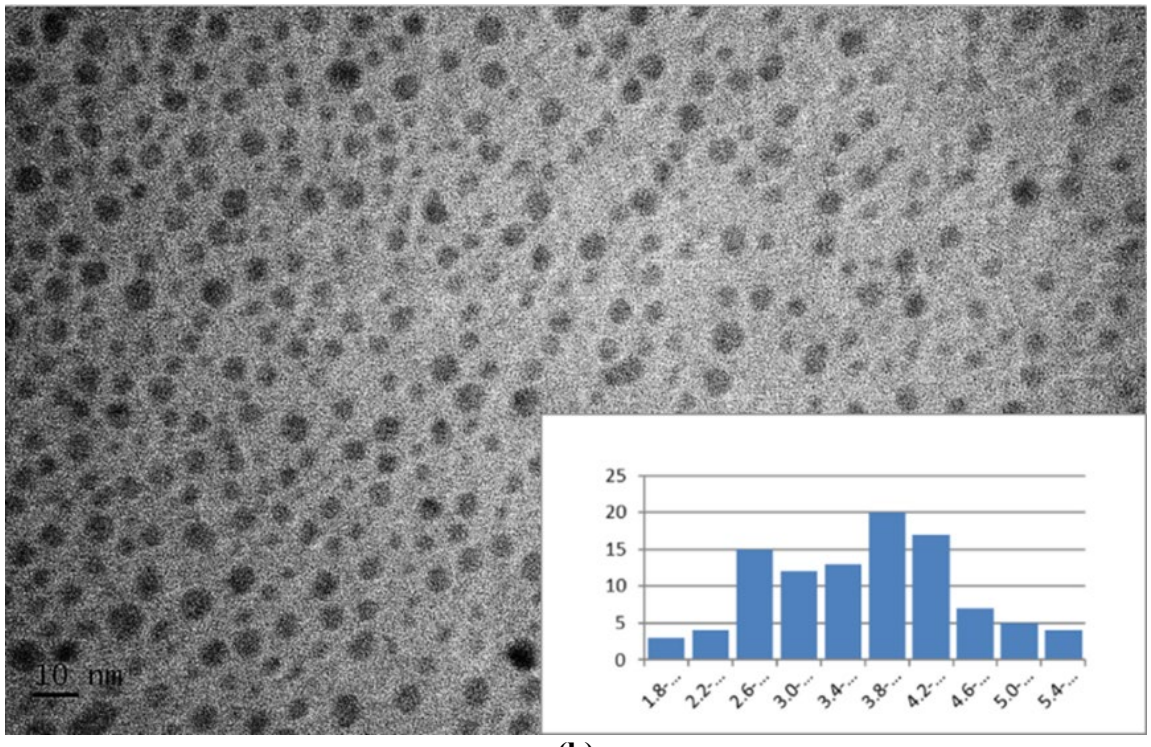
10 nm
25
20
15
10
5
0
1.8-...
2.2-...
2.6-...
3.0-...
3.4-...
3.8-...
4.2-...
4.6-...
5.0-...
5.4-...

**(b)**

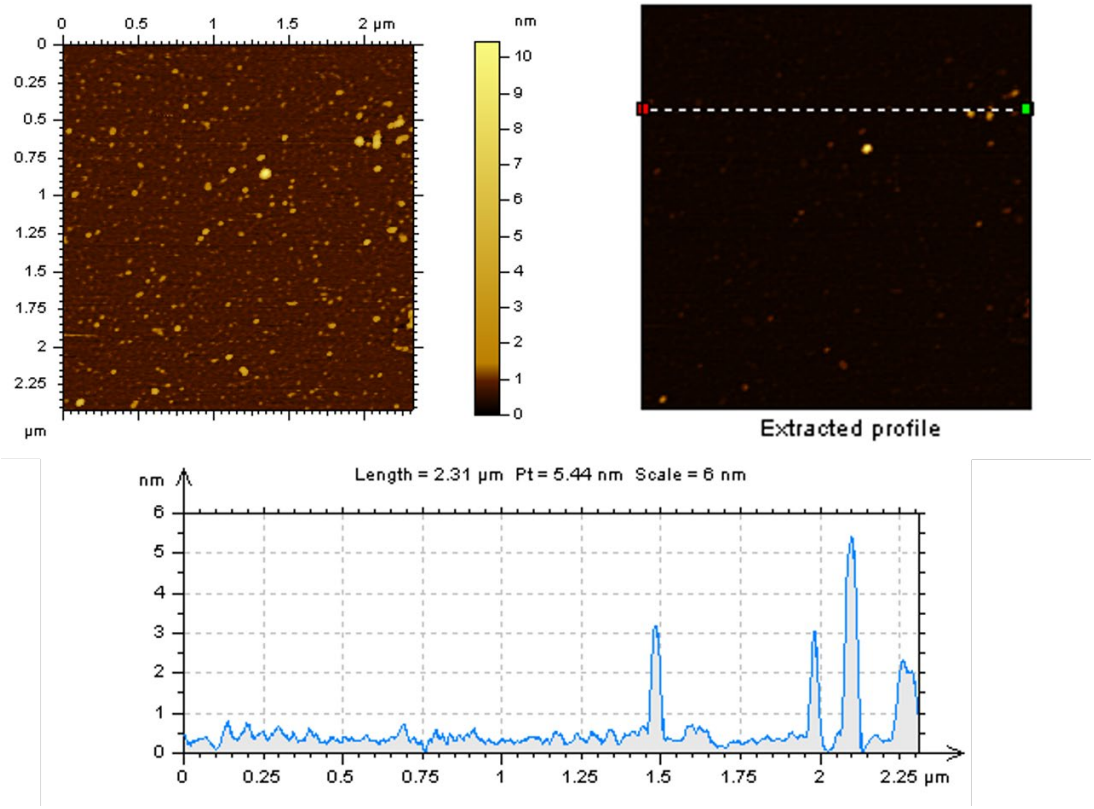
0 0.5 1 1.5 2 µm
µm
nm
Extracted profile
Length = 2.31 µm Pt = 5.44 nm Scale = 6 nm
nm
0 0.25 0.5 0.75 1 1.25 1.5 1.75 2 2.25 µm

**(c)**

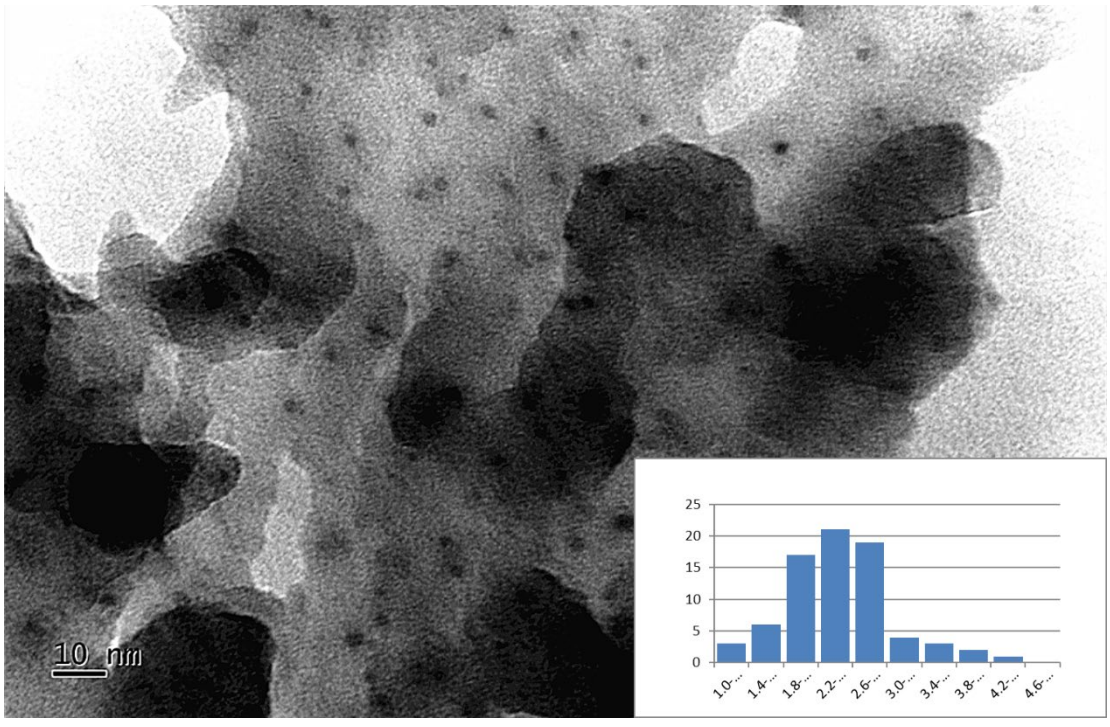
10 nm

**(d)**

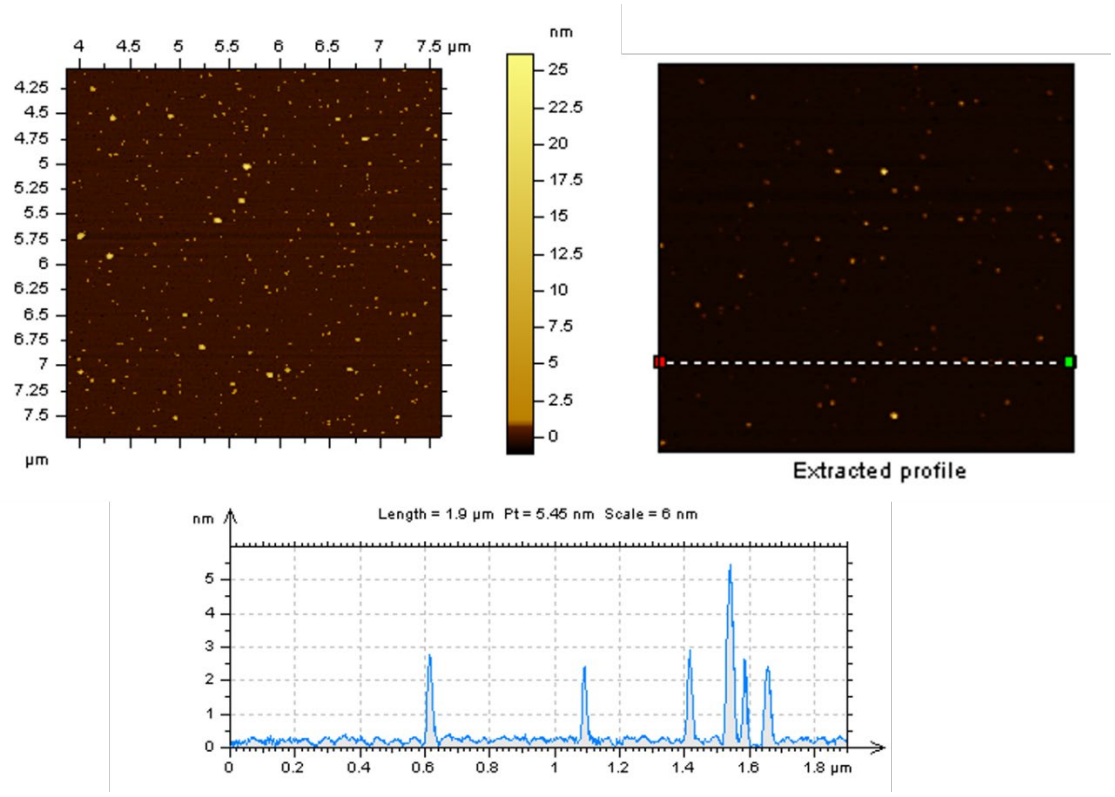
4 4.5 5 5.5 6 6.5 7 7.5 µm
4.25 4.5 4.75 5 5.25 5.5 5.75 6 6.25 6.5 6.75 7 7.25 7.5
µm
nm
25 22.5 20 17.5 15 12.5 10 7.5 5 2.5 0
Extracted profile
Length = 1.9 µm Pt = 5.45 nm Scale = 6 nm
nm
5 4 3 2 1 0
0 0.2 0.4 0.6 0.8 1 1.2 1.4 1.6 1.8 µm

**(e)**

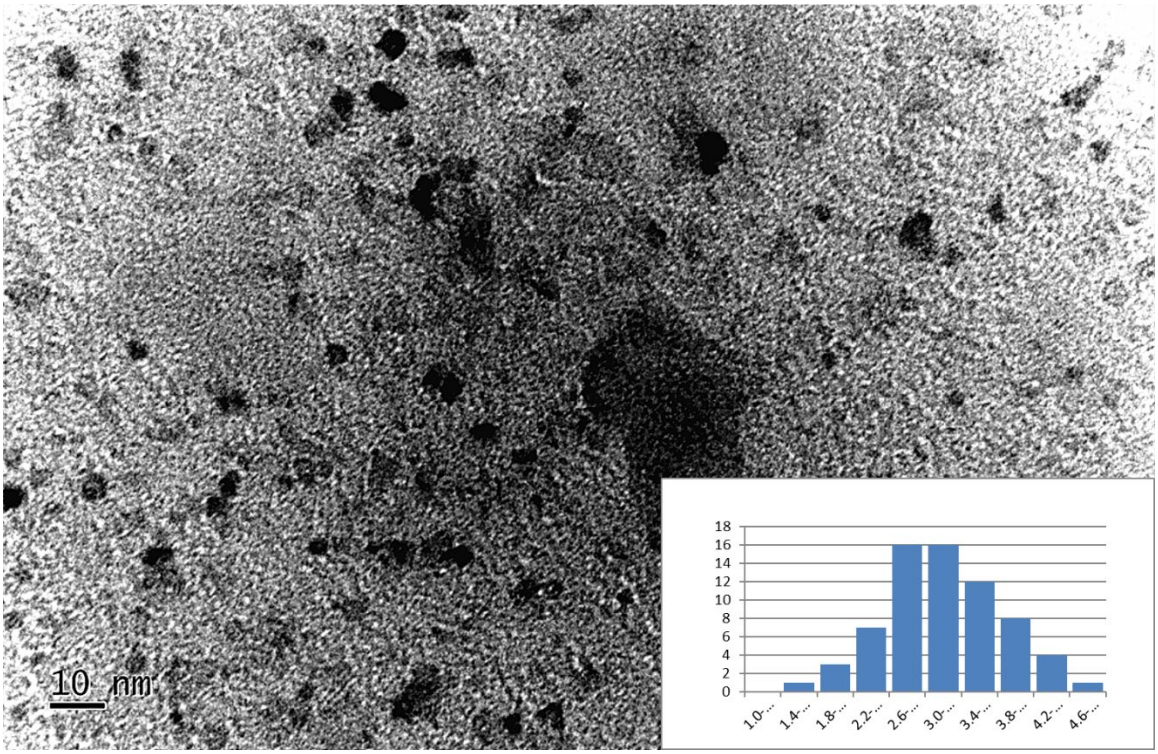
10 nm
18 16 14 12 10 8 6 4 2 0
1.0-... 1.4-... 1.8-... 2.2-... 2.6-... 3.0-... 3.4-... 3.8-... 4.2-... 4.6-...

**(f)**

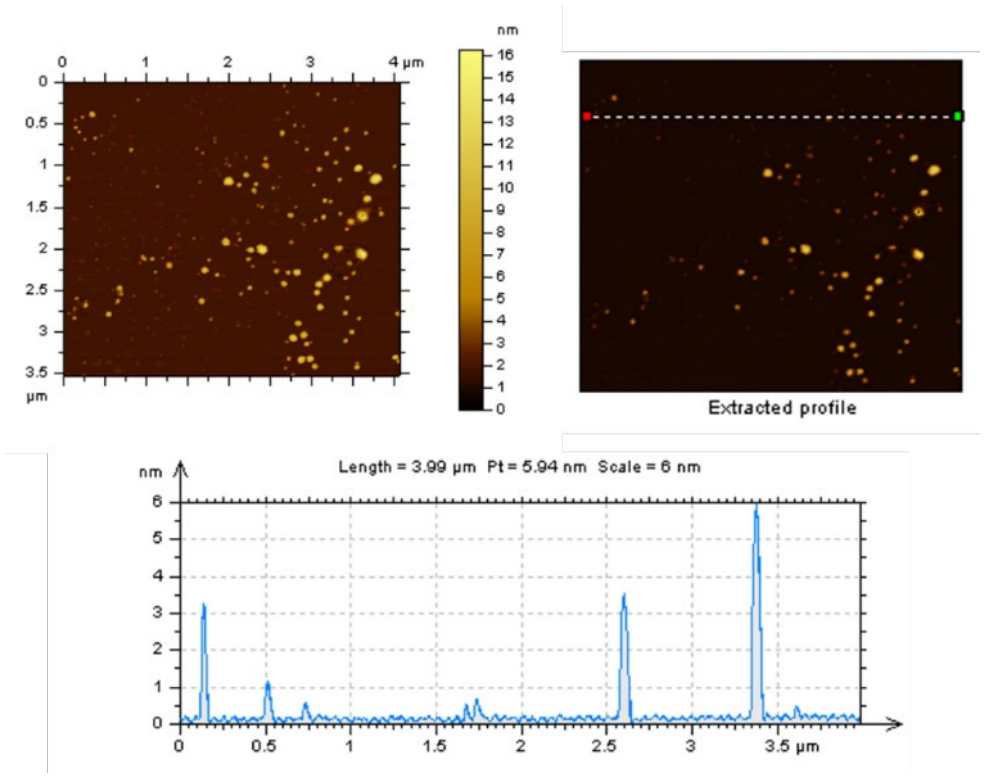


**(g)**

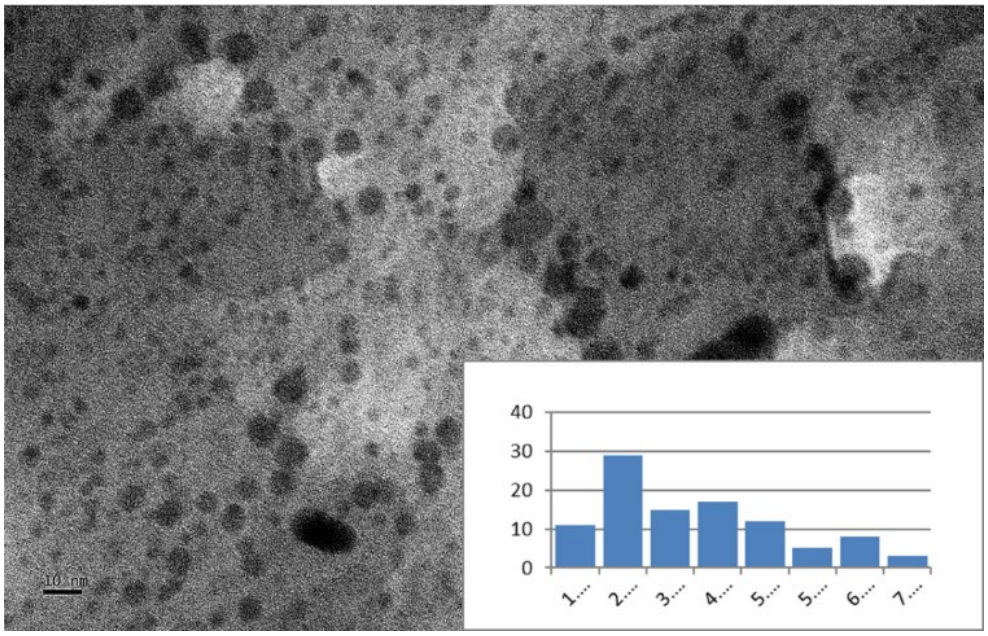


**(h)**

**Figure 2.4** AFM (a, c, e, g) and TEM (b, d, f, h) images of four separate fractions of gel-like CDs. Fraction 1: a, b; Fraction 2: c, d; Fraction 3: e, f; Fraction 4: g, h.

Except TLC, SEC is another separation technique widely used in my group and its mobile phase is usually water. It does not only remove impurities by keeping them in the pores of stationary phase but also causes the lagging effect to separate the CDs in different sizes. For example, we tried to separate gel-like CDs with SEC, but we only obtained one eluent, which suggests the uniformity of gel-like CDs in terms of size of molecular weight. The same result was observed to separate orange CDs. However, when the same precursors were used but the technique altered from ultrasonication to microwave (7 min, 700 W), the obtained CDs could split into three fractions with different PL colors,[50] which is shown in Figure 2.4. In addition, SEC is also often used to separate CDs-drug conjugates from free CDs or drugs. Based on the increase of size or molecular weight, CDs-drug conjugates are supposed to be the first eluent. However, the success of conjugation still needs the confirmation by various spectroscopic characterizations.

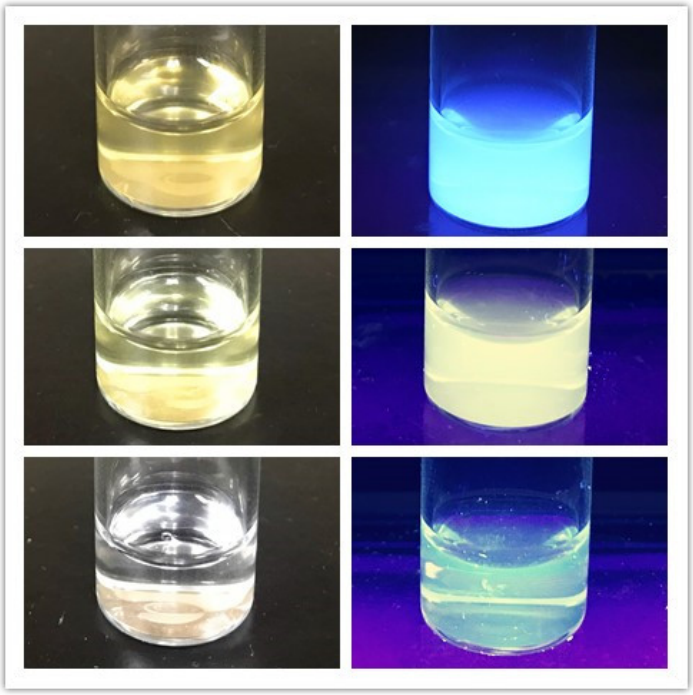

**Figure 2.5** The aqueous dispersions of three CDs fractions with a concentration of 0.1 mg/mL (top-down: fraction 1, 2 and 3) after separation by SEC. (The left column is under white light; the right column is under the UV light at 365 nm).

## 2.3 Summary

In this chapter, CDs were introduced in terms of synthesis, purification and separation. The synthesis of CDs falls mainly into two categories, namely top-down and bottom-up approaches. As to the starting material, it has a wide range. In other words, CDs can be prepared from almost all the carbon-based substances. However, the purification of CDs has never been systematically studied before, which results in the uncertainty of both presence and purity of many reported CDs. In this chapter, purification of CDs has been performed with three different methods, which illustrates that dialysis is not always the optimal purification approach and certain purification method should be applied considering the difference of polarity, molecular weight or size of precursors and resulting CDs. Separation of CDs has aroused much attention and TLC returns to scope of public regarding its availability and efficiency. However, even though SEC can be applied to purify CDs-drug conjugates from free CDs or drugs based on their different sizes, the success of conjugation requires confirmation by various characterization methodologies.

## Chapter 3. Characterization of Carbon Dots

Characterization is necessary to evaluate whether the conjugation of CDs with a compound is successful. Also, characterization is important to determine if CDs can be obtained under a certain reaction condition. In this chapter, many typical techniques to characterize CDs are presented including UV/vis absorption, fluorescence emission, Fourier-transform infrared (FTIR), X-ray photoelectron spectroscopies (XPS), atomic force (AFM), transmission electron microscopies (TEM) and zeta potential measurement. In addition, CDs have many unique properties such as thermal, solvent and salt effects, which will be also illustrated in this chapter.

### 3.1 Instrumental

#### 3.1.1 UV/vis Absorption Spectroscopy

CDs are frequently characterized by their optical properties such as UV/vis absorption and PL. In my group, a Cary 100 UV/Vis spectrophotometer is used to record the UV/vis absorption spectra of CDs in a 1×1 cm quartz cuvette. The UV/vis absorption spectra of CDs usually show two peaks at around 250 and 350 nm as shown in Figure 3.1a, which could be assigned to π-π* transition of C=C conjugate structure and n-π* transition of C=O conjugate structure, respectively.[35] Also, sometimes there are some other peaks besides those two typical ones in the UV/vis absorption spectra of CDs. For instance, in Figure 3.1b, orange CDs display a peak in the low-energy region at 417 nm which can be attributed to the absorption cross-section of $NO_2$.[30] In addition, new peaks or co-existence of all peaks from both spectra of CDs and compound can help examine if CDs successfully conjugate with a compound.

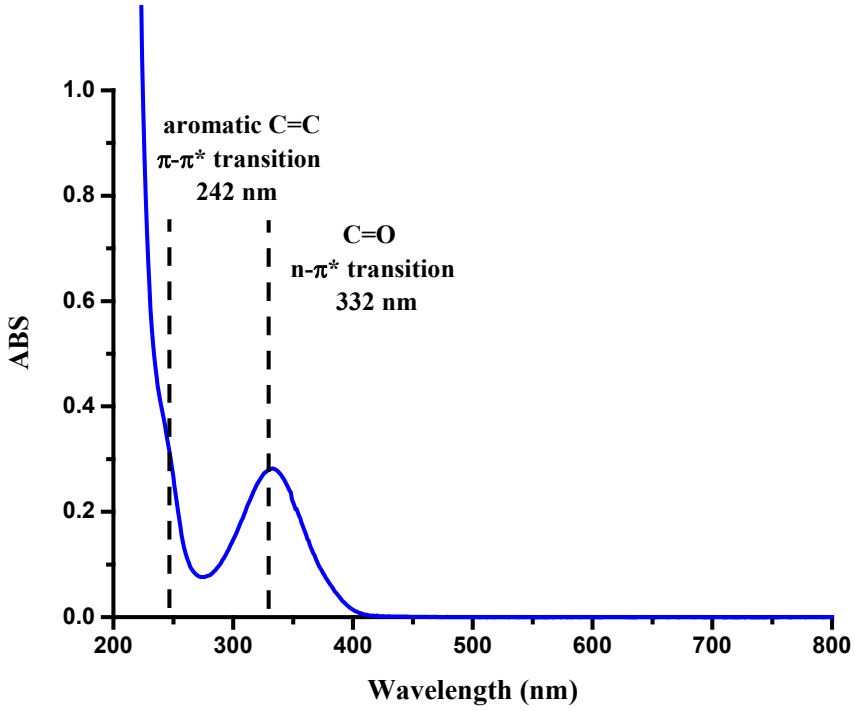


(a)

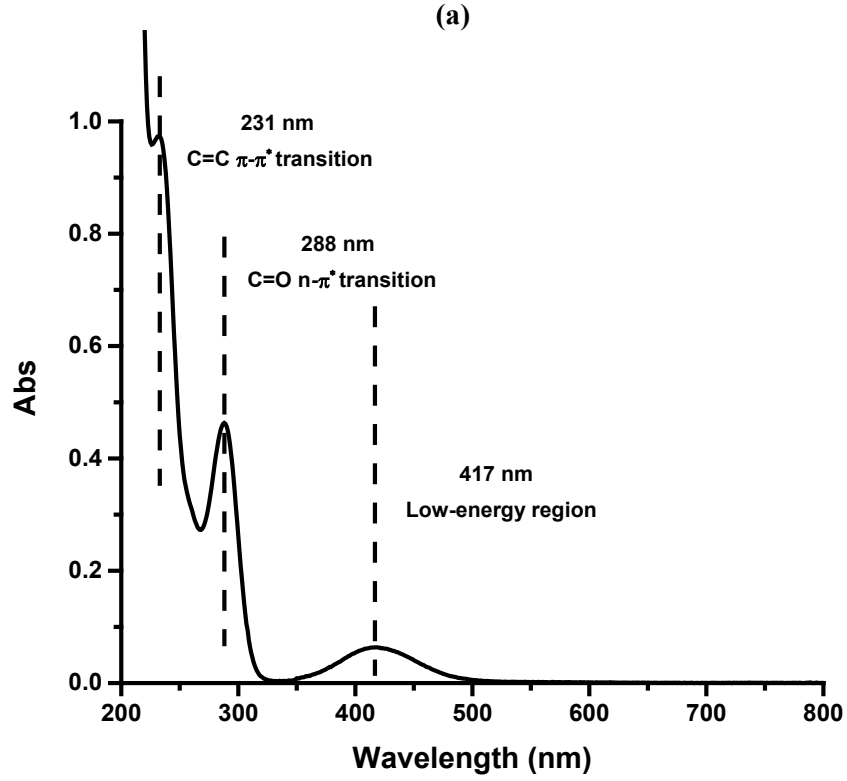


(b)

**Figure 3.1** The UV/vis absorption spectra of gel-like CDs (a) and orange CDs (b). The concentrations of them are 0.60 and 0.03 mg/mL, respectively.

### 3.1.2 Fluorescence Emission Spectroscopy

Except for UV/vis absorption spectroscopy, fluorescence emission spectroscopy is also important to reveal another characteristic optical property of CDs which is PL. In our group, a Fluorolog (Horiba Jobin Yvon) spectrometer is applied to record the fluorescence emission spectra of CDs with a slit width of 5 nm for both excitation and emission. PL process can be simply demonstrated by a surface state theory considering CDs as a semiconductor. The valence band of CDs after absorption of photons will generate excitons (electrons and holes). The generated electrons will transit to the conduction band and move to the energy levels caused by the surface state of CDs after vibrational relaxation. Soon after, electrons will continue to transit back to the valence band and recombine with the holes to release the energy in the form of light emission. Due to a single or multiple energy levels of the surface states, upon excitation at different wavelengths, electrons can transit between a uniform or varied band gaps from the surface states to the valence band while emitting the light at uniform or various wavelengths accordingly. This whole process is illustrated in Figure 3.2. Thus, it explains the observation that CDs either exhibit excitation-dependent or -independent PL as illustrated in Figure 3.3a and b, respectively.

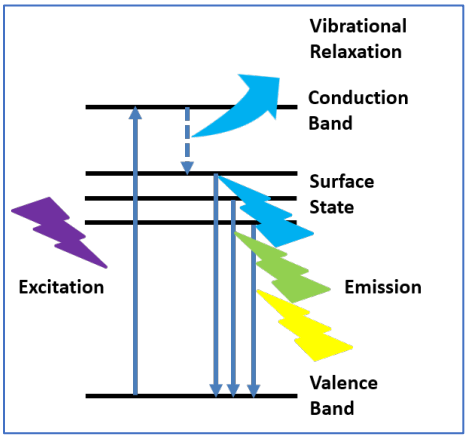


**Figure 3.2** The illustration of electron transition and light emission of CDs upon light excitation.

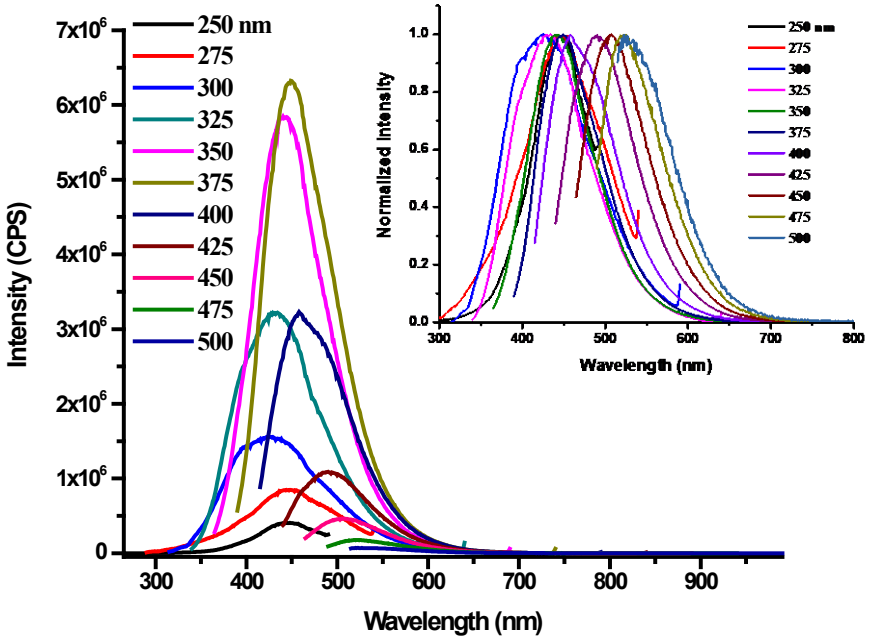


**(a)**

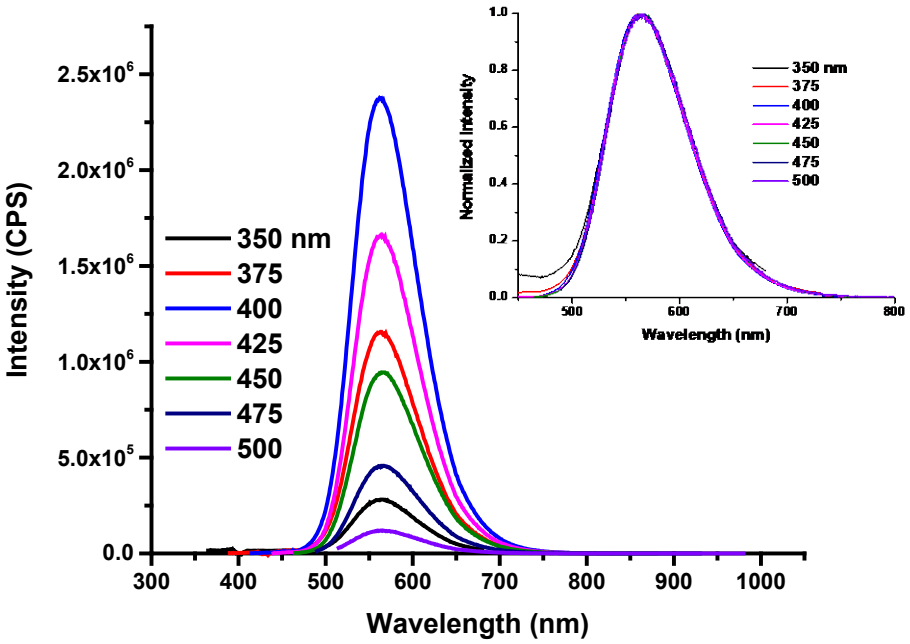


**(b)**

**Figure 3.3** Fluorescence emission spectra of (a) gel-like CDs (0.1 mg/mL) and (b) orange CDs 0.005 (mg/mL) aqueous dispersion excited with various wavelengths (inset: normalized fluorescence spectra of gel-like CDs and orange CDs) in a quartz cell (1 cm).

The excitation dependency of PL of CDs can be converted with different precursors or preparation methods. For example, although orange CDs exhibited excitation-independent PL in Figure 3.3b, when the same precursors were treated with another microwave-mediated method, three fractions were separated by SEC with different PL behaviors, which is shown in Figure 3.4. From Figure 3.4, both fraction 1 (a) and 2 (b) have excitation-independent PL. However, fraction 3 (c) shows excitation-dependent PL. Meanwhile, sometimes the change of excitation dependency of PL can be also achieved by the separation of the as-prepared CDs. For example, as we mentioned previously, when gel-like CDs were separated by TLC, four fractions were obtained. Among them, two fractions (fraction 2 and 3) exhibit excitation-independent PL (Figure 3.5b and c) while the other two fractions (fraction 1 and 4) keep the same excitation-dependent PL behavior as gel-like CDs (Figure 3.5a and d). Moreover, the fluorescence QY of fraction 2 (55%) is even higher than that of gel-like CDs (34%).

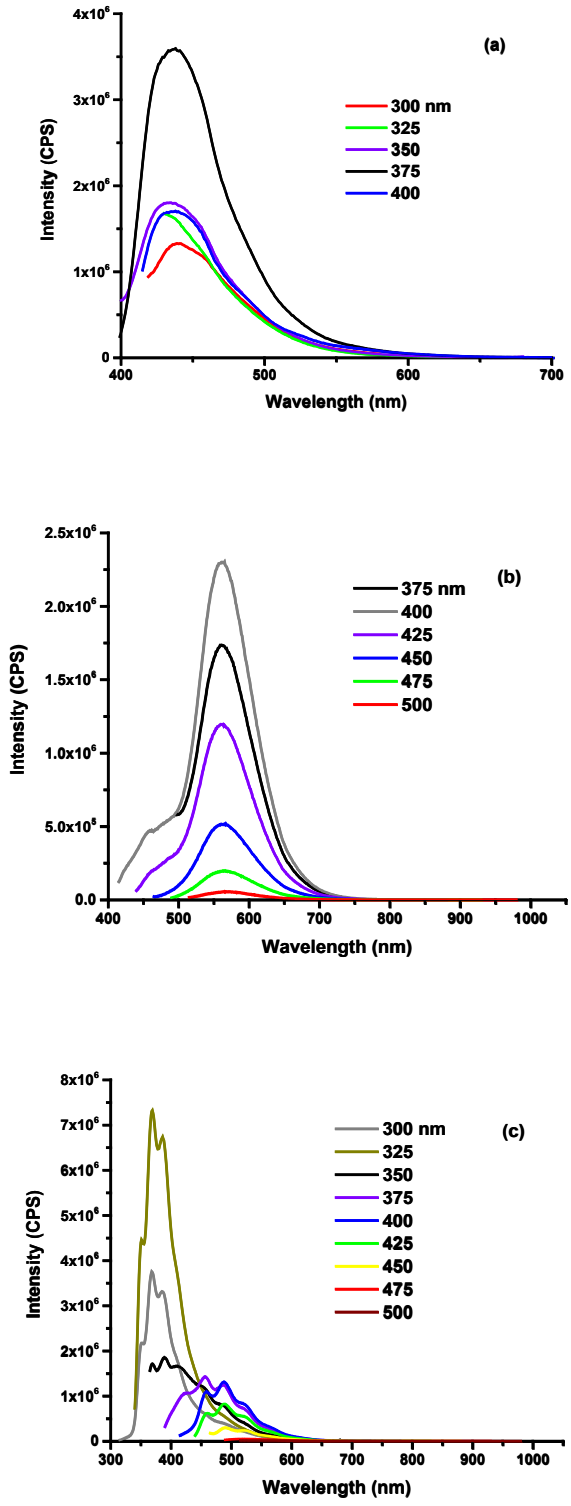


**Figure 3.4** The fluorescence spectra of fraction 1 (a), 2 (b) and 3 (c) of CDs prepared from citric acid and OPD via a microwave-mediated method. The concentration of fraction 1,2 and 3 is $1.9\times10^{-4}$, $5.6\times10^{-2}$ and $2.5\times10^{-1}$ mg/mL, respectively.

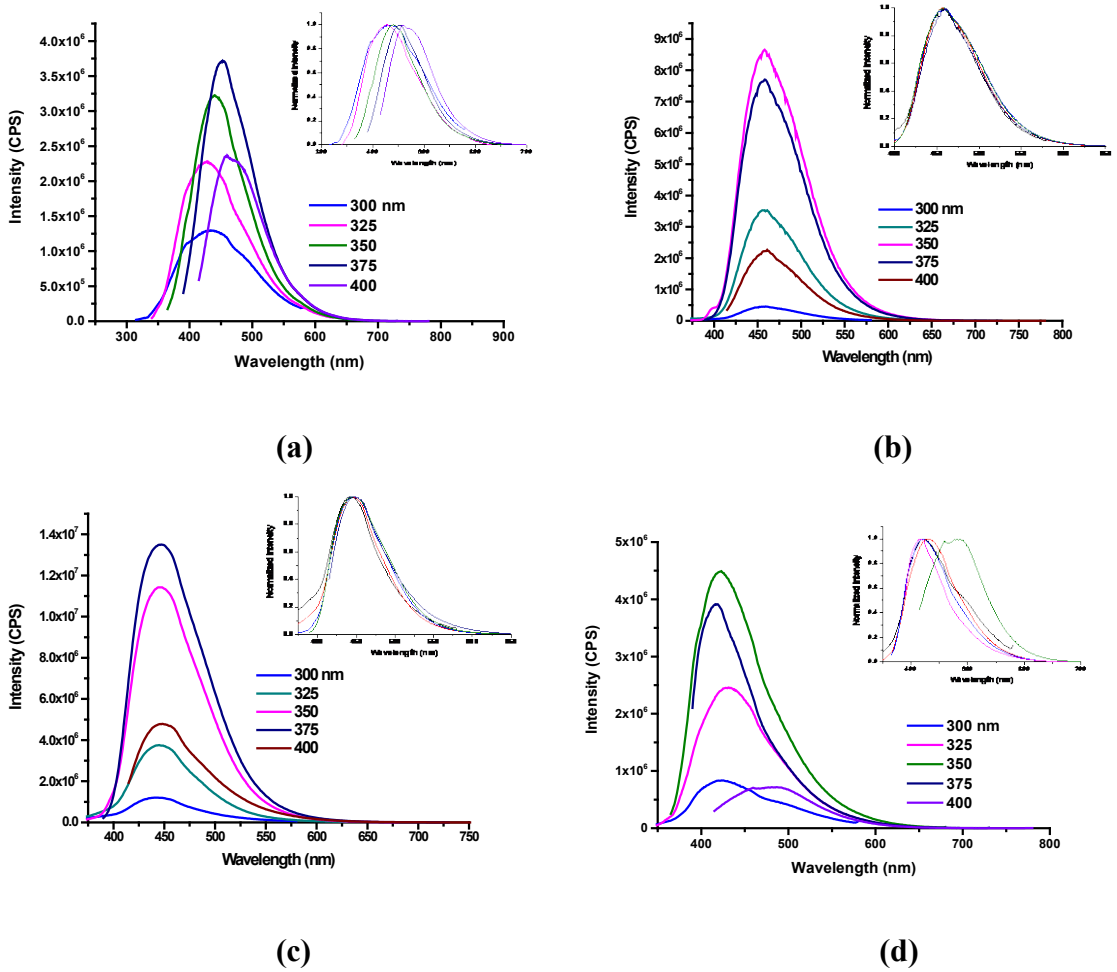


**Figure 3.5** Fluorescence spectra and normalized spectra (inset) of the gel-like CDs fractions (a) 1, (b) 2, (c) 3 and (d) 4 excited at 300, 325, 350, 375 and 400 nm in a quartz cell (1 cm). (The concentration of fractions 1, 2, 3 and 4 were 0.4, 0.3, 0.2 and 0.4 mg/mL, respectively, and the legends in (a), (b), (c) and (d) also apply to their own insets).

Even though the surface state theory can be used to explain the excitation dependency or independency of the emission, some studies reported the emission color can be tuned by the size of NPs such as traditional QDs.[51] Also, molecule state theory provides another viewpoint to inspect the structure of CDs and yield a conclusion that the PL is generated from the fluorophores on the surface of CDs.[52] However, it neglects the significance of the core in the PL of CDs. Actually, core state was put forward together with surface state theory by Giannelis and co-workers in 2012.[53] As to the core state theory, excitons are not

only generated in the surface states but also in the carbon core.[54] However, the core states usually emit light with short wavelength and low fluorescence QY.[53] A highly crystalline core with more uniform functional groups results in higher fluorescence QY while CDs with more traps and fewer surface functional groups have lower fluorescence QY.[55] Even though many theories have been developed to explain the unique PL of CDs, surface state theory is the most popular mechanism.[56]

As a measure of PL, fluorescence QY in the past several years aroused much attention. In order to enhance the fluorescence QY of CDs to meet the requirement of application, various precursors, reaction conditions, and most importantly surface modifications such as N doping,[57-58] S doping[12] and polymer functionalization[59-60] have been applied. The fluorescence QY enhancement of CDs by surface modification might result from the reduction of other non-irradiative emission to intensify the emission in the form of irradiation.[8] With years' endeavor, the fluorescence QY of CDs has been greatly improved up to 93.3%.[25] Table 2 lists the fluorescence QY of some CDs species obtained in my work and the QY calculation was based on the equation.[61] From Table 2, the highest fluorescence QY achieved in my work is 55% of the fraction 2 from the separation of gel-like CDs.

**Table 2.** A summary of the fluorescence QY of various CDs species prepared with different precursors and reaction conditions.

| CDs species | Precursors | Reaction Conditions | Fluorescence QY |
|---|---|---|---|
| Black CDs | Raw carbon powder | $H_2SO_4/HNO_3$, 110 ℃ for 15 h | 1% |
| Gel-like CDs | Citric acid & EDA Molar ratio: 1:14 | Temperature: 120 °C Time: 50 min | 28% |
| Gel-like CDs | Citric acid & EDA Molar ratio: 1:14 | Temperature: 140 °C Time: 50 min | 30% |
| Gel-like CDs | Citric acid & EDA Molar ratio: 1:14 | Temperature: 160 °C Time: 50 min | 34% |
| Gel-like CDs | Citric acid & EDA Molar ratio: 1:14 | Temperature: 180 °C Time: 50 min | 17% |
| Fraction 1 | Gel-like CDs | Temperature: 160 °C Time: 50 min | 4% |
| Fraction 2 | Gel-like CDs | Temperature: 160 °C Time: 50 min | 55% |
| Fraction 3 | Gel-like CDs | Temperature: 160 °C Time: 50 min | 3% |
| Fraction 4 | Gel-like CDs | Temperature: 160 °C Time: 50 min | 12% |
| Orange CDs | Citric acid & OPD Molar ratio: 1:25 | Sonication frequency: 42 kHz Time: 1 hour | 1% |

In addition, fluorescence analysis can help quantify the content of primary amine group on the surface of CDs. On the basis of that fluorescamine can react with primary amine to generate fluorescence, EDA was used as standard. To prepare EDA solution with different concentrations, 0, 2, 4, 6, 8, and 10 μL EDA was added into a 2-mL volumetric flask, respectively, which was filled up with acetone/1×PBS buffer solution with volume ratio 1:1. Then 50 μL solution was transferred to a 5 mL volumetric flask together with 0.5 mg fluorescamine and the flask was filled with the same mixed solution. To avoid the error cause by the emission saturation, each solution was diluted 100 times in the end. Then the fluorescence measurement revealed the linear relation as shown in Figure 3.6. And the linear relationship was used to perform the fluorescence analysis of the content of $-NH_2$ on

both gel-like and orange CDs. Eventually, the -$NH_2$ content on the surface of gel-like and orange CDs is 0.105 and $6.12\times10^{-5}$ mmol/mg, respectively.

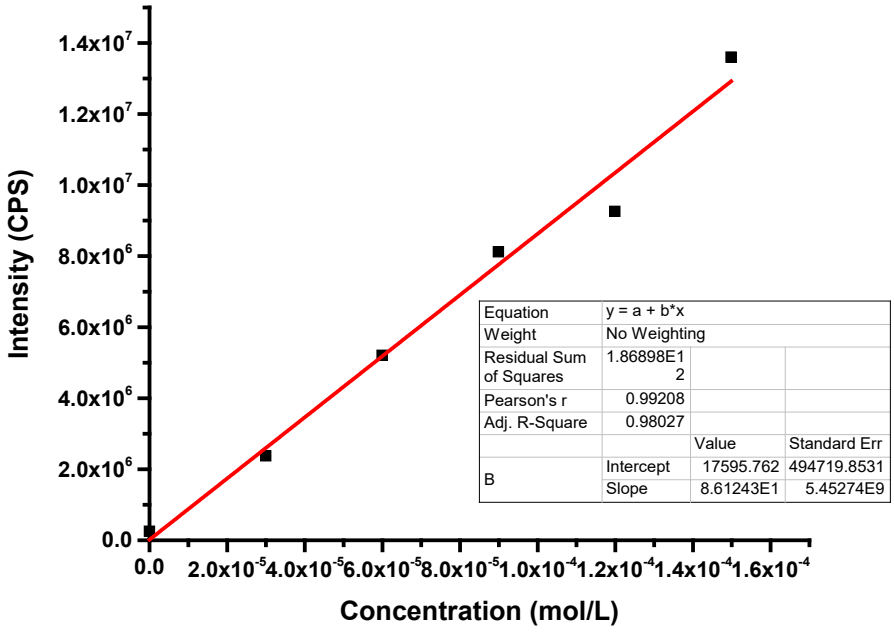


**Figure 3.6** The linear relationship between the fluorescence intensity and concentration of EDA mixed with fluorescamine, which was used as standard to calculate the content of primary amine on both gel-like and orange CDs.

3.1.3 FTIR Spectroscopy

Considering varieties of functional groups carried by precursors, after simple synthesis reaction, the as-obtained CDs will own abundant functional groups which inherit from their precursors. In addition, during the synthesis, the functional groups of precursors may undergo oxidation and dehydration to introduce new functional groups to the resulting CDs. The most straightforward technique to reveal the functional groups species is FTIR spectroscopy. In our group, the FTIR data are usually obtained from a Perkin-Elmer FTIR spectrometer Frontier using air background. With attenuated total reflection (ATR) technique, the chemical composition of the surface of CDs is qualitatively analyzed. Even

though the functional groups on the surface of CDs depend on the precursors, in general, the functional groups observed on CDs include -OH (3640-3200 $cm^{-1}$), $-NH_2$ (3400-3250 $cm^{-1}$), C=C, C=O and C=N (1760-1640 $cm^{-1}$).[35] In Figure 3.7, the FTIR spectrum is used as an example to show the diverse functional groups on the surface of gel-like CDs. Furthermore, compared with UV/vis absorption and fluorescence emission spectroscopies, FTIR spectroscopy can provide a clearer evidence of the conjugation of CDs with a compound by observation of new peaks. However, even though FTIR spectroscopy can provide a fast picture of the surface of CDs, it can't quantitatively analyze the content of each functional group. As a supplementary of FTIR spectroscopy, XPS measurement has to be performed to generate a more comprehensive understanding of the surface of CDs in terms of chemical composition.

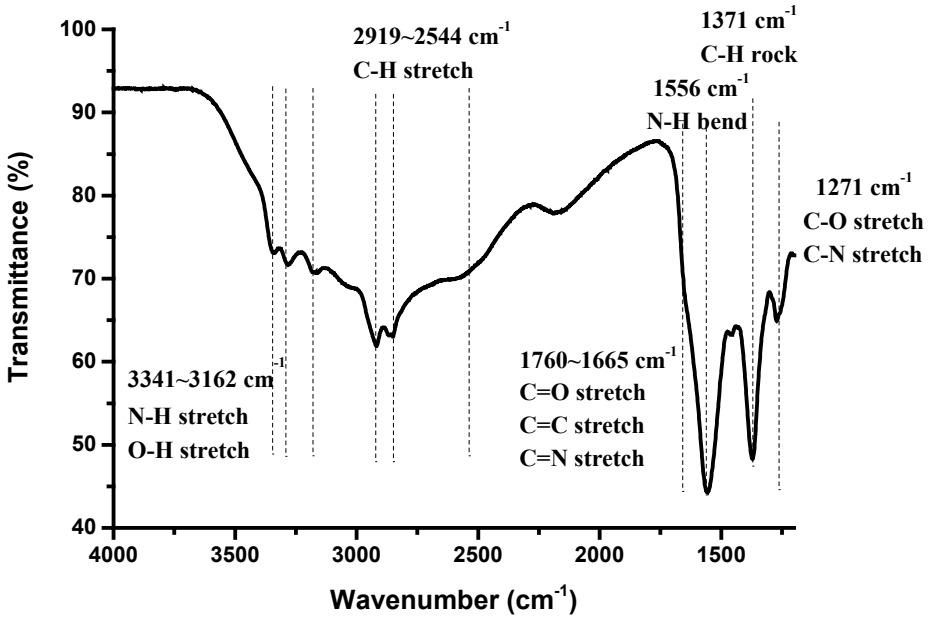


**Figure 3.7** FTIR spectrum of gel-like CDs with air background.

3.1.4 XPS

As mentioned previously, XPS measurement is of great importance to systematically study the functional groups on the surface of CDs on the basis of analysis of FTIR. In our group, the XPS data is acquired using a Perkin-Elmer PHI 560 system with a double-pass cylindrical mirror analyzer operated using a Mg Kα anode with a hυ=1253.6 eV photon energy operated at 250 Watts and 13 kV. From XPS measurement of CDs, we can obtain the percentage of each functional group based on its characteristic binding energy (BE) and integrated peak area. Table 3 shows the XPS analysis of elemental atom percentage and BEs which can help determine the moiety species on the surface of gel-like CDs.

**Table 3.** XPS elemental atom % and BEs of C 1s, O 1s and N 1s core levels of gel-like CDs.

| Orbitals | Atom % | BE (eV) | Functional Groups |
|---|---|---|---|
| C 1s | 75.1 | 284.9 | C=C |
| | | 286.8 | C-OH |
| | | 288.6 | -COOH |
| O 1s | 19.0 | 532.8 | -OH |
| | | 534.1 | C=O |
| N 1s | 5.7 | 399.8 | -NH or -$NH_2$ |

XPS can make up for the deficiency of FTIR measurement. For instance, the overlap of O-H and N-H peaks in FTIR spectrum usually makes it hard to clearly identify the functional group, which is unfavorable for both the demonstration of CDs formation and the conjugation of CDs with a compound. For example, since nitric acid is used in the synthesis of black CDs, nitro was assumed to be introduced to the chemical structure of black CDs. However, due to the accurate elemental analysis of XPS, black CDs turned out to be out of N so nitric acid in the synthesis of black CDs only works as an oxidizing agent to modify the chemical structure of their surface.[19] Also, based on their characteristic BEs,

various functional groups can be identified on the surface of CDs, which can help evaluate whether the CDs can conjugate with the selected compound.

In addition, XPS measurement can help compare CDs synthesized under different reaction conditions. For example, XPS measurement was performed to investigate the thermal effect on the surface elemental composition and optical properties of gel-like CDs.[35] By comparing the surface elemental composition of gel-like CDs prepared at different temperatures in Table 4, we observe that increasing synthetic temperature from 120 to 140 °C reduces oxygen-containing carbon moieties (i.e. O-H, O-C=O groups) but promotes carbonization. Even though carbonization is one essential procedure of CDs formation, high carbonization degree can't guarantee high PL. For example, the fluorescence QY of gel-like CDs decreases from 33 to 17% when reaction temperature increases from 160 to 180 °C. Also comparing the fluorescence QY with atom percentage of separate fractions of gel-like CDs prepared at 160 °C in Table 5, we observe the fluorescence QY of fraction 2>1>3, which matches the O atom percentage of fraction 2>1>3. Therefore, we hypothesize the fluorescence QY is enhanced by enrichment of O on the surface of CDs. However, the comparison to fraction 4 regarding the O atom content and fluorescence QY suggests higher content of O-H may not be beneficial for the improvement of QY. Furthermore, three fractions with different sizes were separated by SEC and collected from CDs prepared with citric acid and OPD via a microwave route.[50] The comparison of XPS data of the three CDs fractions in Table 6 reveals the content of O increases while the content of both C and N decreases with the size of CDs getting smaller.

**Table 4.** XPS atomic percent compositions of gel-like CDs prepared as a function of temperature.

| Orbitals | 120 °C | 140 °C | 160 °C | 180 °C |
|---|---|---|---|---|
| C 1s | 32.2 | 78.8 | 75.1 | 77.0 |
| O 1s | 62.8 | 12.4 | 19.0 | 14.2 |
| N 1s | 5.0 | 8.7 | 5.7 | 8.8 |

**Table 5.** Summary of fluorescence QY and XPS elemental atom % and BEs of O 1s and C 1s core levels of the isolated fractions of gel-like CDs.

| Fraction 1 (QY: 4%) | | |
|---|---|---|
| orbitals | atom % | BE peaks (fwhm, % integrated peak area) |
| O 1s | 76.7 | 532.8 eV (2.9, 85.0%), 534.1 eV (2.6, 15.0%) |
| C 1s | 23.3 | 284.9 eV (3.4, 100%) |
| **Fraction 2 (QY: 55%)** | | |
| orbitals | atom % | BE peaks (fwhm, % integrated peak area) |
| O 1s | 83.6 | 532.8 eV (3.0, 80.4%), 534.1 (2.6, 19.6%) |
| C 1s | 16.4 | 284.9 eV (3.6, 100%) |
| **Fraction 3 (QY: 3%)** | | |
| orbitals | atom % | BE peaks (fwhm, % integrated peak area) |
| O 1s | 74.8 | 532.8 eV (3.0, 75.2%), 534.1 eV (2.6, 24.8%) |
| C 1s | 25.2 | 284.9 eV (3.1, 100%) |
| **Fraction 4 (QY: 12%)** | | |
| orbitals | atom % | BE peaks (fwhm, % integrated peak area) |
| O 1s | 98.2 | 532.8 eV (2.9, 100%) |
| C 1s | 1.8 | 284.9 eV (2.7, 100%) |

**Table 6.** XPS elemental atom % and BEs of C 1s, N 1s, and O 1s core levels in the CDs fractions.

| **Fraction 1** | | |
|---|---|---|
| **Orbitals** | **Atom %** | **BE peaks (fwhm, % integrated peak area)** |
| C 1s | 87.1 | 284.9 eV (2.8, 84.0%), 288.3 eV (3.1, 16.0%) |
| N 1s | 1.6 | 399.1 eV (3.6, 100%) |
| O 1s | 11.4 | 532.7 (2.8, 51.6%), 530.9 eV (2.7, 48.4%) |
| **Fraction 2** | | |
| **Orbitals** | **Atom %** | **BE peaks (fwhm, % integrated peak area)** |
| C 1s | 78.5 | 284.9 eV (2.9, 88.9%), 288.3 eV (3.1, 11.1%) |
| N 1s | 1.0 | 399.1 eV (3.3, 100%) |
| O 1s | 20.5 | 532.7 eV (2.5, 72.1%), 530.9 eV (2.2, 27.9%) |
| **Fraction 3** | | |
| **Orbitals** | **Atom %** | **BE peaks (fwhm, % integrated peak area)** |
| C 1s | 66.1 | 284.9 eV (2.8, 92.2%), 288.3 (2.9, 7.8%) |
| N 1s | 0.7 | 399.1 eV (4.1, 100%) |
| O 1s | 33.2 | 532.7 eV (2.5, 87.5%), 530.9 eV (2.0, 12.5%) |

### 3.1.5 AFM/TEM

AFM and TEM are two common techniques to characterize the size of CDs. It is necessary to use them in conjunction with each other as TEM supplies excellent XY-plane information as shown in Figure 3.8a while AFM is only able to provide the height of CDs along the z-axis as shown in Figure 3.8b. Therefore, the combination of both techniques can provide overall 3D information and enable to show us that CDs are spherical. In my group, AFM images of CDs are obtained on an Agilent 5420 atomic force microscope. To take AFM measurement, one drop of CDs aqueous dispersion has to be diluted 1000 times and dropped on a clean silica mica slide, which then will be transferred to do the screening using tapping mode. TEM images are acquired using a JEOL 1200X TEM with a drop of CDs aqueous dispersion placed on a carbon-coated copper grid and air dried. The morphological features of CDs have minor variations based on different preparation methods and the CDs prepared in my work vary in size between 2-6 nm with narrow distribution.[19, 35, 62] In addition, high-resolution TEM (HRTEM) can even display the graphitic crystalline core of CDs and estimate the lattice spacing (Figure 3.9).[48] Furthermore, there are often a few clusters shown in AFM and TEM images caused by the aggregation of CDs, which reminds us to keep CDs evenly distributed in water by using ultrasonic bath (42 Hz, 5 min) or digital vortex mixer (2 min) before AFM and TEM screening.

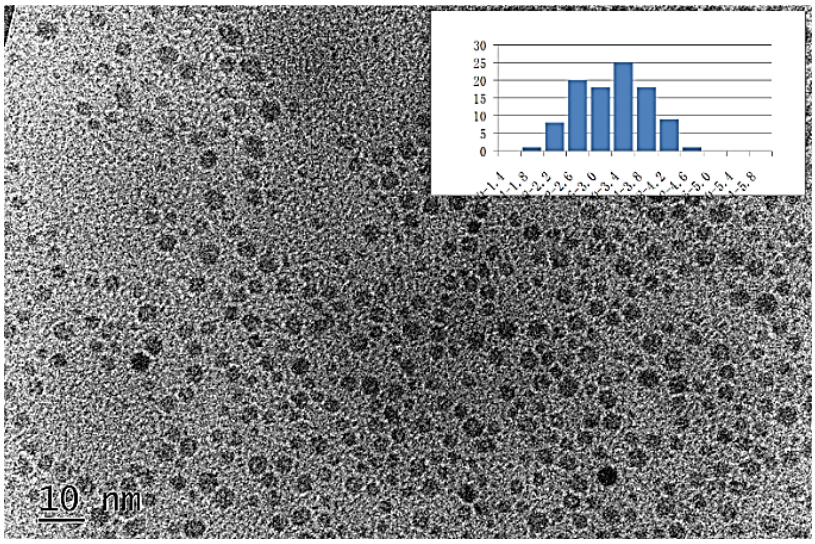


**(a)**

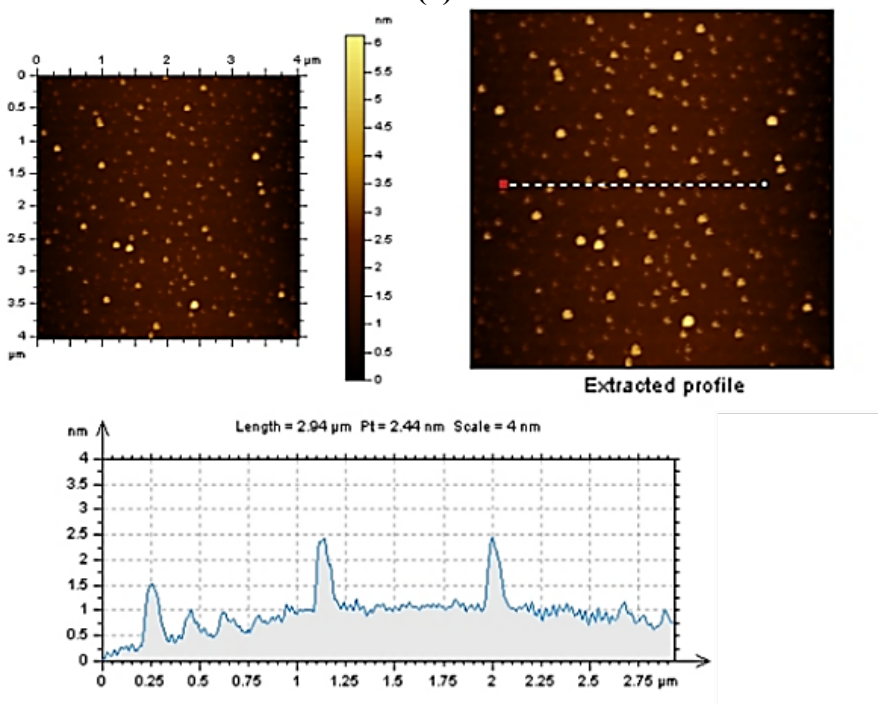


**(b)**

**Figure 3.8** Images of (a) AFM and (b) TEM of gel-like CDs.

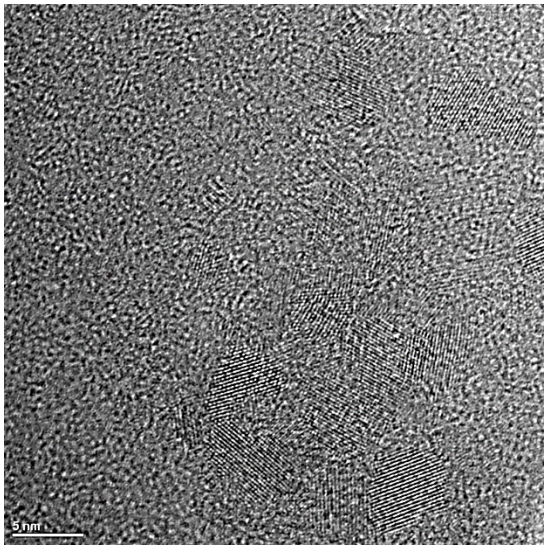


**Figure 3.9** HRTEM image of fraction 2 of gel-like CDs.

3.1.6 Zeta Potential

Even though most CDs carry negative charge due to abundant nucleophiles on the surface, the aggregation of CDs indicates the repulsive interaction between CDs is not strong, which is revealed by their zeta potential values acquired from Malvern, Zetasizer nano series. Zeta potential is related to the surface functional groups and usually used to explain the stability of a colloid from the viewpoint of the repulsive force between particles. A large absolute value (>20 mV) indicates that there will be interparticle repulsion leading to well-dispersed colloidal solutions. For example, black CDs exhibit the largest zeta potential absolute value (-38 mV) due to the large presence of carboxylic functionality, which explains the good stability of their aqueous dispersion.[20] However, when zeta potential value is closer to zero, particles in solution are much more likely to experience agglomeration. For instance, due to the presence of both amine and carboxyl functional groups, the surface of orange CDs tends to be electrically neutral and the zeta potential value is close to zero (-12.2 mV).[30] That explains why the aqueous dispersion of orange CDs is not stable and occurs agglomeration.

## 3.2 Properties

### 3.2.1 Thermal Effect

Some properties of CDs such as fluorescence QY have been found to be tuned by varying reaction temperature of CDs synthesis.[63] In my work, four different temperatures (120, 140, 160 and 180 °C) were applied to synthesize gel-like CDs with the same precursors (citric acid and EDA, molar ratio 1:14).[35] Characterizations revealed a gradual change of many properties of these gel-like CDs. For example, Figure 3.10 is a graphical illustration of the change of PL intensity under UV lamp (365 nm). With the temperature increased from 120 to 160 °C, the fluorescence QY increased up to 33%. However, due to the increasing carbonization extent, the fluorescence QY decreased when the synthesis was heated up and maintained at 180 °C. In addition, the average particle size decreased upon the increase of synthesis temperature from 120 to 180 °C, which was confirmed by both AFM and TEM measurements. And the more compact structure might result from a higher carbonization degree of gel-like CDs synthesized in higher temperatures. From XPS measurement, we observed the decrease of oxygen content as the reaction temperature increased, which revealed that increasing temperature facilitated the desorption of oxygen-containing moieties (i.e. O-H, O-C=O groups). Furthermore, due to the special gel network, the volume of gel-like CDs could be affected by environmental temperature. To be specific, gel-like CDs shrunk in cold environment (0 °C) while swelled when they were heated.

**Figure 3.10** Gel-like CDs prepared at 120, 140, 160, and 180 °C (respectively, from left-to-right) in the white light (above) and under UV light (365 nm) (below).

3.2.2 Solvent Effect

Another interesting effect observed in some CDs is solvent effect, which means CDs in different solvents will exhibit different PL behaviors including shift of the maximum emission peak and the alteration of excitation-dependent or -independent emission. For example, when orange CDs were dispersed in different common solvents including water, methanol, acetone and tetrahydrofuran (THF), there was a blue shift in the PL color with the decrease of polarity index of solvents (Figure 3.11).[30] Furthermore, the PL color was explained by the fluorescence spectra shown in Figure 3.12. With orange CDs dispersed in water (a), methanol (b), acetone (c) and THF (d), the maximum emission wavelength occurs a blue shift from 570, 539, 512 to 507 nm, respectively. Additionally, the PL intensity and fluorescence QY increased with the polarity index decreasing, which might be due to higher dispersity of orange CDs in organic solvents considering the abundant

hydrophobic functional groups on the surface such as C=C and C=N.[30] Based on the unique solvent effect, orange CDs can be considered as one of the few reported amphiphilic CDs species.[64]

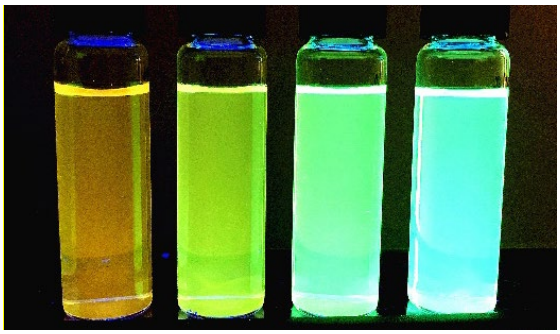

**Figure 3.11** Orange CDs aqueous dispersion under the irradiation of UV light (365 nm). From left to right, orange CDs were dispersed in water, methanol, acetone and THF.

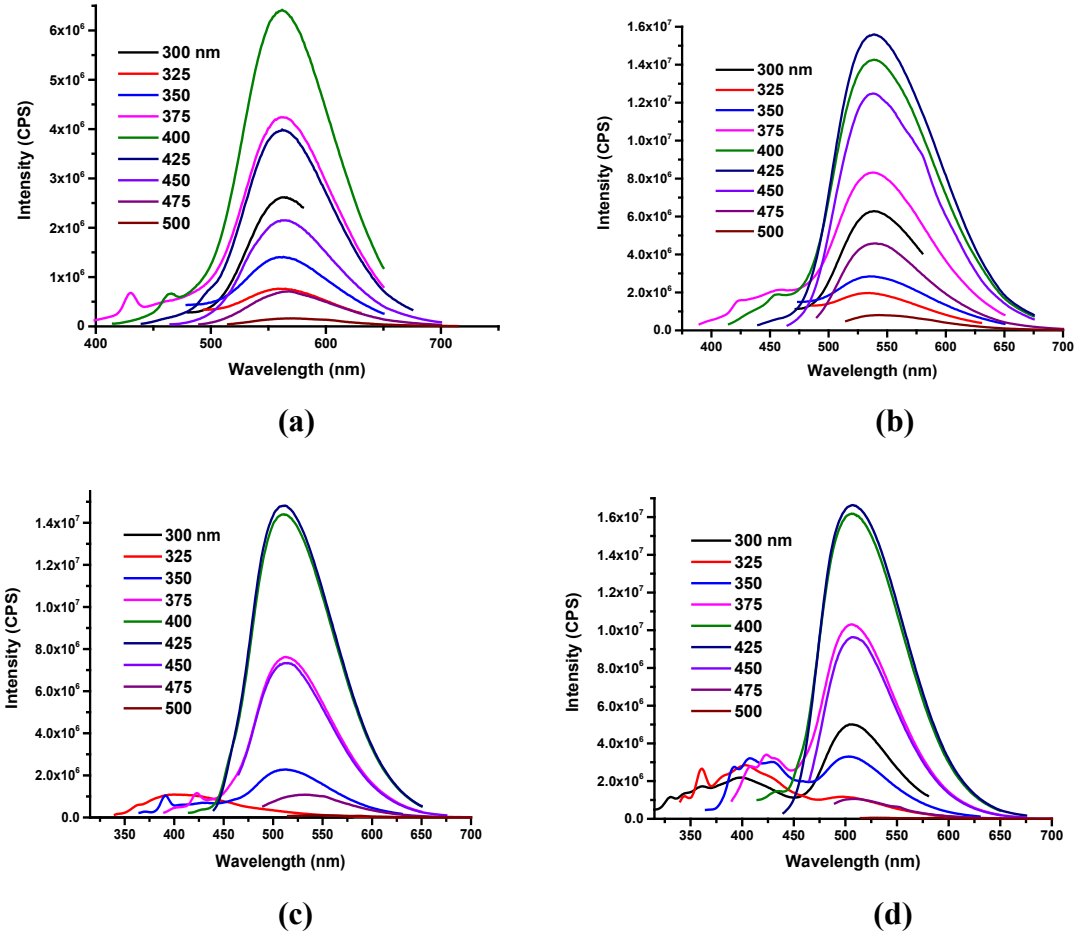


**Figure 3.12** The fluorescence emission spectra of orange CDs dispersed in (a) water, (b) methanol, (c) acetone and (d) THF (0.15 mg/mL).

### 3.2.3 Gel Behavior and Tyndall Effect

Tyndall effect is a well-known characteristic of colloid. It is the scattering of light as a light beam passes through a colloid. The individual dispersion particles scatter and reflect light, which makes the beam visible. The amount of scattering depends on the frequency of the light and density of the dispersion particles. In addition, a colloid contains disperse phase (the suspended particles) and continuous phase (the medium of dispersion). According to different dispersed phases and dispersion media, colloids can be specifically categorized. For example, when the dispersed phase is liquid while the dispersion medium is solid, the colloid is a gel. On the contrary, when the dispersed phase is solid while the dispersion medium is liquid, the colloid is a sol. Therefore, when gel-like CDs were prepared and observed to behave like a viscous gel or sol, considering that CDs particles are solid while there might be remnant EDA as the dispersed medium, gel-like CDs were presumed to be a sol. However, the disperse and continuous phases are not fixed. For example, after purification with acetone wash, gel-like CDs lost 20% EDA and CDs might become the continuous phase in reverse. It was confirmed by the immobility upon inversion of the vial containing gel-like CDs that gel-like CDs behaved more like a gel after purification (Figure 3.13a). Furthermore, a clear red beam was observed with a narrowband red laser applied to irradiate gel-like CDs from one side (Figure 3.13b), which exhibited the Tyndall effect. Even though there were previously some reports that CDs aqueous dispersion displayed the Tyndall effect,[65] it is the first time to observe the Tyndall effect in the pure CDs owing to the special gel network.

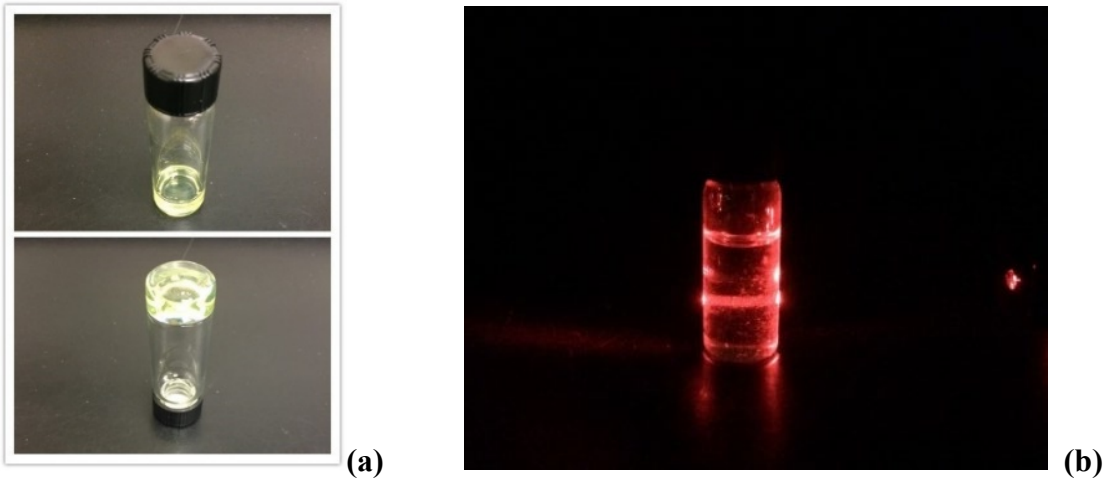

**(a)** **(b)**

**Figure 3.13** (a) Gel-like CDs upright (upper-left photo) and inverted (lower-left photo); (b) The Tyndall effect of gel-like CDs.

3.2.4 pH Effect, Salt Effect and Photoluminescence Quenching

The effect of pH was observed in gel-like CDs. pH test demonstrated that the gel network could maintain at pH 8-9. Otherwise, gel-like CDs would solidify as a result of coagulation when the pH of environment became strongly acidic (pH 1-4) or basic (pH 11).

In addition, when gel-like CDs (1 g) was mixed with NaCl (1 g) or $CaCl_2$ (0.5 g), coagulation occurred immediately. Due to the negative zeta potential of gel-like CDs, the addition of $Na^+$ or $Ca^{2+}$ might neutralize the charge on their surface to cause the aggregation of these NPs.

Inspired by the coagulation caused by the addition of salt, different cations including $Na^+$, $K^+$, $Ag^+$, $Mg^{2+}$, $Ca^{2+}$, $Cu^{2+}$, $Mn^{2+}$, $Cd^{2+}$, $Pb^{2+}$ and $Fe^{3+}$ were added in the form of chlorides or nitrates to analyze the effect of different cations on the behaviors and optical properties of gel-like CDs. The detailed process is as follows. 0.3 mg/mL of gel-like CDs stock aqueous dispersion was prepared. Then 5 mL of the gel-like CDs stock aqueous dispersion was added with 5 mL of each chloride or nitrate solution (0.01 mol/L) and thoroughly mixed. During the addition of different cations, there were several interesting

observations. Firstly, when gel-like CDs were mixed with $Ag^{+}$, $Ag^{+}$ was reduced to Ag which coated the bottom of test tube. Secondly, the color of solution containing $Cu^{2+}$ turned from blue to purple upon its addition to gel-like CDs. Thirdly, there was immediate white precipitation formed with the addition of $Pb^{2+}$. Furthermore, the fluorescence measurement in Figure 3.14 reveals a slight increase of the PL intensity of gel-like CDs aqueous dispersion upon the addition of $Ag^{+}$. Meanwhile, $Cu^{2+}$ leads to the decrease of PL by 30% and $Fe^{3+}$ quenches the PL. In comparison, all other cations have no appreciable effect on the PL of gel-like CDs.

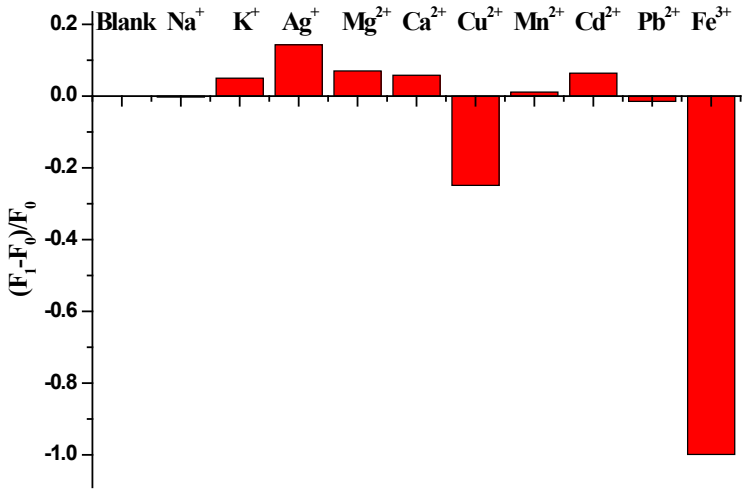


**Figure 3.14** Fluorescence measurement of gel-like CDs aqueous dispersion (0.3 mg/mL) with the addition of different cations (0.01 mol/L).

### 3.3 Summary

CDs are often characterized by UV/vis absorption, fluorescence emission, FTIR, XPS, AFM, TEM and zeta potential. UV/vis absorption and fluorescence emission spectroscopies reveal the optical properties of CDs. Among them, PL is one of the most important properties. FTIR can be used to demonstrate the chemical structure of the surface

of CDs in pair with XPS measurement. The morphology studies of CDs rely on AFM and TEM scanning, which can provide an overall 3D information of the size and shape of CDs.

Furthermore, specific CDs species have many unique excellent properties. For example, gel-like CDs own thermal effect, Tyndall effect, pH effect and salt effect. Meanwhile, orange CDs exhibits solvent effect. These special properties will allow CDs to have a wider application prospect. And PL quenching induced by cations including $Cu^{2+}$ and $Fe^{3+}$ was observed on both CDs species while the common cations such as $Na^{+}$, $K^{+}$, $Mg^{2+}$ and $Ca^{2+}$ don't affect their PL. The PL quenching induced by specific cations suggests that CDs can be fabricated as biosensors for the detection of $Cu^{2+}$ and $Fe^{3+}$.

In the past 15 years, the focus of CDs study was mostly on their optical properties. Based on their excellent optical properties, CDs have been widely applied to many areas such as drug delivery,[66] bioimaging,[21] biosensing[67] and printing.[35] **Chapter 4** and **5** will demonstrate the development of CDs in drug delivery. And **Chapter 6** will present the application of CDs in printing. However, similar to traditional QDs, CDs are semiconductors. Therefore, CDs may have excellent electrical, catalytic and magnetic properties, which is worth much more investigation in the future. Among them, photocatalytic capability of bare CDs will be discussed in the **Chapter 7: Future Work**.

## Chapter 4. Specific Bone Targeting with Carbon Dots

From **Chapter 3**, many excellent properties of CDs especially their optical properties were discovered. In this chapter, CDs are applied to a biological model, zebrafish (*Danio rerio*), to study drug delivery with CDs as specific drug nanocarrier. To be specific, black CDs were found to "light up" the bones of zebrafish. Therefore, the later study will involve the specificity of CDs species in targeting the bone, cytotoxicity of CDs and CDs drug loading ability.

### 4.1 The Specificity of Black Carbon Dots for Bone Targeting

Bone-related diseases and dysfunctions are heavy burdens on our the increasingly aged society. One important strategy to relieve this problem is through early detection and treatment of bone-related diseases. Towards this goal, there has been constant interest in developing novel bone-specific materials for imaging and drug delivery. Currently, however, materials that have high affinity and specificity towards bone are very limited. Black CDs were observed to bind to calcified bones of zebrafish *in vivo* with high affinity and specificity.[20] In this chapter we show that bone binding is highly specific to black CDs and this binding is non-toxic. Significantly, CDs derived from other precursors did not show any bone binding properties. These differences are attributed to the differences in surface chemistry of CDs preparations, highlighting the heterogeneous nature of different CDs species. Importantly, bone-binding by black CDs is not significantly altered by chemical functionalization of their surface. These unique properties indicate the potential applications of black CDs as highly bone-specific bioimaging agents and drug nanocarriers.

When black CDs were injected into the yolk sac of zebrafish, although they don't have high fluorescence QY, we found the bones of zebrafish larvae were specifically lighted

up.[68] The use of zebrafish as the model brings two major advantages. Firstly, zebrafish larvae have developing bones, which are easy to be targeted. Secondly, zebrafish larvae are transparent, which will be convenient for observation. In order to examine the specificity of black CDs in targeting the bone, gel-like CDs and another CDs species prepared from glycerin were used as comparison.[20] As a result shown in Figure 4.1, only black CDs can target the bones of zebrafish, which illustrates the specificity of black CDs.

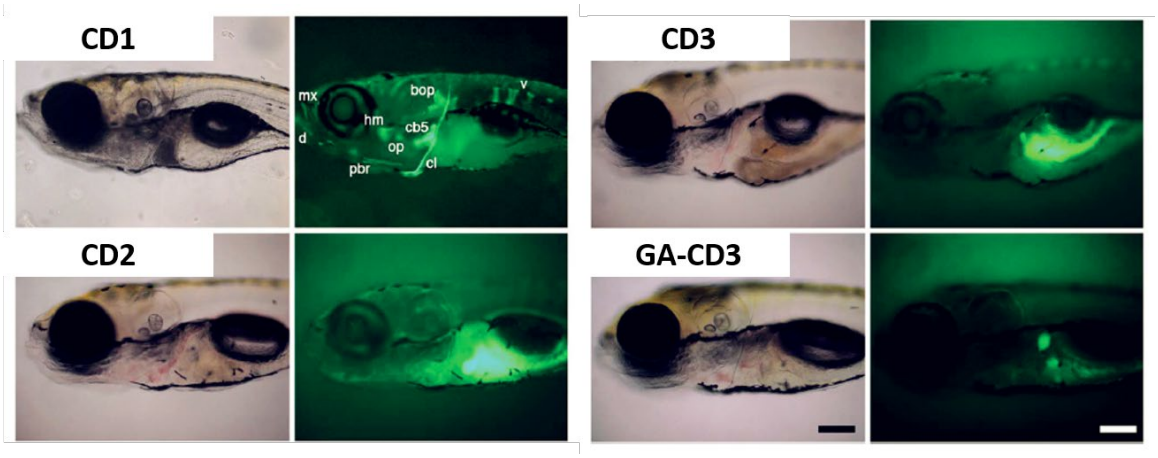


**Figure 4.1** Transmitted and fluorescence images of 8-day old larvae injected at 6-day post fertilization with black CDs (CD1), citric acid (CD2), glycerin (CD3), and glutamic acid (GA) conjugated glycerin derived CDs (GA-CD3). In the image of CD1, bones are dentary (d), maxilla (mx), posterior branchiostegal ray (pbr), hyomandibula (hm), opercle (op), ceratobranchial 5 (cb5), clei- thrum (cl), basioccipital articulatory process (bop), and vertebrae (v). Images of CD2 and CD3 were overexposed to demonstrate that CD2 and CD3 do not bind to bones; the autofluorescence seen in the gut tissues is a result of image over exposure. In the image of GA-CD3, the two stained structures correspond to primitive kidneys (pronephros). Scale bar is 100 microns.

### 4.2 Mechanistic Studies of the Interaction between Carbon Dots and Bone

The mechanism of the increasing PL in the bones might be related to the interactions of black CDs with the bones. There were two opinions put forward. First, the PL of black CDs could be enhanced by the bone microenvironment due to the abundance of calcium in the form of hydroxyapatite (HT).[69] HT could've interacted with the black CDs by electrostatic force between $Ca^{2+}$ and negative charge carrier by black CDs. However, there was no

evidence to prove the increase of PL of CDs-HT mixture was due to their interaction since HT itself has PL and the fluorescence spectrum of the mixture was possibly the simple overlap of each individual spectrum. Furthermore, the addition of $Ca^{2+}$ to CDs solution didn't show the enhancement of PL of black CDs, which confirmed that the interaction with HT was not the reason for the increasing PL of bones. Another mechanism is relevant to cartilage. During the embryo development, cartilage mineralization plays a key role in the formation of vertebrate bones.[70] And cartilage contains large amount of chondroitin sulfate, which may trap circulating black CDs as the tissue mineralizes. Therefore, the interaction between black CDs and chondroitin sulfate sodium salt (CSSS) was analyzed with fluorescence spectroscopy. However, similarly, CSSS has fluorescence with the maximum emission peak at 493.5 nm. It is not convincing to account for the increasing PL intensity and shift of the maximum emission peak of CDs-CSSS mixture by the interaction between black CDs and CSSS. Therefore, the mechanism remains to be understood.

**4.3 Cytotoxicity Test**

To test potential cytotoxicity, we followed the survival of 6-day old larvae injected with different amounts of black CDs (3.1 ng to 25.0 ng). We did not observe any loss of viability in the larvae injected with black CDs compared to the mock control, from day 7- to day 12-post fertilization (Figure 4.2). The loss of viability was observed in all experimental and control groups from day 12- to day 17-post fertilization when the experiment was terminated (Figure 4.2). The similarities in survival curves between control and experimental larvae demonstrate that black CDs up to 25 ng are well tolerated by the organism without any detrimental effects.

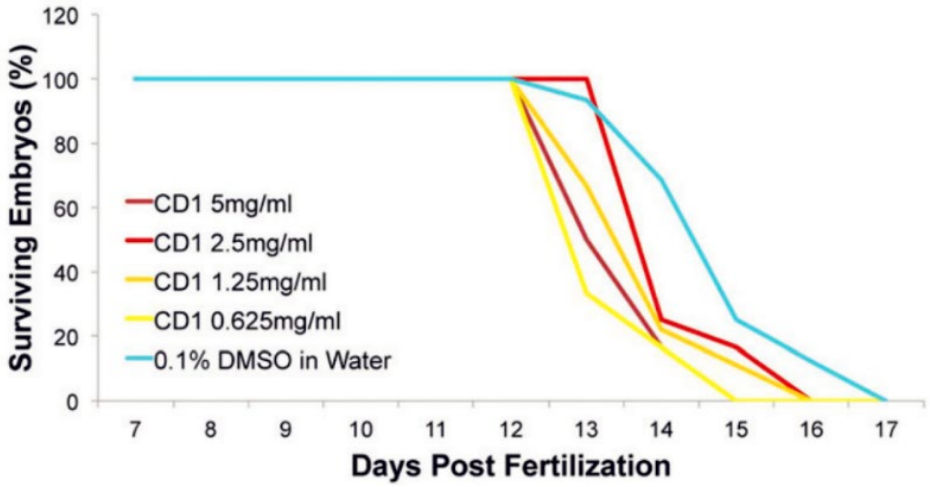


**Figure 4.2** Survival curves of larvae injected with different amounts of black CDs. Survival curves for the control (0.1% DMSO in water) and CDs injected larvae are not significantly different (n≥25 larvae per condition in at least two independent experiments).

Although only CD1 exhibited bone-binding affinity, we wanted to test the cytotoxicity of all CDs preparations. Thus, we repeated the survival assay using 25 ng of CD2, CD3 or GA-CD3. We did not observe any loss of viability in the treated larvae for the first 5 days after injection (Figure 4.3). Starting at day 12-post fertilization, and continuing until day 16, the larvae viability was lost under all conditions, including the control (Figure 4.2 and 4.3). The similarity in the survival of the control and experimental groups suggests that for the developmental stages tested, none of the CDs species are toxic.

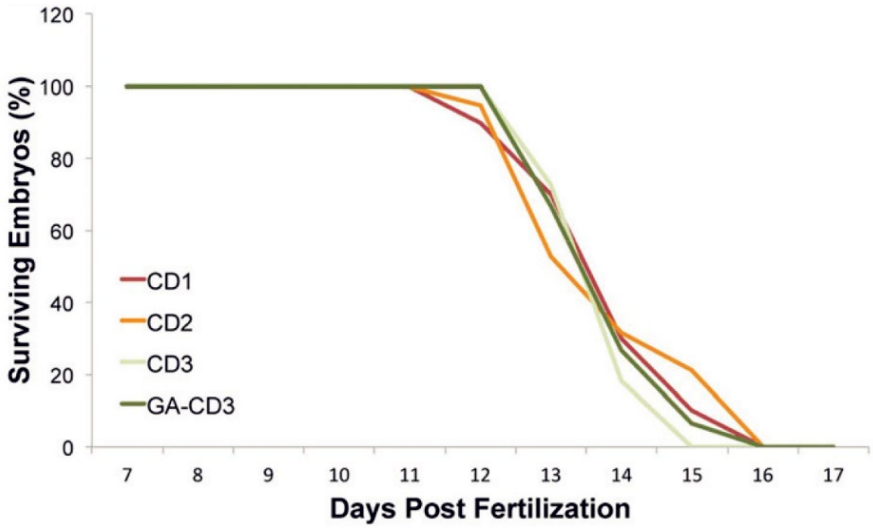


**Figure 4.3** Survival curves of larvae injected with different CDs preparations. All conditions have similar survival rates (n≥25 larvae per condition).

Finally, we tested whether surface modifications altered the cytotoxicity of black CDs, using our larvae survival assay. We analyzed the loss of viability in the 6-day old larvae after injecting 20 ng of EDA conjugated CDs (EDA-CD1), 25 ng of GA conjugated CDs (GA-CD1), or 25 ng of unmodified CD1 (control). No loss in the larvae viability was observed in the first 5 days post-injection (Figure 4.4). The loss of viability was observed under control and experimental conditions starting at day 12-post fertilization and continuing until day 16 (Figure 4.4). The similarity in the survival of the control and experimental groups suggests that the modified black CDs are nontoxic, at least for the developmental stages tested. This finding supports the potential of black CDs to be used as nanocarriers for bone-specific applications including bioimaging and drug delivery.

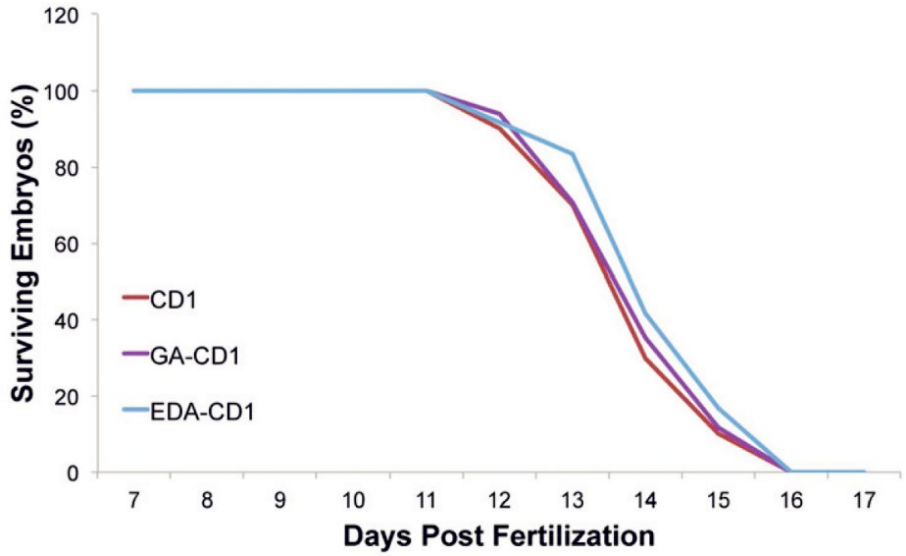


**Figure 4.4** Survival curves of larvae injected with CD1, EDA-CD1, and GA-CD1. All conditions have similar survival rates (n≥25 larvae per condition).

### 4.4 Drug Delivery

The high binding affinity and specificity of black CDs towards bones make them promising materials for bone-specific applications. Black CDs have extensive carboxyl moieties at their surface,[71] which may promote bone binding but also limit the types of cargo chemicals that can be delivered to the tissue. To function as effective bioimaging agents or drug delivery platforms, one may require modification of the surfaces of black CDs to accommodate drug or bioagents. In such occasions, it is important to know whether the bone binding properties are retained after surface modifications. We modified the surface of black CDs in two ways via a conventional EDC/NHS method to increase the bone binding affinity as well as the cargo carrier capacity. To increase the bone-binding affinity we attached GA, and to expand the repertoire of molecules that can be attached to black CDs we conjugated EDA that provides amine groups.

4.4.1 1,2-Ethylenediamine and Glutamic Acid

To conjugate black CDs with EDA, 8.34 mg of 1-ethyl-3-(3-dimethyl-aminopropyl)carbodiimide hydrochloride (EDC) was added to 2.0 mL of 2.5 mg/mL black CDs aqueous dispersion in PBS buffer at pH 7.4. After 20 min, 2.6 mg of EDA were added to the mixture, which was stirred at room temperature for 3 h. The product of the reaction was subjected to a SEC column (Sephacryl S-300) for purification. The sample was lyophilized to obtain solid EDA-modified black CDs (EDA-CD1), and then characterized by standard methods.

To conjugate black CDs with GA, 8.34 mg of EDC was added to 2.0 mL of 2.5 mg/mL black CDs aqueous dispersion in PBS buffer at pH 7.4. After 20 min, 10.66 mg of GA were added, and the mixture was stirred at room temperature overnight. The resulting solution was then dialyzed with a semi-permeable membrane dialysis bag (MWCO 3500) against pure water for 2 days to remove the unreacted GA. The conjugates (GA-CD1) were obtained after the removal of water by lyophilization, and then characterized by standard methods.

In Figure 4.5, we observed that compared to the control, neither modification significantly changed the black CDs deposition in calcified bones: the abdominal injection of 20 ng of EDA-CD1 or 25 ng of GA-CD1 in the 6-day old larvae resulted in strong and highly specific bone fluorescence 2 days after injection. Under all conditions, the number of vertebrae labeled by black CDs was the same, although in some cases the vertebrae appeared thinner. We attributed these differences to the natural variation between individual larvae in our population,[72] as all types of individuals were observed under all

conditions tested. Together, these results suggest that carboxyl or amine group surface modifications do not affect the black CDs binding affinity and specificity for bones.

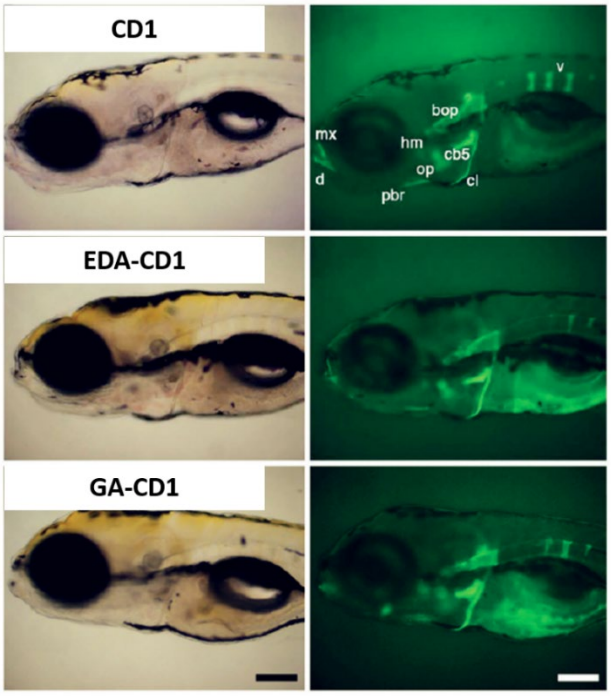


**Figure 4.5** Transmitted and fluorescence images of 8-day old larvae injected at 6-day post fertilization with CD1, EDA-CD1 or GA-CD1. The names of bones are only indicated in the CD1 image, as described in Figure 4.1, but are present under all conditions. Scale bar is 100 microns.

4.4.2 Biotin

Biotin is a water-soluble B vitamin. It is involved in a wide range of metabolic processes, both in humans and in other organisms, primarily related to the utilization of fats, carbohydrates, and amino acids. And it plays an important role in the development of bones and can benefit the heal of fractured bones.

Considering the chemical structure of biotin, its conjugation with black CDs was supposed to be easy. To conjugate black CDs with GA, 11.1 mg of EDC was added to 2.0 mL of 2.5 mg/mL black CDs aqueous dispersion in PBS buffer at pH 7.4. After 30 min, 2.4 mg of biotin were added, and the mixture was stirred at room temperature overnight.

The conjugation was later purified by SEC and confirmed by characterizations using UV/vis absorption, fluorescence emission and FTIR spectroscopies. UV/vis absorption spectra in Figure 4.6a indicate CDs-biotin conjugate has only one peak, which is located between 263 and 287 nm. The peak position is different from either black CDs or biotin alone. The fluorescence emission spectrum of CDs-biotin conjugate in Figure 4.6b and its normalized spectrum in Figure 4.6c show an excitation-dependent PL. And the maximum excitation and emission are 350 and 500 nm, respectively, which coincides with the maximum excitation wavelength of biotin and the maximum emission wavelength of black CDs. Thus, the conjugate inherits the optical properties from both black CDs and biotin, which can be considered as a proof for their conjugation. As mentioned in **Chapter 3**, FTIR measurement can provide the most straightforward evidence for the conjugation. In Figure 4.6d, the co-existence of the -OH peak (3339 $cm^{-1}$) of black CDs and C-H peak (2924 $cm^{-1}$) of biotin on the CDs-biotin conjugate confirms the successful conjugation.

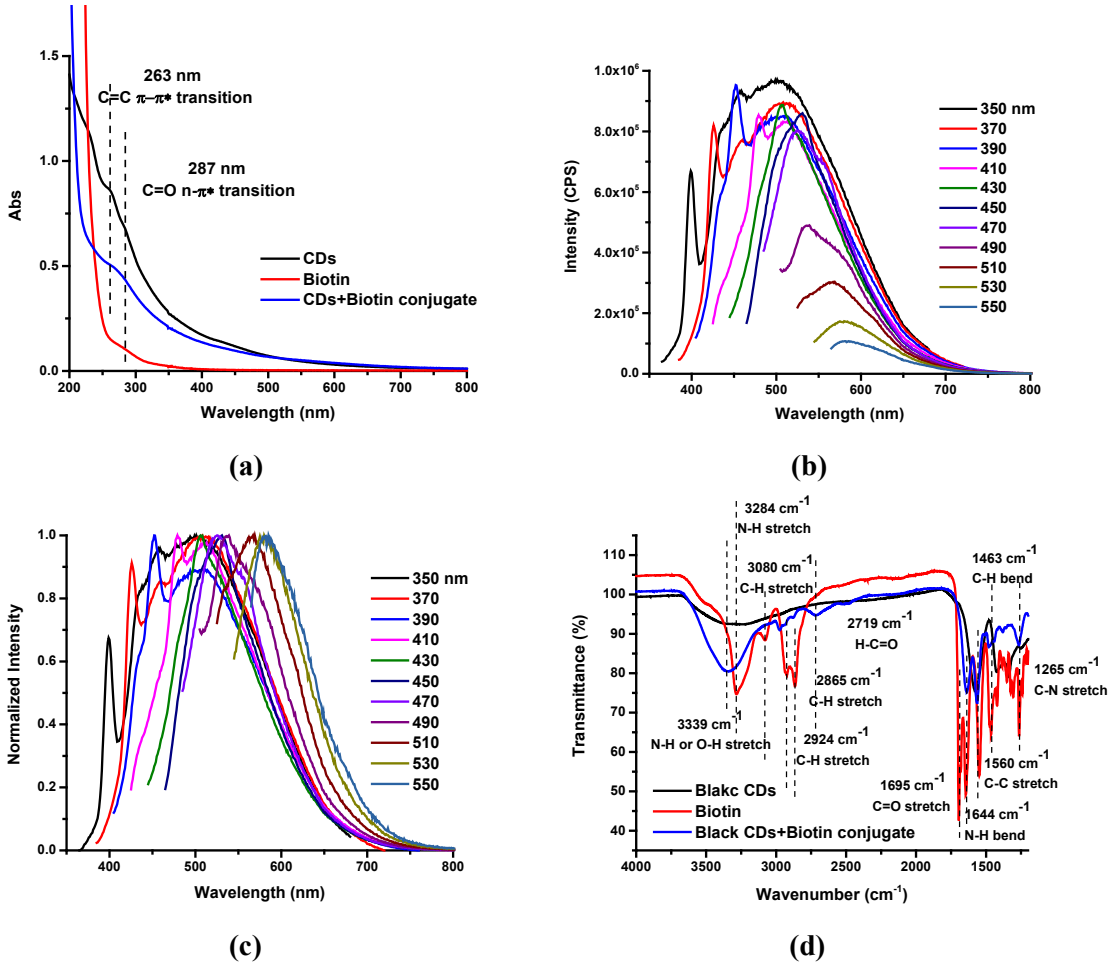


**Figure 4.6** Characterizations of CDs-biotin conjugate. (a) UV/vis absorption spectra of black CDs (0.02 mg/mL), biotin (0.2 mg/mL), and their conjugate (0.2 mg/mL); (b) Fluorescence emission spectrum of the CDs-biotin conjugate (0.1 mg/mL); (c) Normalized fluorescence spectrum of the conjugate; (d) FTIR spectra of black CDs, biotin, and their conjugate with air background.

### 4.4.3 Retinoic Acid

Retinoic acid is recognized as a key regulator of bone mineralization.[73] Either excessive or insufficient retinoic acid alters bone mineral density and compromises bone health, leading to serious diseases, such as osteoporosis. Recent evidence demonstrates that retinoic acid is critical in balancing the production of unmineralized osteoid bone matrix versus mineralized bone matrix,[73] making it a potential target for treatment of bone mineralization diseases. However, a significant barrier in developing retinoic acid-based therapies is that

retinoic acid is an important and potent physiological regulator in numerous other tissues. Any treatment using traditional methods to deliver retinoic acid drugs to bones will also disrupt homeostasis in other tissues. To overcome this important barrier, it is critical to develop novel drug delivery methods that precisely deliver retinoic acid drugs exclusively to the bones. And one novel method of drug delivery is to conjugate retinoic acid with black CDs.

Figure 4.7 shows the chemical structure of retinoic acid and the only functional group that can be used for conjugation with black CDs is carboxyl group. However, since black CDs only contain carboxylic groups, the conjugation between black CDs and retinoic acid is challenging because the anhydride formed by carboxyl groups is not stable. Therefore, we separated the conjugation process into two steps. The first step is the surface modification of black CDs by doping polyethylenimine (PEI) on black CDs via a classic EDC/NHS method to gain amine groups, which will serve as a linker to benefit their further conjugation with retinoic acid.

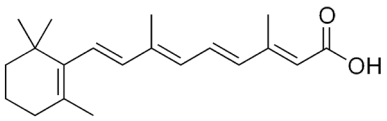


**Figure 4.7** The chemical structure of retinoic acid.

After purification by SEC, CDs-PEI conjugate was characterized by UV/vis absorption, fluorescence emission and FTIR spectroscopies. Figure 4.8a shows the UV/vis absorption spectra of black CDs, PEI and their conjugate. However, since PEI doesn't have absorption peak and the spectrum of the conjugate is similar to the one of black CDs, UV/vis spectroscopy doesn't provide enough information such as absorption peak shift caused by conjugation. Fluorescence emission spectrum and its normalized spectrum in Figure 4.8b and c, respectively, show that CDs-PEI conjugate exhibits excitation-dependent PL. And

the maximum excitation and emission wavelengths are 325 and 421 nm, respectively. This result matches the PL properties of PEI, which illustrates that the surface of black CDs is coated by PEI. However, the excitation-dependent PL is indicative of the PL behavior of black CDs. Therefore, the overall PL behavior exhibits a codominance relation of black CDs and PEI. Figure 4.8d is the FTIR spectra of black CDs, PEI and their conjugate with air background. It can be clearly observed that the CDs-PEI conjugate have all peaks from both black CDs and PEI, which confirms their conjugation.

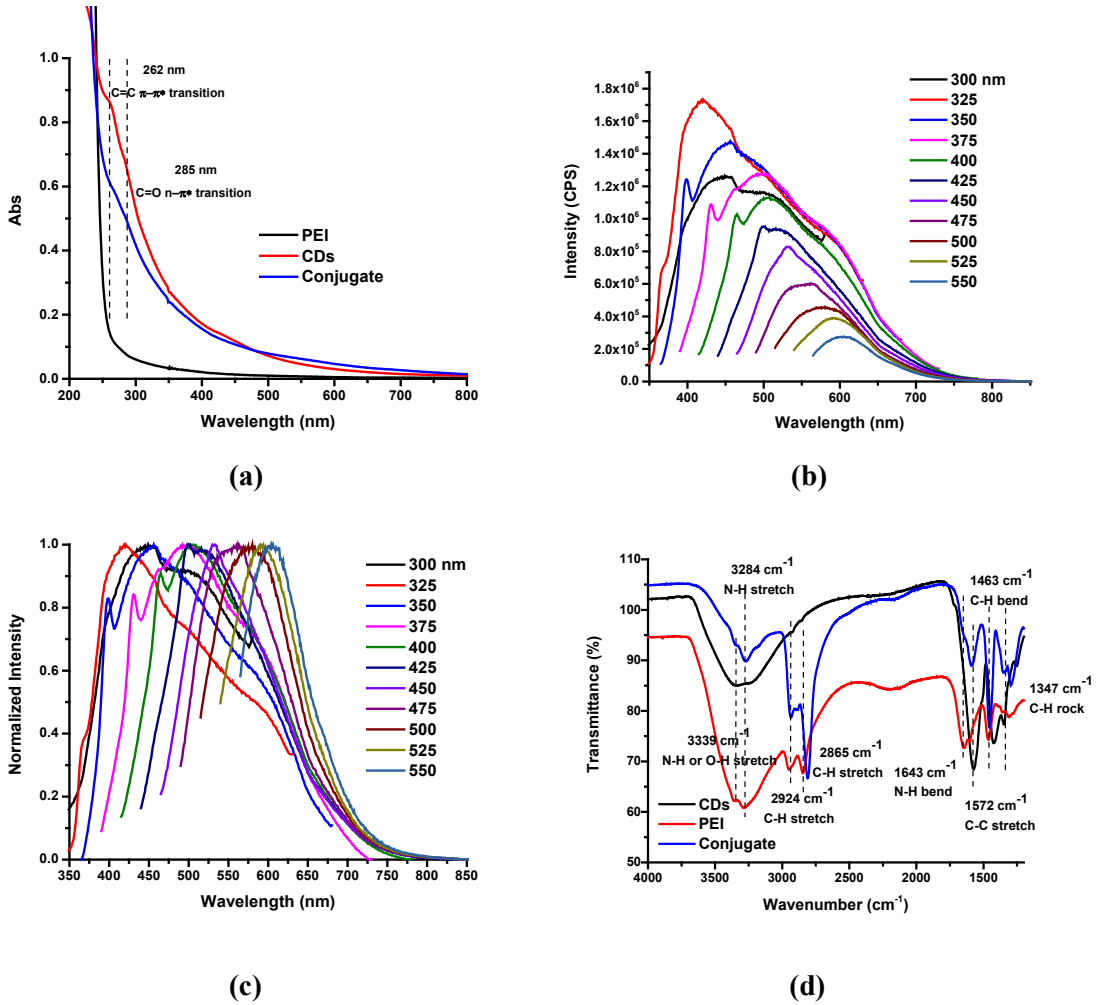


**Figure 4.8** Characterizations of black CDs modified with PEI. (a) UV/vis absorption spectra of black CDs (0.025 mg/mL), PEI (10 mg/mL), and their conjugate (0.5 mg/mL); (b) Fluorescence emission spectrum of CDs-PEI conjugate (0.5 mg/mL); (c) Normalized fluorescence spectrum of the conjugate; (d) FTIR spectra of black CDs, PEI, and CDs-PEI conjugate with air background.

After surface modification, the second step is the conjugation of CDs-PEI with retinoic acid. Since PEI can't dissolve in water but can dissolve in DMSO, PEI was dissolved in DMSO before added to CDs-PEI aqueous dispersion. The conjugation was achieved by the same EDC/NHS approach. After purification by SEC and lyophilization, the conjugate of CDs-PEI with retinoic acid was obtained in powder, which was followed by a series of common spectroscopic characterizations. The new CDs-PEI-retinoic acid shows a new peak at 338 nm in the UV/vis absorption spectra (Figure 4.9a), which indicates the presence of retinoic acid. However, since retinoic acid can't dissolve in water, the UV/vis absorption spectrum of retinoic acid is not shown in Figure 4.9a for comparison. Besides, fluorescence emission spectrum and its normalized spectrum (Figure 4.9b and c, respectively) illustrate the PL of CDs-PEI-retinoic acid conjugate is excitation-dependent. The maximum excitation and emission wavelengths are 350 and 459 nm, respectively. Considering the maximum excitation and emission wavelengths of retinoic acid,[74] the redshift of both wavelengths of CDs-PEI-retinoic acid conjugate confirms the success of conjugation between CDs-PEI with retinoic acid. Figure 4.9d is the FTIR spectra of retinoic acid, CDs-PEI and their conjugate. However, because there are only a few simple peaks in the FTIR spectrum of retinoic acid, the conjugation between retinoic acid and CDs-PEI doesn't seem as convincing as the other two spectroscopies.

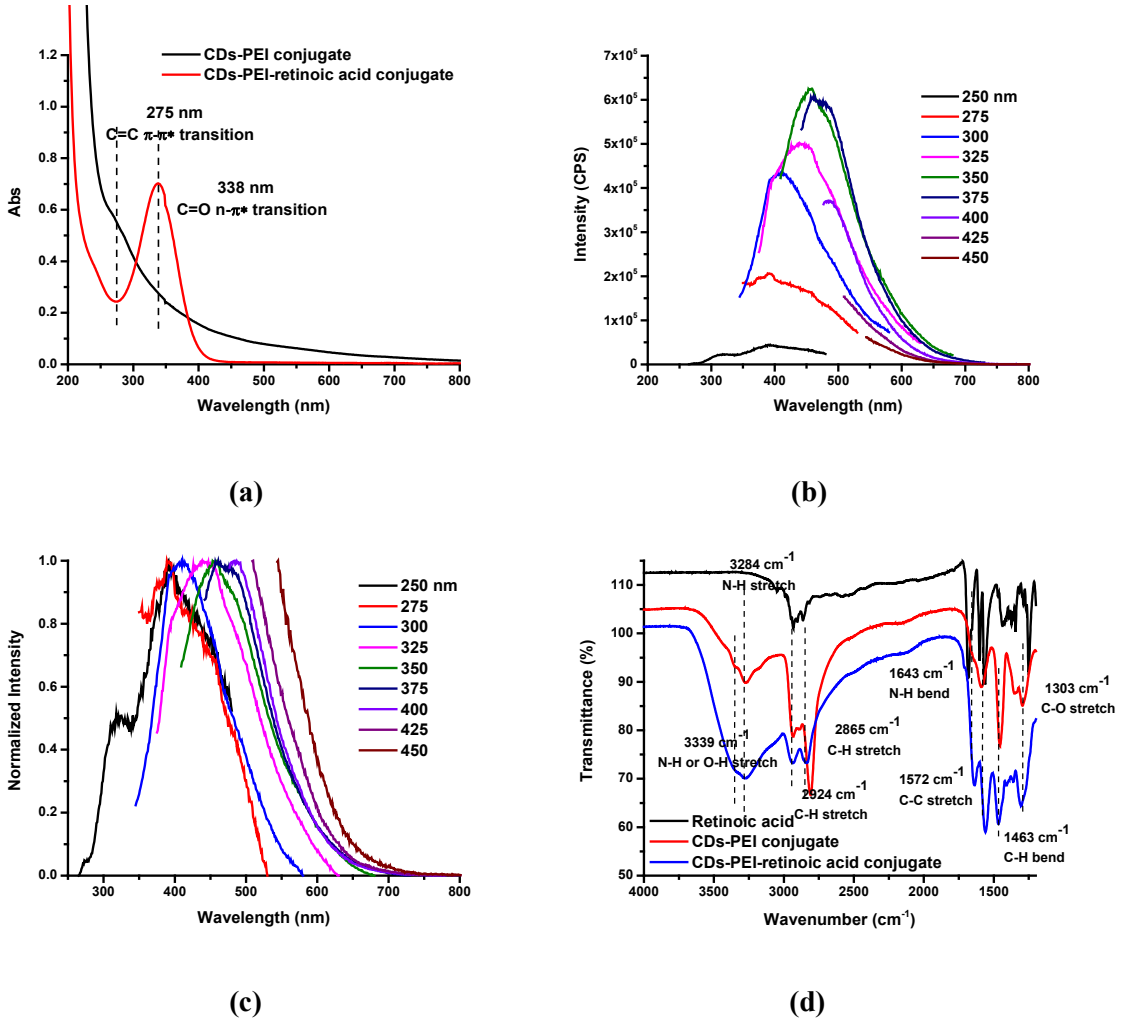


**Figure 4.9** Characterizations of CDs-PEI conjugated with retinoic acid. (a) UV/vis absorption spectra of CDs-PEI and CDs-PEI-retinoic acid conjugate; (b) Fluorescence emission spectrum of CDs-PEI-retinoic acid conjugate; (c) Normalized fluorescence spectrum of the conjugate; (d) FTIR spectra of CDs-PEI, retinoic acid, and their conjugate.

### 4.4.4 Gel-like CDs

From the conjugation of black CDs with biotin and retinoic acid, we learn that the sole presence of carboxyl group greatly limits the available drug species for conjugation by covalent bond. In order to broaden the availability of drug species, even though we can modify the drugs, it is time-consuming to modify each drug from conjugation to confirmation by performing various spectroscopic characterizations. Therefore, instead of modifying drugs, the most direct way is to modify the drug carrier, namely CDs.

Black CDs have been tried to conjugate with compounds containing abundant amine groups such as GA, biotin and PEI. Except for them, gel-like CDs have abundant amine groups on the surface. So, we tried to conjugate for the first time, black CDs and gel-like CDs. Since black CDs can specifically target bones of zebrafish while gel-like CDs have high PL and abundant amine groups, the conjugation is expected to enhance the fluorescence QY of black CDs and their drug loading ability.

After purification by SEC and lyophilization, characterizations of their conjugation were performed using UV/vis absorption (Figure 4.10a), fluorescence emission (Figure 4.10b and c), FTIR spectroscopies (Figure 4.10d), AFM (Figure 4.10e) and TEM (Figure 4.10f). In Figure 4.10a, we observe the conjugate of black and gel-like CDs has a peak at 258 nm, which is assigned to C=C conjugate structure. In addition, contributed by the black CDs, the UV absorption starts from 700 nm. Fluorescence emission spectrum and its normalized spectrum in Figure 4.10b and c, respectively, show the maximum excitation wavelength of the conjugate is 350 nm, which is attributed to gel-like CDs. However, the maximum emission wavelength occurs a slight redshift compared with that of gel-like CDs, which might be caused by the presence of black CDs. FTIR spectrum in Figure 4.10d demonstrates the addition of gel-like CDs to black CDs introduced several new peaks such as 2920~2582 $cm^{-1}$ and 1645 $cm^{-1}$. AFM and TEM images in Figure 4.10e and f, respectively illustrate the increase of the size from about 3 to 6 nm by the combination of two types of CDs. Therefore, the conjugation between black and gel-like CDs is confirmed with various characterization methodologies.

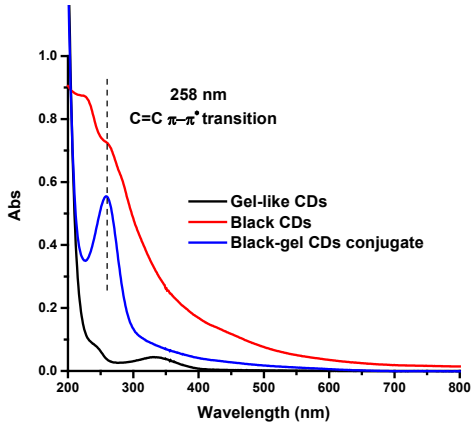
258 nm
C=C π–π* transition
Gel-like CDs
Black CDs
Black-gel CDs conjugate
Abs
Wavelength (nm)

(a)

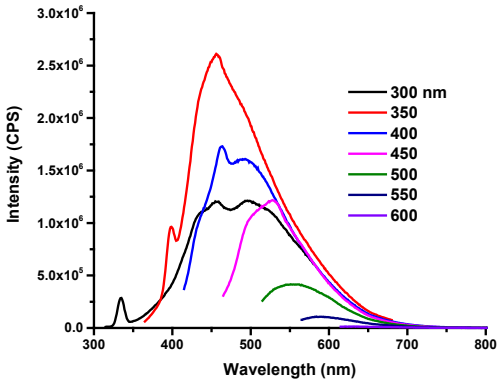
300 nm
350
400
450
500
550
600
Intensity (CPS)
Wavelength (nm)

(b)

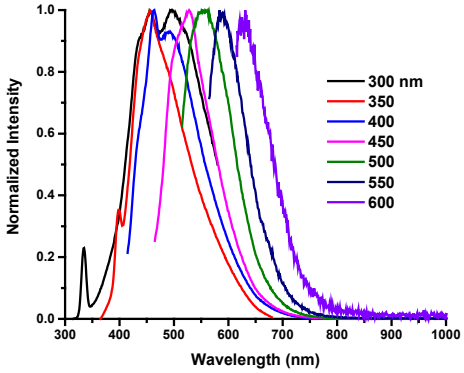
300 nm
350
400
450
500
550
600
Normalized Intensity
Wavelength (nm)

(c)

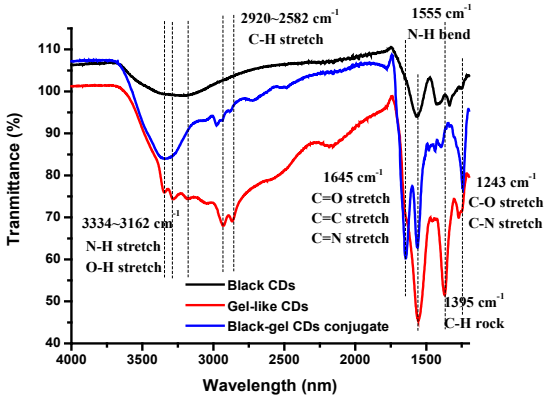
2920~2582 cm-1
C-H stretch
1555 cm-1
N-H bend
1645 cm-1
C=O stretch
C=C stretch
C=N stretch
1243 cm-1
C-O stretch
C-N stretch
3334~3162 cm-1
N-H stretch
O-H stretch
1395 cm-1
C-H rock
Black CDs
Gel-like CDs
Black-gel CDs conjugate
Tranmittance (%)
Wavelength (nm)

(d)

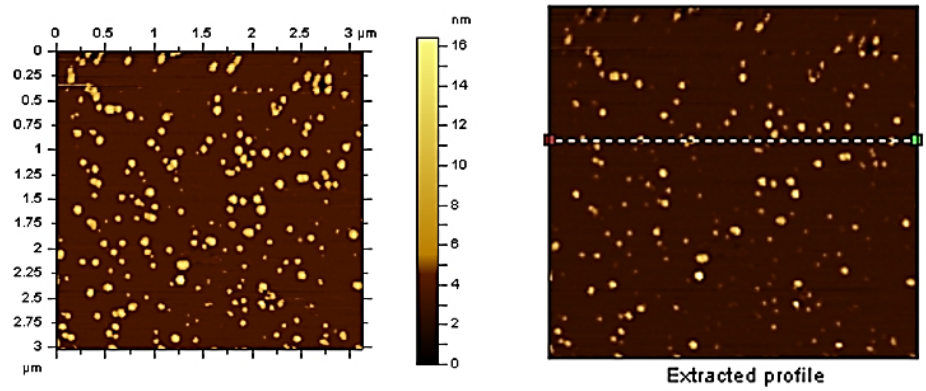
nm
Extracted profile

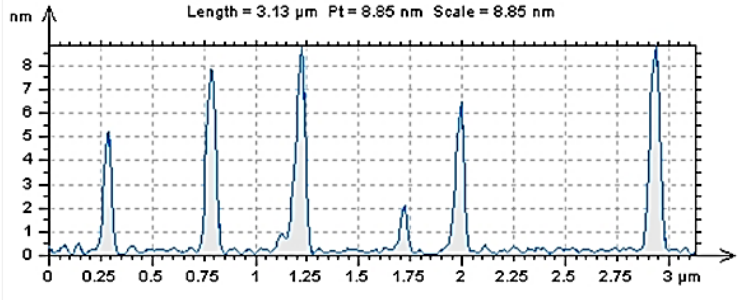
Length = 3.13 µm Pt = 8.85 nm Scale = 8.85 nm
nm

(e)

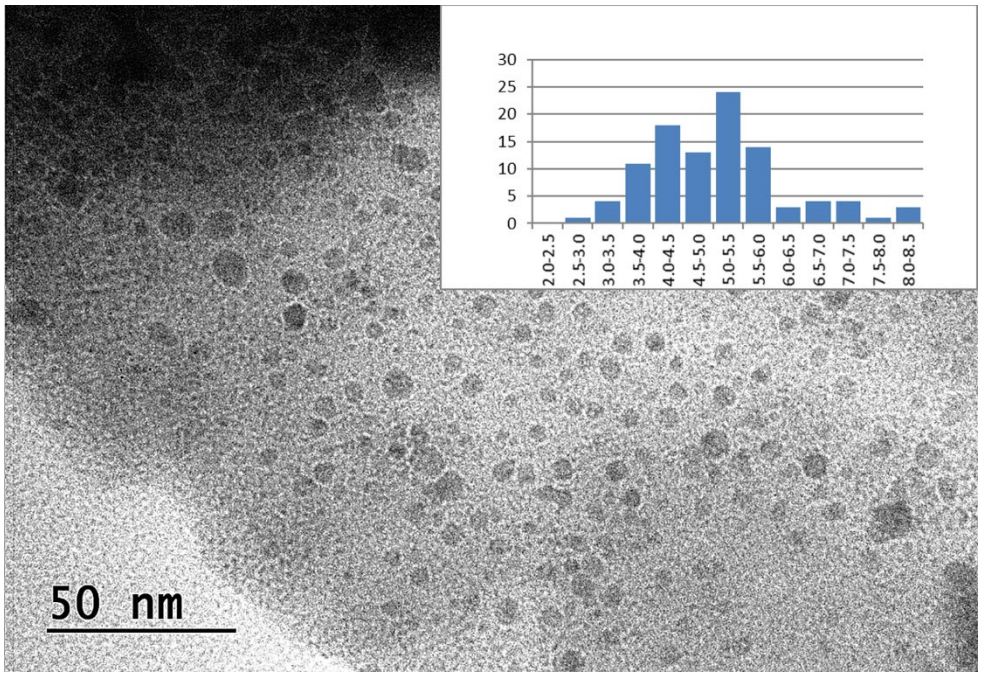


**(f)**

**Figure 4.10** Characterizations of the conjugation between black and gel-like CDs. (a) UV/vis absorption spectra of black CDs (0.03 mg/mL), gel-like CDs (0.1 mg/mL), and their conjugate (0.1 mg/mL); (b) Fluorescence emission spectrum of the conjugate (0.1 mg/mL); (c) Normalized fluorescence spectrum of the conjugate; (d) FTIR spectra of black CDs, gel-like CDs, and their conjugate; (e) AFM and (f) TEM image of their conjugate with air background.

Furthermore, 6-day post-fertilization zebrafish was injected with the black-gel-like CDs conjugate (5 mg/mL) to the yolk sac, and we observed the fluorescence of the bones of zebrafish under excitation of 405 and 458 nm using Leica confocal microscope (Figure 4.11). Since the maximum excitation wavelength of black CDs is 440 nm, the green emission obtained at 458 nm-excitation is because of black CDs. However, the blue emission acquired under 405 nm-excitation might be led by the presence of gel-like CDs because black CDs emit green light while gel-like CDs emit blue light under the excitation of 405 nm.

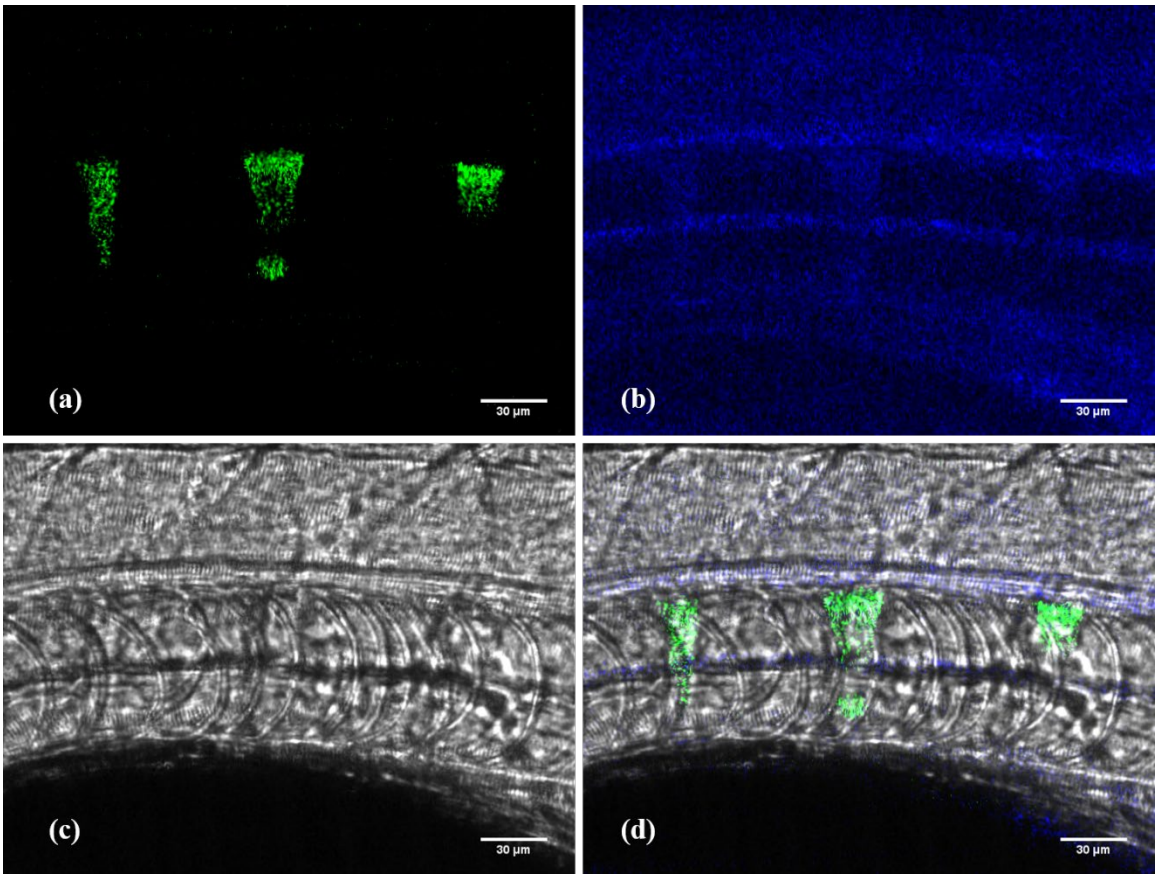


**Figure 4.11** Confocal image of 6-day post-fertilization zebrafish injected with black-gel-like CDs conjugate excited at (a) 458 nm, (b) 405 nm, (c) bright field, and (d) overlap.

### 4.5 Summary

In this chapter, the specificity of black CDs is presented in targeting the bones of zebrafish in comparison to the other two CDs preparations. Also, the mechanism is hypothesized from the interaction of black CDs with HT and CSSS. However, none of them is convincing so the mechanism remains to be understood. Meanwhile, black CDs are found nontoxic, which is confirmed by the survival rate of zebrafish injected with black CDs at different concentrations. To test whether black CDs can be used as a novel DDS, we conjugated black CDs with a series of bioagents and drugs such as EDA, GA, biotin and retinoic acid. Also, considering that the only functional group of black CDs that can be applied for conjugation is carboxyl group, surface modification was conducted by doping PEI and even

gel-like CDs. After doping gel-like CDs, the black-gel-like CDs conjugate was injected into the yolk sac of zebrafish. Under confocal microscope, we observed the fluorescence of zebrafish bones under excitation of 405 and 458 nm, which suggests the conjugate will be the next promising DDS for specific bone targeting. Compared with either black or gel-like CDs, their conjugate will have better PL behavior and enhanced drug loading ability.

Drug delivery is a promising research area by taking advantage of the excellent PL property of CDs. Black CDs have shown excellent application in the specific drug delivery to the bones of zebrafish. However, given the species number of CDs synthesized with different methods, high PL, tunable surface and their application in drug delivery, there is still a large room for the development of CDs, especially in the area where drug delivery is challenging such as drug delivery across the BBB.

## Chapter 5. Crossing the Blood-Brain Barrier with Carbon Dots

As concerned in **Chapter 4**, black CDs have been proved to be a promising drug nanocarrier for bone diseases and more studies of CDs in terms of drug delivery should be focused on the area where drug delivery is challenging such as drug delivery across the BBB. Therefore, drug delivery across the BBB using CDs as nanocarrier is the focus of this chapter. And I will explain the transport of CDs across the BBB in combination of different CDs used in my work from two different mechanisms, namely carrier-mediated endocytosis and passive diffusion.

### 5.1 Crossing the Blood-Brain Barrier with Nanoparticles

The BBB is a membrane barrier formed by the brain microvascular system which separates blood from the extracellular fluid of brain in the central nervous system (CNS) of most vertebrates that include amphibians, reptiles, birds, and mammals.[75-76] The BBB protects the brain from foreign substances in the blood that may damage the brain and keep a constant brain environment.[77] However, the actual membrane barrier was not observed until the scanning electron microscopy (SEM) was invented in 1937 and later widely introduced into the medical research field.

From the anatomic viewpoint, the BBB is composed of five constituent parts, namely the pericytes, astrocytes, neurons, basement membrane, and junctional complexes.[78-79] Among them the astrocyte endfeet, basement membrane and the tight junctions between endothelial cells are the most basic compositional elements (shown in Figure 5.1). Due to the presence of tight junctions instead of large fenestration between endothelial cells, the passage of the drugs through the BBB is primarily restricted.[80] Also, as is known there exists high electrical resistance (1500–2000 $\Omega \cdot cm^2$ ) between the endothelial cells caused

by the encapsulation of capillaries by the pericytes and astrocytes.[81] Only small molecules such as water, some gases, and some lipid-soluble compounds can penetrate through the BBB by passive transcellular diffusion. On the other hand, the transport of large molecules with high electric charge, polarity and hydrophilicity (i.e., glucose, amino acids and most drugs) has to rely on specific proteins via active transport routes.[82] Therefore, the delivery and release of drugs into the brain is a challenging topic. Nonetheless, it attracts much attention due to the increasing population of neurodegenerative diseases such as Alzheimer's,[83] Parkinson's[84] and Huntington's disease,[85] and HIV encephalitis.[86]

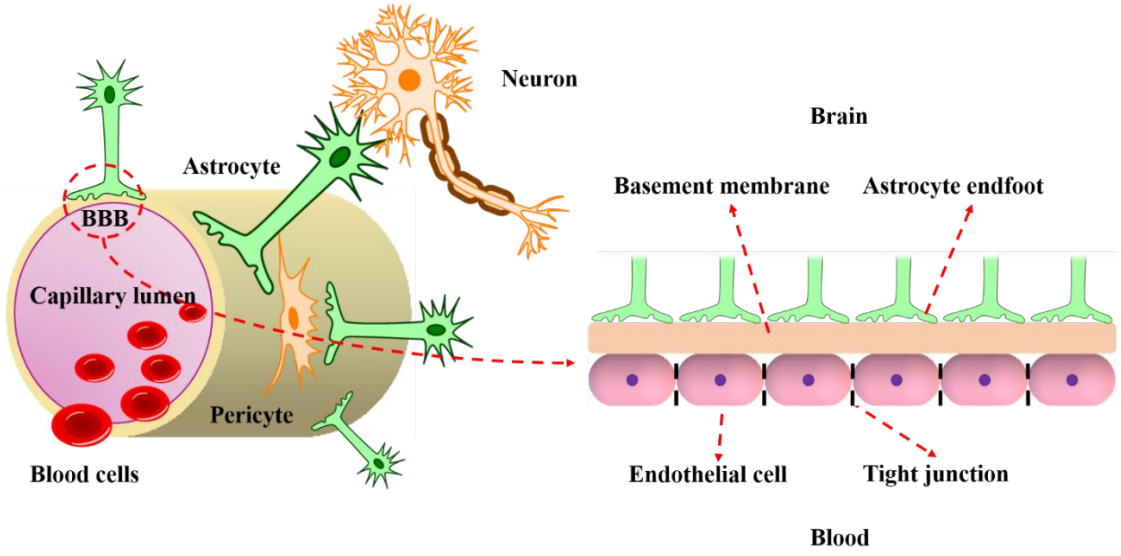


**Figure 5.1** The schematic representation of the structure of the BBB.

In order to efficiently release drugs into the brain, various strategies have been developed. They include chemical modification of drug and prodrugs, temporary disruption of the tight junctions, local delivery into the brain by neurosurgery and NP-mediated delivery.[87] However, the temporary disruption of tight junctions inducing the opening of the BBB with osmotic pressure,[88] microbubbles[89] and ultrasound[90] are risky. They will damage the integrity of the BBB and cause an uncontrolled influx of medicines and unwanted toxins

or molecules into the CNS during the opening of the tight junctions.[91] On the contrary, NPs assisted drug delivery across the BBB is a relatively mitigatory method and the supporting NPs indicate solid colloidal particles with a size range of 1–1000 nm. In terms of drug species, the first drug delivered by NPs to the brain was hexapeptide dalargin (Tyr-D-Ala-Gly-Phe-Leu-Arg).[92] To date, drugs delivered with NPs carriers have covered peptides,[93] proteins,[85] nucleic acid,[94] antibodies,[95] antiretroviral,[96] and anticancer drugs.[97] In general, drug delivery with NPs offers many advantages such as non-invasiveness, low cost, good biodegradability and long-term stability, ease of synthesis, high targeting efficiency, and high controllability to load and release drugs across the BBB.[98-99]

NPs that have been developed and applied to cross the BBB mainly include polymeric NPs such as PBCA,[95] poly(lactic-co-glycolic acid) (PLGA) and poly(lactic acid) (PLA) NPs,[100] liposomes[101] and inorganic composites such as gold, silver and zinc oxide NPs (shown in Figure 5.2).[102-104] QDs with excellent PL properties have also been utilized to cross the BBB;[105] however, drug delivery strategies to pass the BBB using QDs gradually lost their popularity in the past decade due to their potential intrinsic toxicity. In light of this, CDs have emerged as a green alternative for constructing drug delivery systems (DDS) to cross the BBB considering their polymeric core structure, high biocompatibility and relatively nontoxic nature (carbon-based material).[35, 106-107]

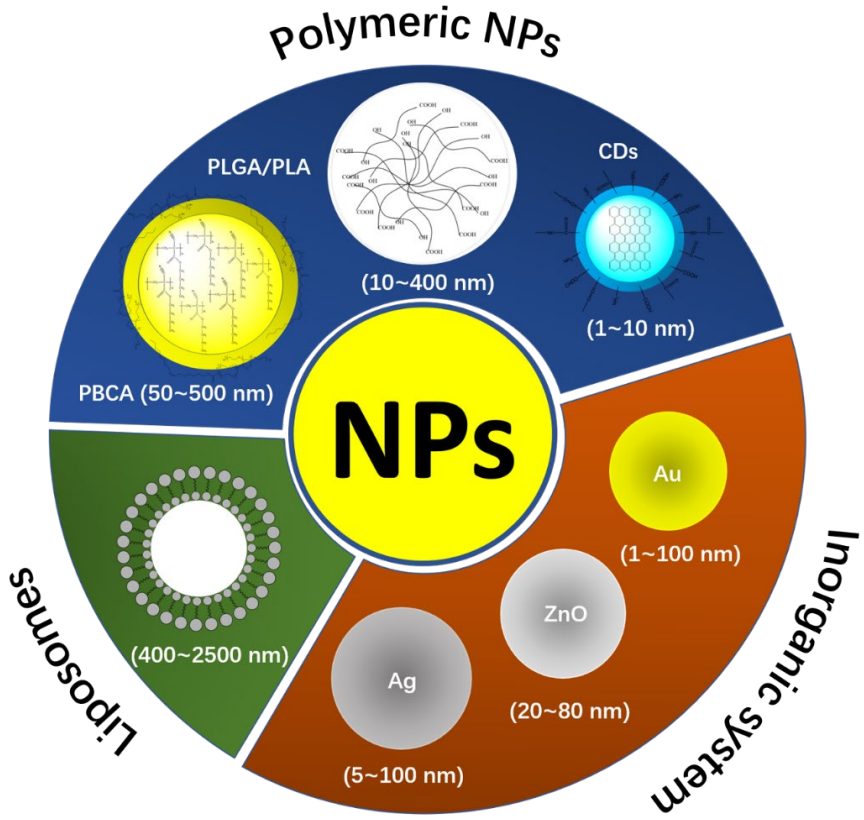


**Figure 5.2** The NPs developed in the past decade assisting drugs across the BBB.

The BBB penetration mechanism can be divided into active and passive transport routes as shown in Figure 5.3.[108] The passive transport routes indicate energy-independent processes, for instance, simple diffusion.[109] And the passive diffusion of drugs usually applies in tumor cells via the enhanced permeability and retention effect (EPR).[110] Oppositely, the active transport routes include receptor- and adsorption-mediated endocytosis and carrier-mediated transport, which all require the hydrolysis of adenosine triphosphate (ATP).[111-113] Also, the drug transported vary according to different NPs and mechanisms. For instance, the small and stereospecific pores in the carrier-mediated transport system restrict the transport of large-molecule drugs.[114] Instead, most CDs have an ultra-small size (1–10 nm) and versatile surface functionalities,[115] which would be in

favor of the delivery of large drug molecules via the carrier-mediated transport by covalently conjugating with drugs.[106]

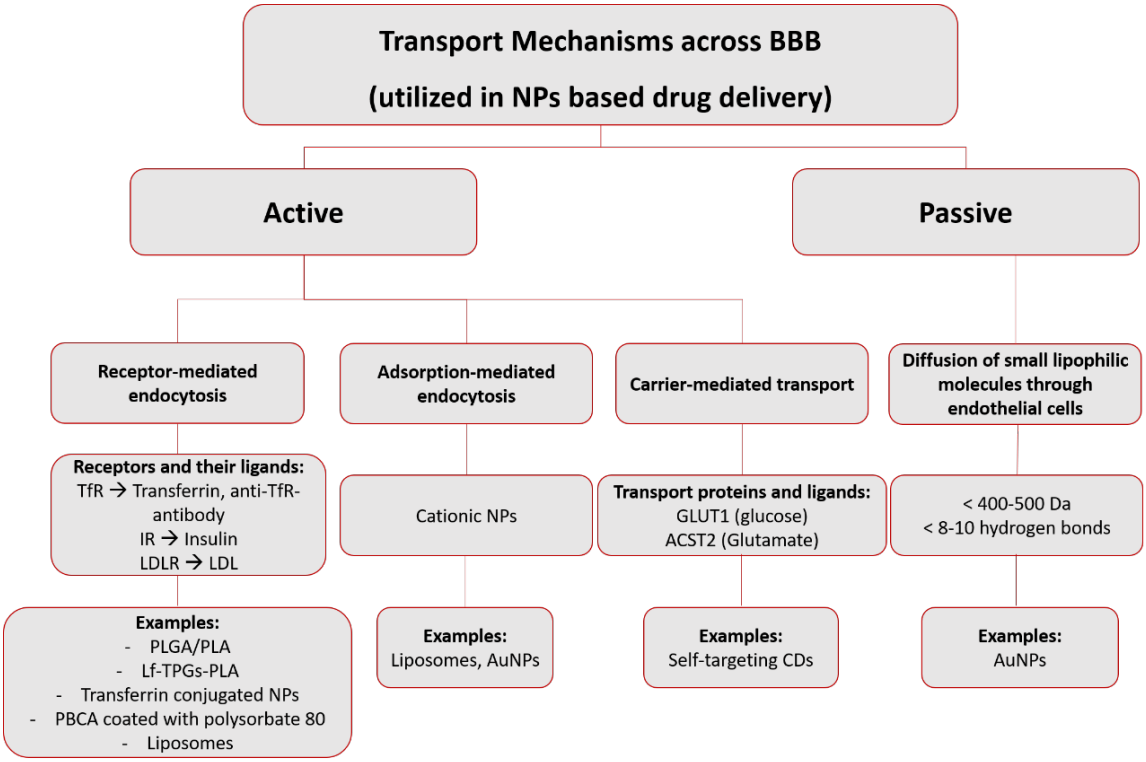


**Figure 5.3** Flowchart of the BBB penetration mechanisms of NPs (to simplify the chart, some of the mechanisms that are not used in NPs based DDS are not shown in the flowchart (example: tight junctions)). Small lipophilic molecules (<400 Da) diffuse passively through endothelial cells.[116] The penetration of charged molecules such as cationic NPs depends on adsorption-mediated endocytosis while the delivery of large molecules with high hydrophilicity such as transferrin requires active transport route (i.e., receptor-mediated endocytosis). Abbreviation: TfR, transferrin receptor; IR, insulin receptor; LDL, low-density lipoprotein; LDLR, low-density lipoprotein receptor; Lf, lactoferrin; TPGS, D-α-tocopheryl polyethylene glycol 1000 succinate.

### 5.2 Carbon Dots across the Blood-Brain Barrier via Carrier-Mediated Endocytosis

Due to the small size (1-10 nm) and abundant surface functional groups, CDs have an incomparable advantage over other NPs to serve as the drug nanocarrier either via the passive diffusion or active transport. In our group, we have explored the potential of CDs across the BBB by itself using zebrafish as the biological model. The CNS of zebrafish includes the brain and spinal cord which are connected by the cerebral spinal fluid that

circulates through ventricles of the brain that are contiguous with the central canal of the spinal cord.[21] Any fluorescent species that is able to penetrate the BBB will be easily observed in the central canal of the spinal cord. Therefore, the ability of CDs injected into the vasculature to reach the spinal cord and especially the central canal (shown in Figure 5.4) is our main assay for crossing the BBB.

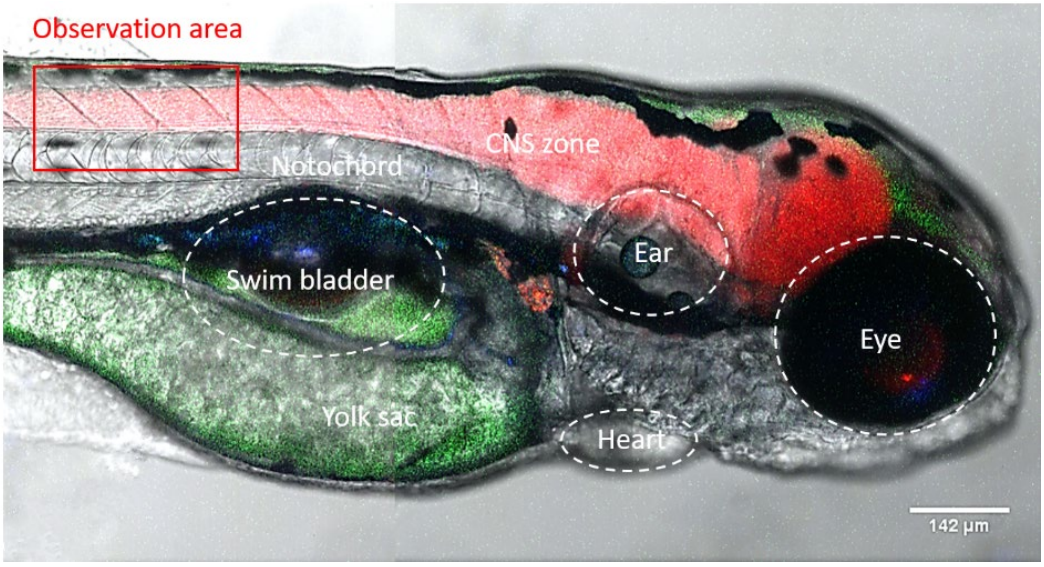


**Figure 5.4** The light micrograph of the mcherry-expressed transgenic zebrafish body at 6 days after fertilization. The red box is the major observation area to study the CDs across the BBB.

CDs prepared from tryptophan with EDA (CD-EDA) and urea (CD-Urea) were co-injected intravascularly with 10,000 MW fluorescein dextran into the heart of transgenic zebrafish expressing mcherry (tg:HuC-mCherry) in all neurons to examine the ability of CDs to cross the BBB (Figure 5.5). The 10,000 MW of fluorescein dye is too large for the molecule to cross the BBB. When the injection accurately targets the heart, fluorescein is restricted to the vasculature as can be seen in the control experiment. When CD-Urea was injected with the dye, similar images were obtained as the control experiment. These CDs cannot be observed excited at 405 nm, which was probably caused by the low fluorescence

QY (21.5 ± 3.2%) and the discrepancy between the excitation of the channel (405 nm) and the maximum excitation wavelength of these CDs (350 nm). In contrast, upon the injection of CD-EDA mixed with the dye, we can observe the blue PL of the zebrafish vasculature in the CDs channel. Also, in the location of the central canal of spinal cord, blue PL was weak but also seen, as highlighted in Figure 5.5. (Notice: for convenience of display, blue PL was replaced by white color). This injection was repeated 3 times on batches of 6 fish (18 fish total). This provides evidence of the CD-EDA penetrating the BBB to reach the CNS. The reason for CD-EDA crossing the BBB is hypothesized to be due to the greater amount of tryptophan molecules on the surface of CD-EDA as shown by UV/vis absorption spectrum and XPS data.[21] It is also easier to observe CD-EDA than CD-Urea due to the differences in fluorescence QY. Since, the LAT1 transporter is not specific for tryptophan, but recognizes several large amino acids, it is able to recognize tryptophan on the surface of CD-EDA and transports the whole system across the BBB into the CNS.

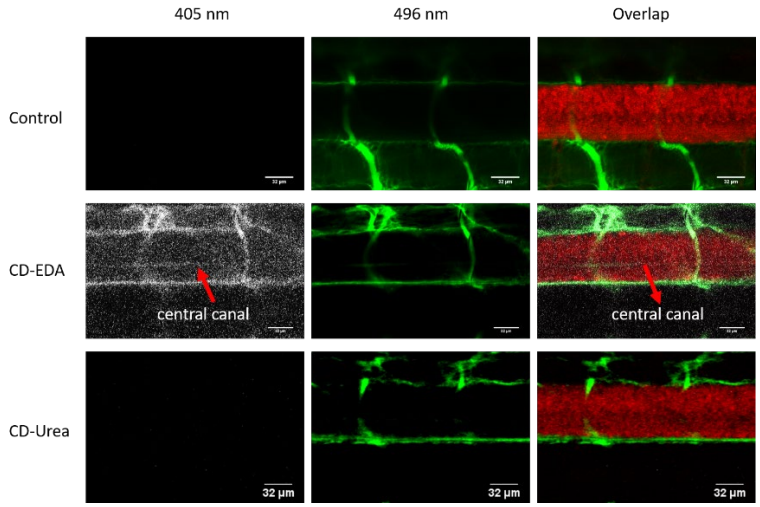


**Figure 5.5** Confocal microscopic images of a six-day-old, transgenic zebrafish larvae expressing mcherry (585 nm) in the CNS. The larvae were injected with either 10,000 MW fluorescein dextran dye (496 nm) alone (control, top row), or a combination of dye and CD-EDA (second row) or a combination of dye and CD-Urea (third row). Fluorescence from trp-CDs (405 nm) that cross the blood brain barrier can be seen in the central canal that is highlighted with the red arrows.

### 5.3 Crossing the Blood-Brain Barrier by Passive Diffusion

Since orange CDs are small in size (~2 nm), less hydrophilic and charged, they are hypothesized to be able to cross the BBB via passive diffusion. Therefore, after orange CDs (0.1 mg/mL) were injected intravascularly into the heart of wild-type zebrafish (5 day old), the zebrafish was mounted on glass bottom dish with the help of low-melting agar immediately. And the central canal of spinal cord was examined carefully with the use of confocal microscope. Considering the maximum excitation of orange CDs is 400 nm, the injected zebrafish was irradiated under the excitation of 405 nm. Then Figure 5.6 was obtained showing the yellow fluorescence exhibited by the central canal of spinal cord, which confirmed that orange CDs have the potential to cross the BBB. However, even though orange CDs have many optimal properties that enable them to cross the BBB via passive diffusion, the mechanism of orange CDs overcoming the BBB remains to be figured out.

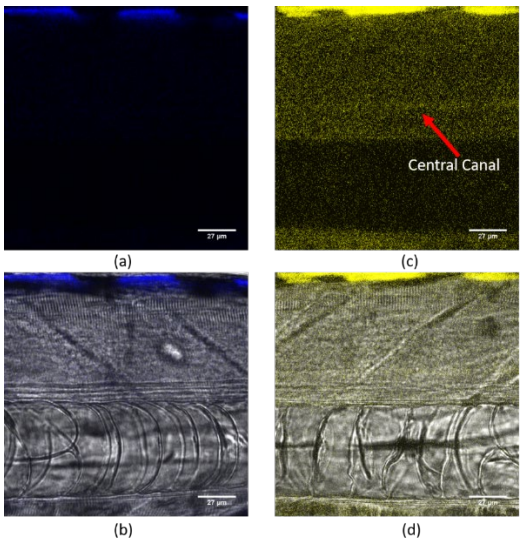


**Figure 5.6** Confocal images of orange CDs aqueous dispersion (0.1 mg/mL) across the BBB. (a) and (c) are under excitation of 405 nm; (b) and (d) are overlaping the images under both white light and excitation of 405 nm. (a) and (b) are control without injection; (c) and (d) show zebrafish injected with orange CDs aqueous dispersion and the arrow in (c) indicates the central canal of spinal cord.

Another phenomenon was observed when zebrafish was soaked in the orange CDs aqueous dispersion (1.25 mg/mL) instead of injection. After zebrafish (5 day old) was soaked in the orange CDs aqueous dispersion overnight, it was mounted on a glass-bottom plate and observed under confocal microscope that orange CDs permeated all over the body of zebrafish (Figure 5.7). And most importantly, we observed the orange CDs entered the CNS, which further confirms the hypothesized mechanism. The observation of orange CDs across the BBB by passive diffusion was significant because it eases the administration and reduces death of zebrafish cause by injection.

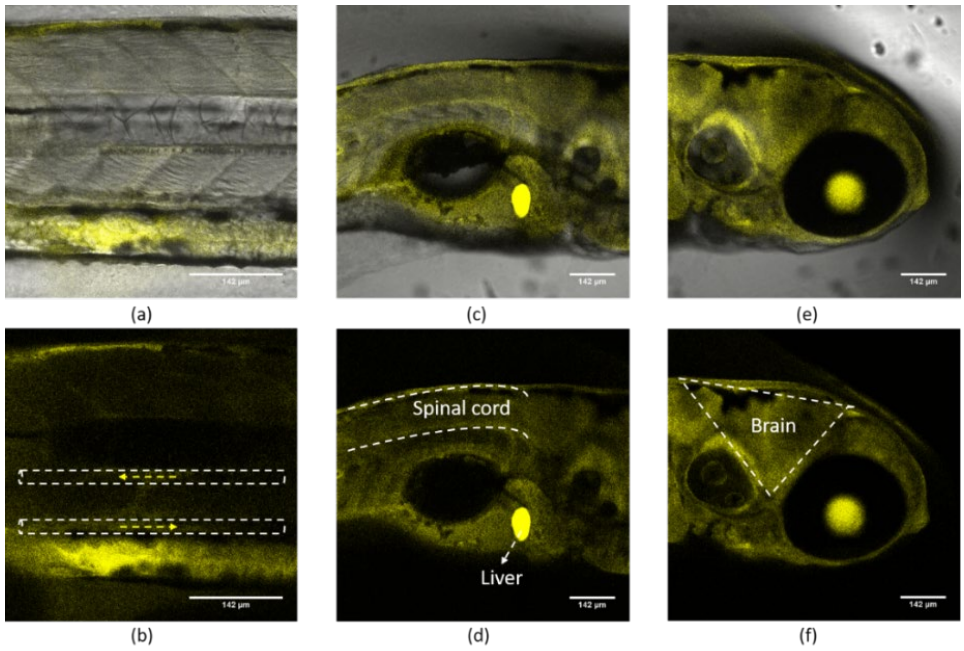


**Figure 5.7** Orange CDs permeation into blood (a, b) and CNS including spinal cord (c, d) and brain (e, f). (a, c, e are overlaped images under both white light and excitation of 405; b, d, f are images under the excitation of 405 nm).

The ability of orange CDs to be used in biological applications was tested by conducting in *in vitro* viability assays. Both normal healthy (HEK293) and cancer (SJGBM2, 4CHLA200) cell lines were used to understand the cytotoxicity of prepared orange CDs. Orange CDs were dispersed in the same culture media of the cells for the treatment. The

cells were incubated in different concentrations of orange CDs such as 1 µM, 10 µM, 100 nM for 72 hours before the cytotoxicity measurement using the MTS assay. MTS assay is a colorimetric method for sensitive quantification of living cells in proliferation and cytotoxicity assay based on the generation of a colored formazan product along with the redution of MTS tetrazolium compound by living cells. Then the cell viability was averaged after three replicates of the cytotoxicity assay and compared with the viability of non-treated cells. As shown in Figure 5.8, at all the concentrations of the orange CDs the viability of the treated cells was comparable to the non-treated cells. It is noteworthy to mention that even at a significantly high concentration as 10 µM, the cell viability was high and remained above 90% for both cancer (SJGBM2) and normal healthy (HEK293) cells. The only exception was that CHLA200 viability lowered about 15% at 10 µM but at lower concentrations this also showed high viability. These results confirm that the orange CDs are non-toxic and can be used in biological applications.

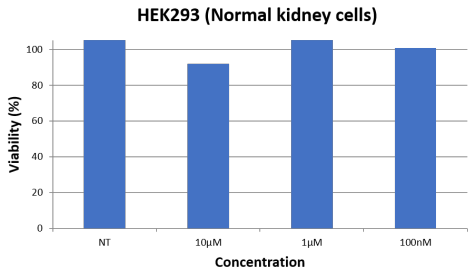


(a)

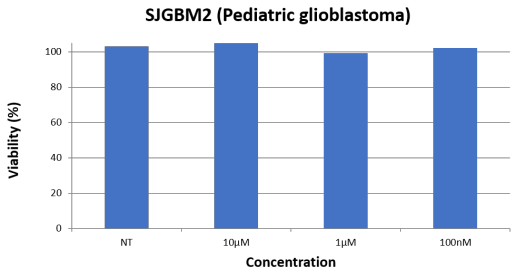


(b)

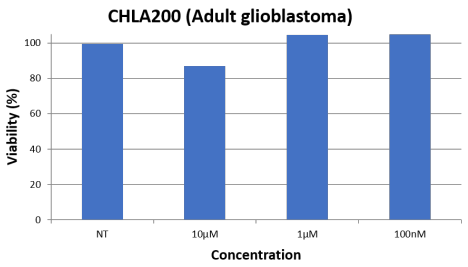


(c)

| O-CDs | | | | |
|---|---|---|---|---|
| | HEK293 | | | |
| Concentration | NT | 10µM | 1µM | 100nM |
| Viability (%) | 105.6278 | 92.0282 | 105.9724 | 100.6887 |
| | SJGBM2 | | | |
| Concentration | NT | 10µM | 1µM | 100nM |
| Viability (%) | 103.1997 | 104.9854 | 99.12354 | 102.2839 |
| | CHLA200 | | | |
| Concentration | NT | 10µM | 1µM | 100nM |
| Viability (%) | 99.29345 | 86.99829 | 104.3571 | 104.8868 |

(d)

**Figure 5.8** Cytotoxicity test of orange CDs with different cell lines: (a) normal kidney cells HEK293; (b) Pediatric glioblastoma SJGBM2; (c) adult glioblastoma CHLA200. *NT-Nontreated (without any orange CDs). (d) are the averaged data sets used above.

## 5.4 Summary

NP-mediated drug delivery can alleviate the side effect brought by the traditional physical therapies. As a new family member of NPs, CDs have been studied for their ability to cross the BBB. Some CDs species showed the capability to cross the BBB via an active transport mechanism due to their precursors such as tryptophan. Meanwhile, some CDs species was able to cross the BBB by passive diffusion because of some favorable properties. For example, orange CDs are small in size, amphiphilic and less charged, which endows them with the ability to overcome the BBB. Their cytotoxicity was studied, which demonstrated their non-toxicity. Therefore, CDs showed the potential as promising drug nanocarrier across the BBB. However, the mechanism of CDs and their drug conjugate across the BBB remains to be investigated with endothelial cells.

## Chapter 6. Printings and Cosmetics with Carbon Dots

CDs have shown great potential in drug delivery. Due to their high fluorescence QY, CDs have also been applied in other field such as printing and cosmetics. In this chapter, plenty of creative inventions using CDs will be exhibited with their detailed making process.

### 6.1 Invisible Text Printing

Since the discovery of CDs in 2004, their high PL has attracted much attention. The application of high PL can be of great help in human's daily life. For example, CDs have been applied in the text printing via plenty of techniques including handwriting, inkjet printing,[117] relief printing,[118] screen printing,[119] intaglio printing,[118] and micro-trace transferring.[118] Also, since most CDs are excitation wavelength dependent and highly photoluminescent, CDs were usually used for multicolor printing.[22] Except being used as ink, CDs could also be applied in making a thin film for presenting the effect of printing. For example, CDs could be mixed with polymers such as poly(vinyl alcohol) (PVA) to form a transparent composite film as ink-free substrates for pattern as it was reported by Chen et al.[118] However, there are also many research groups that merely mentioned the potential in the use as the ink,[120] and in most research group involved in the design of text printing using CDs, some details to print or modify the printer are either hidden or complicated.[121] Nonetheless, our group reported how we used the gel-like CDs to prepare the ink for text printing. And the printing was conducted in the real inkjet printer on a non-fluorescent paper. After printing, the text can be seen only though the UV light with a narrow wavelength of 365 nm (Figure 6.1). On the contrary, in the ambient light, the words didn't show until it is dried and oxidized after 3 years. Also, different from the most CDs,[122]

the gel-like CDs can be erased by water easily without leaving any trace and the paper can be reused, which will greatly reduce the cost in the text printing.

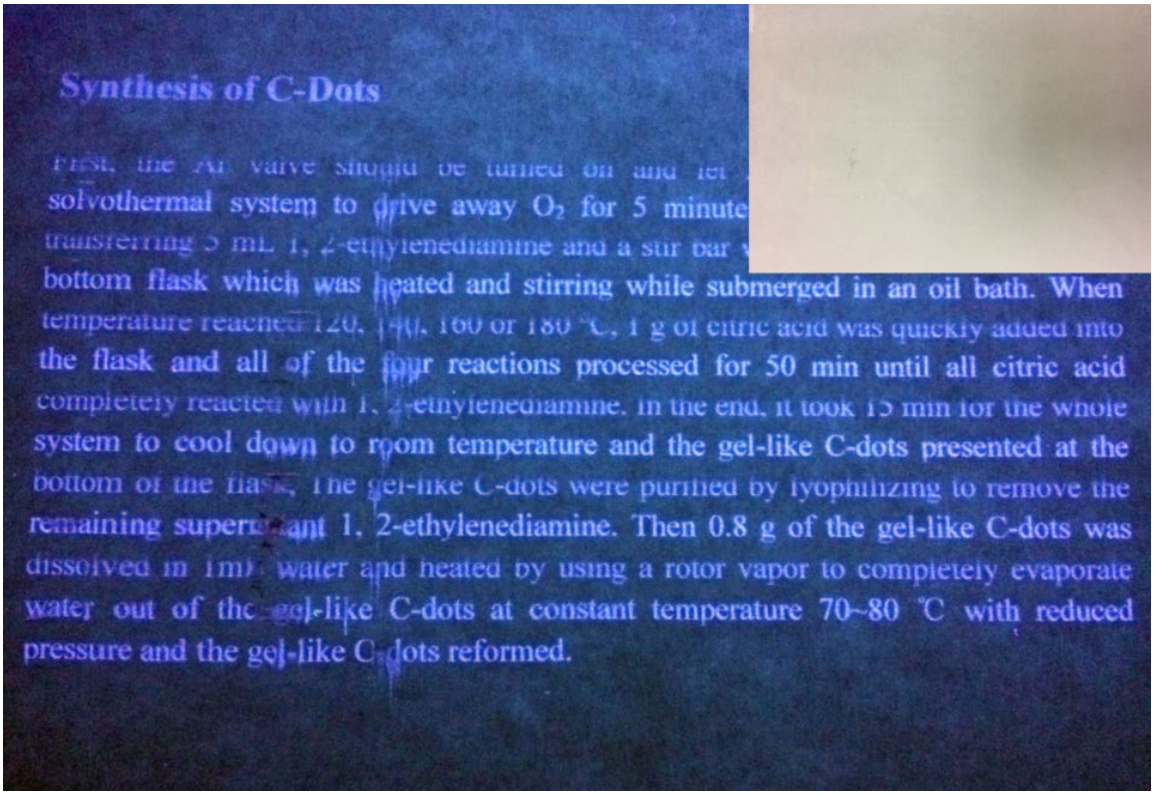


**Figure 6.1** Text printed with gel-like CDs aqueous dispersion as the photoluminescent ink irradiated by UV light (365 nm) and white light shown in the inset in the up-right corner.

**6.2 3D Printing**

Except for 2D text printing, 3D printing is a hot topic in the contemporary world. However, due to the limitation in the 3D printing, the ink materials are restricted such as acrylonitrile butadiene styrene (ABS), polylactic acid (PLA) and nylon, which significantly limits the application of the printed figures. Therefore, new functional materials as ink for 3D printing have to be discovered.

Since CDs have varieties of excellent properties, CDs were considered as a promising functional material. However, due to the low yield, 3D printing with CDs alone is hard to achieve. Inspired by the property of Orbeez beads that Orbeez beads can take in water and

grow larger, we speculated whether CDs can be embedded into Orbeez beads or their precursor which is superabsorbent polymer. Superabsorbent polymers can take in and retain extremely large amounts of a water relative to their own mass through hydrogen bonding with water. Therefore, we turned the attention toward the embedment of CDs into sodium polyacrylate (SPA), a common superabsorbent polymer. Then the use of CDs-embedded SPA will allow for 3D printing which requires high amounts of ink materials.

To start with, we prepared CDs aqueous dispersion with gel-like CDs and added five Orbeez beads in it to observe if the Orbeez beads can still adsorb water to grow larger. The result was unpredicted since the addition of ions has been reported to limit the growth of Orbeez beads. However, shortly, we observed these Orbeez beads grew large and took in all the water leaving the glass vial empty. Clearly, CDs didn't restrict the growth of Orbeez beads as ions. Moreover, after we rinsed the Orbeez beads with DI water three times, the Orbeez beads exhibited blue PL under the irradiation of UV light (365 nm). Figure 6.2a shows the Orbeez beads collected after the treatment of gel-like CDs aqueous dispersion (0.1 mg/mL) and their control with only water, which suggest gel-like CDs entered the Orbeez beads. To confirm the universality of CDs embedment in the Orbeez beads, orange CDs aqueous dispersion (0.1 mg/mL) was prepared and added with Orbeez beads, which yielded yellow photoluminescent Orbeez beads under the excitation of 400 nm (Figure 6.2b). Furthermore,

**(a)** **(b)**

**Figure 6.2** Orbeez beads treated by (a) water (left), gel-like CDs aqueous dispersion (0.1 mg/mL) (right), and (b) orange CDs aqueous dispersion (0.1 mg/mL) irradiated by UV light (365).

Then orange CDs were selected for the preparation of aqueous dispersion and mixed with SPA powder to achieve evenly distribution. After the SPA powder naturally lost water, it was grounded into refined powder as the feedstock for 3D printing. With the help of a Formlabs SLA 3D printer, a figure of the statue of liberty was printed with the SPA powder that embeds orange CDs. Figure 6.3a shows the printed figure in comparison with a one-dime coin. And in Figure 6.3b, we observed the figure containing CDs on the left exhibited yellow PL under the blue light (400 nm) while the control without CDs on the right reflected the light of irradiation. With the embedment of orange CDs in SPA, CDs and SPA are reported for the first time as the ink for 3D printing and the printed figure demonstrated excellent optical properties. Therefore, it opens a new avenue for more functional materials to be applied for 3D printing or additive manufacturing.

**(a)** **(b)**

**Figure 6.3** (a) The comparison of the printed figure with a one-dime coin; (b) 3D printing of "statue of liberty" with CDs-SAP conjugate (left) and control without orange CDs (right).

### 6.3 Fingerprint

Fingerprint is a unique characteristic for the identification of individuals and it is one of the most important tools in forensic science. When a finger touches a solid surface, an imprint of finger's edge pattern will be left on the surface. Such fingerprint is invisible to naked eyes. Traditionally, in order to reveal the latent fingerprint, powder dusting technique was usually employed,[123] and the used powders include lead carbonate/sulfate, ferric oxide, ninhydrin spraying and fluorescent dye staining.[124] However, in the traditional techniques, some toxic agents were involved, it is necessary to find nontoxic materials for the fingerprint identification. In the past few years, CDs have been widely studied as fingerprints since they are nontoxic and biocompatible as mentioned previously.[125-126] Moreover, CDs are photoluminescent, which endows another useful feature to the ink prepared with CDs for fingerprint. As is observed, the study regarding the application of CDs for fingerprints sharply increased in 2017-2018 and various PL colors of fingerprint

have been achieved ranging between blue and red by tuning different excitation wavelengths or with different synthetic approaches.[124, 127-128] However, to make the ink for fingerprints, CDs were either prepared as aqueous dispersion or in powder form, which lacks the consideration for the stability and recovery of fingerprints.

Surprisingly, the use of gel-like CDs has solved both problems. Figure 6.4 shows fingerprints of me and another colleague. In our study, we brushed the gel-like CDs onto the thumb and pressed the thumb on a non-fluorescent paper. The fingerprint took advantage of the gel network and high PL of CDs and could stick onto the non-fluorescent paper to make a nontoxic, stable and photoluminescent fingerprint.

**(a)** **(b)**

**Figure 6.4** Thumb fingerprints of (a) me and (b) another colleague using gel-like CDs as ink.

### 6.4 Nail Polish

CDs were also applied in the design of beauty product such as nail polish and this is the first time to report CDs as the additive for making nontoxic fluorescent nail polish. Compared with the control experiment shown in Figure 6.5b, Figure 6.5a shows the orange

CDs mixed with commercial nail polish, which endows the nail with the orange PL under UV light (365 nm) (right) while colorless in the white light (left).

**(a)** **(b)**

**Figure 6.5** (a) Orange CDs were mixed with commercial nail polish to make nails yellow photoluminescent under UV light (365 nm); (b) Control experiment without orange CDs in the nail polish doped on the nails under UV light (365 nm).

### 6.5 Hair Colorant

Hair is a protein filament that grows from follicles found in the dermis. On the surface of hair, the interaction between CDs and protein can contribute to the discovery of a permanent hair colorant made of CDs. The work was inspired by a study reported in 2018 when Huang et al. prepared graphene oxide (GO) and reduced graphene oxide (r-GO) mixed with chitosan at various loading level as hair dyes.[129] In the study, they sprayed as-prepared dye solutions on hair and observed that the coating of both GO and r-GO could render new properties to the hair such as antistatic performance and heat dissipation. On the basis of known properties of GO and r-GO, these coatings may have even more functionalities including UV protection, antibacterial, and odor absorption. After hair was dried, the coating of both compounds kept adhesive to the hair and resistive to washing with shampoo due to the contribution of chitosan, which met the requirement for being a

permanent hair colorant. In addition, the change of hair color in terms of shades and gradients was achieved by tuning the loading level of dopants. Without any doubt, the use of GO or r-GO as an alternative of traditional hair dyes reduces the organic solvents or toxic molecules involved in the ingredients, which protects hair from damage caused by undesired chemicals. However, the selection of hair color can merely be tuned in a narrow range from dark yellow to black and the hair coloring process relied on chitosan, which is widely used to form hydrogel and might be able to inhibit the exhibition of many properties of GO and r-GO.

Therefore, considering many excellent properties including high water-dispersity, tunable PL, abundant surface functional groups and nontoxicity, we believed CDs could be an even better alternative for the conventional hair dyes. 13 CDs species were synthesized using different approaches including hydrothermal, solvothermal, microwave-mediation, and ultrasonication. The purification methods are composed of dialysis, solvent wash and SEC. And the precursors covered both lab-fabricated compounds and daily-consumed products including wine, tea, coffee and goat cheese. When CDs aqueous dispersions were applied onto the human hair, after rinse we found only three types of CDs could make the hair "glow" under the UV light (365 nm). The hair coloring effect is shown in Figure 6.6. When the wavelength of irradiation shifted to 254 nm, the PL was still observed as demonstrated in Figure 6.7. In comparison, these three CDs species have higher hydrophobicity, which was confirmed by their low absolute zeta potential value. After drying hairs doped with the three CDs species with a commercial hair dryer, we still observed the fluorescence of hair with the same intensity by naked eyes. When dry hair was washed by water or methanol, we didn't see the elimination of PL as illustrated in

Figure 6.8, which confirms the stability of CDs on hair and demonstrates that CDs can be used to make permanent photoluminescent hair colorants. Also, SEM images in Figure 6.9 revealed the presence of CDs in the form of slight aggregation.

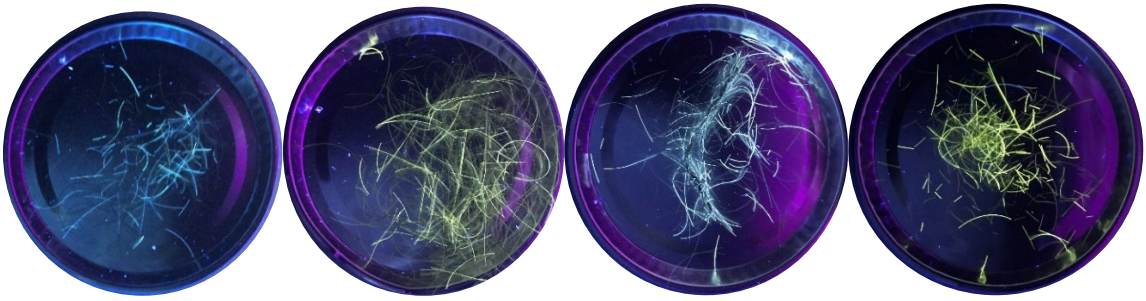

**(a)** **(b)** **(c)** **(d)**

**Figure 6.6** Various CDs species as hair colorant on hair excited under 365 nm. (a) hair alone, (b) O-CDs doped hair, (c) fraction 1 doped hair, (d) fraction 2 doped hair.

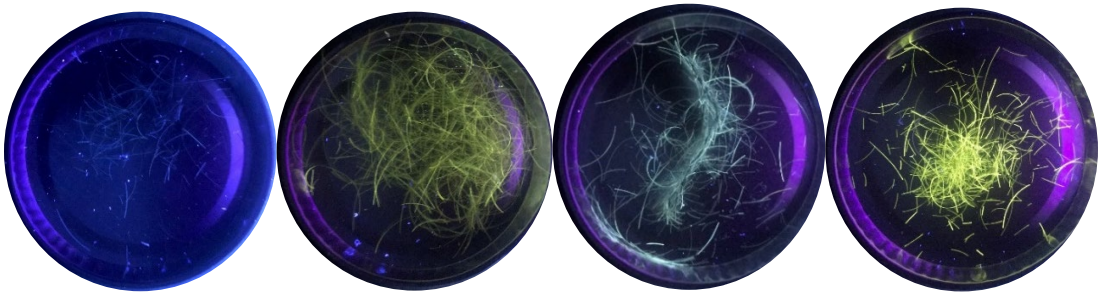

**(a)** **(b)** **(c)** **(d)**

**Figure 6.7** Various CDs species as hair colorant on hair excited under 254 nm. (a) hair alone, (b) O-CDs doped hair, (c) fraction 1 doped hair, (d) fraction 2 doped hair.

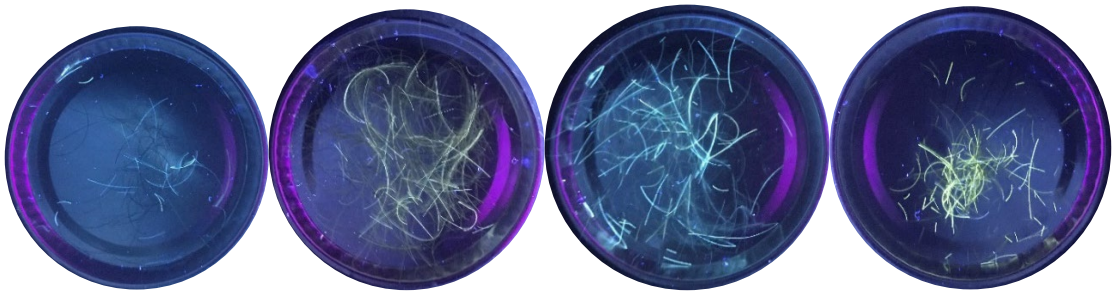

**(a)** **(b)** **(c)** **(d)**

**Figure 6.8** Stability test of various CDs species as hair colorant on hair after being washed. (a) hair alone, (b) O-CDs doped hair, (c) fraction 1 doped hair, (d) fraction 2 doped hair.

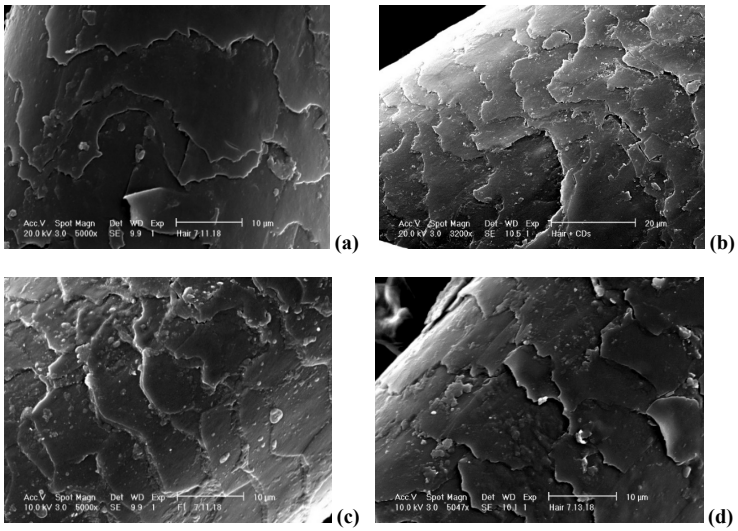


**Figure 6.9** SEM images of various CDs species as hair colorant on hair. (a) hair alone, (b) O-CDs doped hair, (c) fraction 1 doped hair, (d) fraction 2 doped hair.

## 6.6 Summary

Due to high fluorescence QY, CDs have been widely applied in text printing and fingerprint. However, in many previous reports, the details of text printing are missing or not easy to follow. In this chapter, we have designed a CDs-based ink for text printing with making procedure explained in detail. In addition, 3D printing has become a new and hot topic. We designed a novel method with the help of SAP to realize 3D printing with CDs and obtained photoluminescent figures. Also, CDs can be used for nontoxic fingerprint, nail polish and permanent hair colorant due to their excellent optical properties.

To date, applications related to the optical properties of CDs have been widely investigated. However, as a new family member of NPs, there might be many properties of CDs still unknown to public. For example, we believe CDs are semiconductors. The electric and magnetic studies of CDs have not been much reported. Also, even though there are many studies that report CDs can enhance the photocatalytic activity of many known photocatalyst materials,[130] the photocatalytic activity of CDs alone is seldom reported. Therefore, more promising applications will be proposed in **Chapter 7: Future Work**.

## Chapter 7. Future Work

To date, most CDs studies have been developed because of the excellent optical properties of CDs. As a derivative of QDs, CDs are semiconductors, which suggests that they have a definite conduction-valence band gap and great potential as photocatalyst. In this chapter, we are going to study the photocatalytic activity of bare CDs. In addition, since black CDs can target bones of zebrafish while orange CDs can permeate the whole body of zebrafish, in this chapter, we are going to present the ongoing project conjugating both CDs species to investigate if the conjugate can both cross the BBB and target the bones of zebrafish.

### 7.1 Photocatalytic Activity with Bare Carbon Dots as Photocatalyst

Environmental protection and energy crisis are two critical issues brought by the rapid growth of population and increasing daily demand. To avoid the implications of these issues, while considering the sustainability in the development, new resources are being widely explored such as solar energy. For this, photoactive materials are drawing much attention due to the unlimited sunlight energy and potential application as a catalyst for hydrogen generation via water splitting and for pollutants degradation.[131-132] Since hydrogen is considered as a renewable and sustainable energy resource, photocatalysis has become one promising solution to solve both issues.

Since the discovery of $TiO_2$ as the photocatalyst by Honda and Fujishima in 1972, in the past 40 years,[133] much efforts have been devoted to developing photocatalysts that act efficiently under visible light irradiation. To date, there are varieties of photocatalyst including metal oxides such as $TiO_2$,[134] $Fe_2O_3$,[135] ZnO,[136] ZnS,[137] $BiVO_4$,[138] metal chalcogenides, for example, CdS and $MoS_2$,[139] and nitrides, especially graphitic carbon nitrides.[140] However, the majority of photocatalysts contain metals, which poses a risk of

secondary pollution to water bodies after the degradation of the contaminants. In addition, sulfides are not stable and photocorrosion is easy to occur.[141] Even though oxides are stable in aqueous solution and low cost, most of them usually possess large band gap.[142] Therefore, the development of nontoxic, stable and efficient photocatalysts is desirable for applications such as the photocatalytic water splitting and the photocatalytic degradation of pollutant.

Since CDs are photoluminescent semiconductors with a specific energy band gap between the valence and the conduction bands,[143] they have the potential to drive photocatalytic redox reactions. For instance, these properties make CDs a good candidate for photocatalytic water splitting into hydrogen and oxygen.[144] Furthermore, the photocatalytic redox activity of CDs was utilized *in vivo* to generate reactive oxygen species (ROS) to cause the death of hypoxic tumor cells.[145] However, though photocatalytic water splitting is promising for hydrogen generation and photodynamic therapy, it has been challenging to design photocatalysts with efficient solar to hydrogen conversion due to the recombination of the electron/hole pairs and the fast backward reactions.[146] In addition, most traditional photocatalysts, such as $TiO_2$ and ZnO can only utilize UV light with band gaps greater than 3.0 eV.[133] Therefore, the development of stable photocatalyst that absorb in the visible light with narrow band gap is very much sought. Carbon-based materials such as graphitic carbon nitride (g-$C_3N_4$) has emerged as a promising photocatalyst with a band gap of 2.7 eV that is situated for visible light reactions.[147] Therefore, considering the similar polymeric structure of CDs as g-$C_3N_4$, and the abundant electron donors and acceptors on CDs, the photocatalytic properties of CDs should be investigated. Recently, CDs have been integrated in heterostructures to enhance the activity of various photocatalysts[148-149] and

they are able to play manifold roles in heterogeneous photocatalysis. For example, they are photoelectron mediator and acceptor, photosensitizer, reducing agent, and they can enhance adsorption capacity.[150-151] Furthermore, there are many advantages that facilitate the application of CDs as photocatalyst. First, they are well-dispersed in water, which yields a homogeneous phase to efficiently absorb water on their surface.[63] Additionally, CDs are nontoxic, they will not contaminate the body of water or have adverse effect on the human health. However, even though CDs have been utilized to enhance the photocatalytic activity of various metal oxide nanomaterials such as $Fe_2O_3$,[152] $TiO_2$,[153] ZnO,[154] $SnS_2$,[155] and BiOBr,[156] there are fewer studies on the photocatalytic properties of bare CDs, especially on the photocatalytic dye degradation.[157] Otherwise, the photocatalytic activity of bare CDs is usually negligible.[158]

Herein, in this study, we will focus on the study of the photocatalytic activity of the bare CDs as well as the influence of size on the photocatalytic performance. The CDs were synthesized via a microwave-assisted reaction of citric acid as carbon precursor and OPD as nitrogen dopant. After purification by SEC, as observed from the AFM images (Figure 7.1), the three fractions exhibited different sizes as we previously expected from the CDs separation through the SEC. The size of fraction 1, 2, and 3 is estimated to be around 5, 3 and 2 nm, respectively, according to Figure 7.1a, b and c). The average particle size of each fraction has been confirmed by the TEM images shown in Figure 7.1d, e and f. From the histograms of TEM images, we observe the sizes of fractions 1, 2 and 3 to be $4.48 \pm 1.38$, $3.61 \pm 0.92$ and $2.24 \pm 0.45$ nm, respectively. The combination of AFM and TEM data revealed typical spherical CD morphology with narrow size distributions.

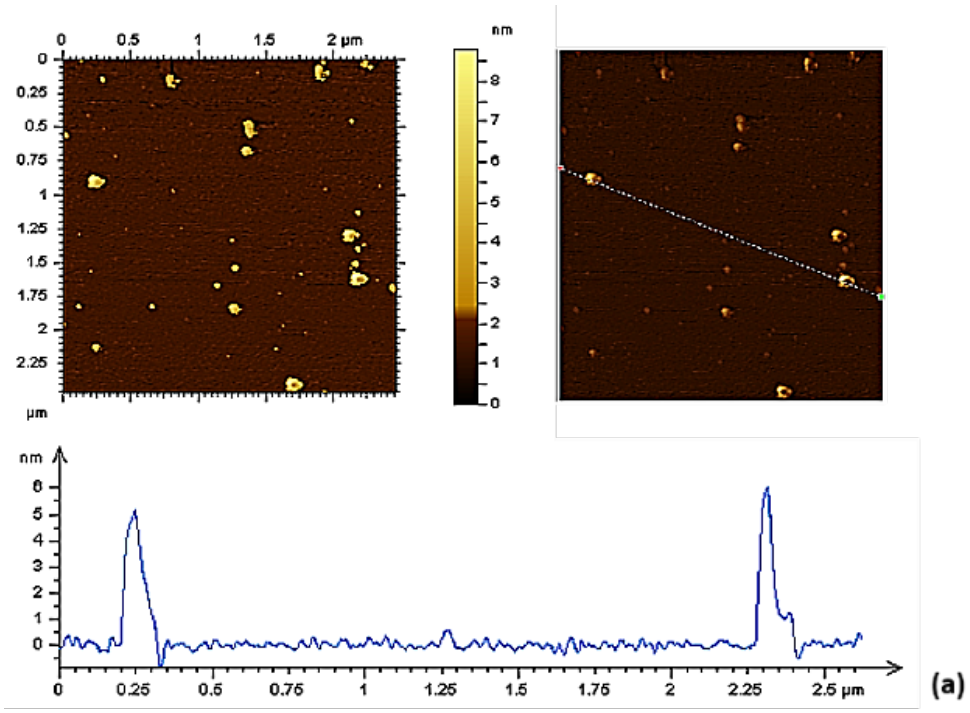
0 0.5 1 1.5 2 µm
nm
µm
nm
0 0.25 0.5 0.75 1 1.25 1.5 1.75 2 2.25 2.5 µm

(a)

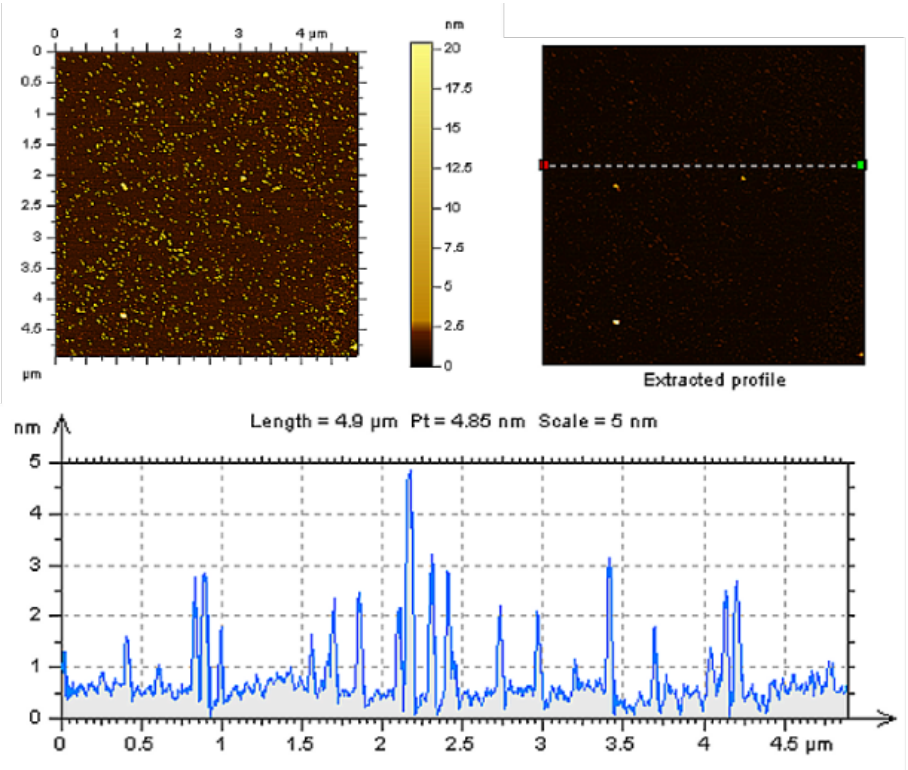
0 1 2 3 4 µm
nm
µm
Extracted profile
Length = 4.9 µm Pt = 4.85 nm Scale = 5 nm
nm
0 0.5 1 1.5 2 2.5 3 3.5 4 4.5 µm

(b)

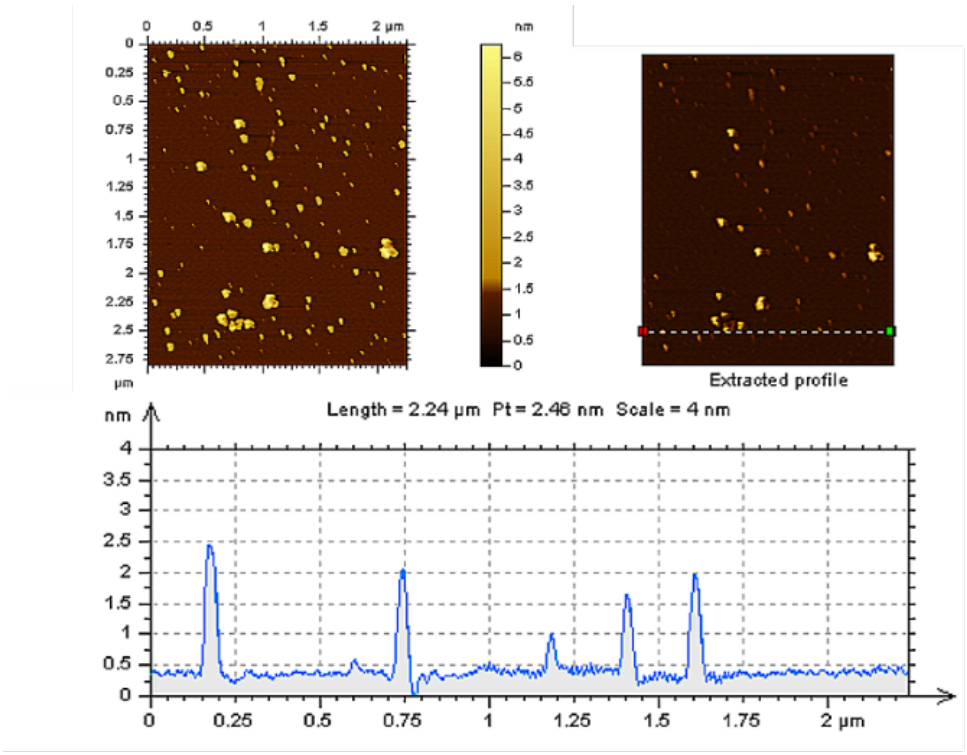
Extracted profile
Length = 2.24 µm Pt = 2.48 nm Scale = 4 nm
nm
µm

(c)

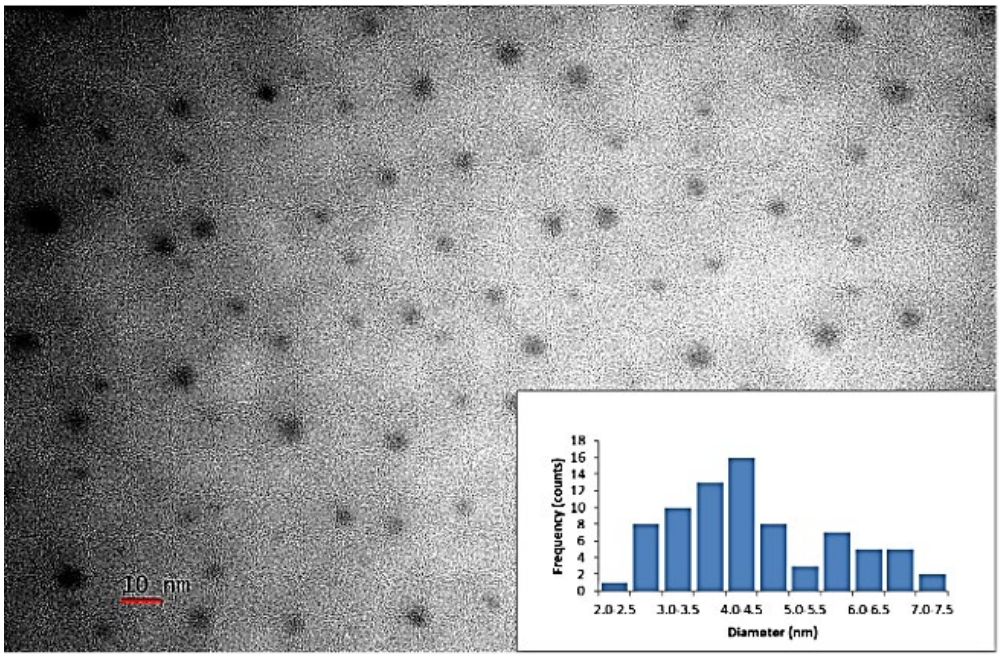
10 nm
Frequency (counts)
Diameter (nm)

(d)

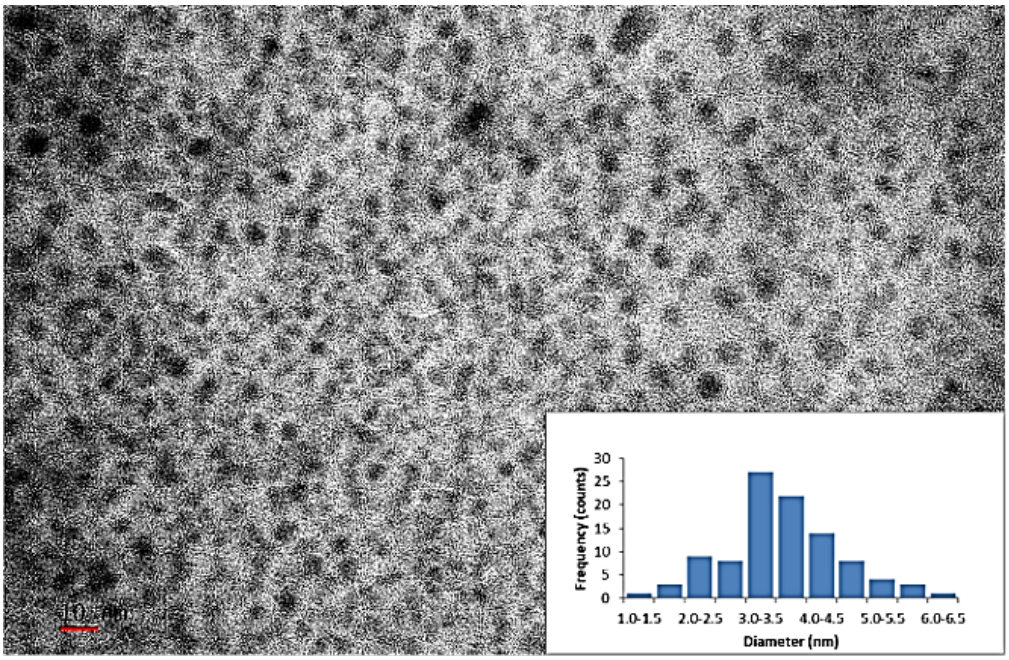


(e)

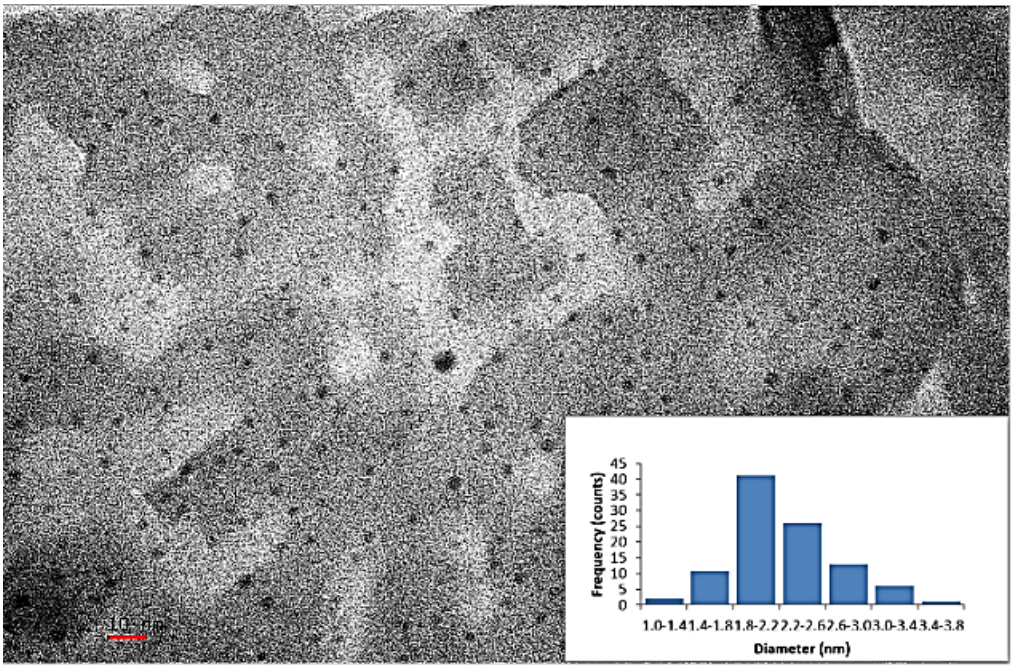


(f)

**Figure 7.1** The AFM images of fraction 1 (a), 2 (b) and 3 (c); the TEM images of fraction 1 (d), 2 (e) and 3 (f). The scale bars represent 10 nm.

In order to explore the photocatalytic activity of the as-prepared CDs, considering the negative zeta potential of CDs fractions, positively charged organic dyes were selected for

photocatalytic dye degradation. Therefore, the degradation of rhodamine B (RhB) and methylene blue (MB) was conducted in presence of 0.75 mg/mL of CDs under simulated sunlight. Neither RhB or MB was degraded in the presence of fraction 1 (Figure 7.2a and b). As the size of CDs decrease to 3 nm in fraction 2, partial degradation of MB was noticed only in the first 20 min (Figure 7.2d). On the other hand, no significant degradation of RhB was found for reactions catalyzed with fraction 2 (Figure 7.2c). On the contrary, the 2-nm CDs of fraction 3 demonstrated significant degradation of RhB and MB, which was both completed in 150 min (Figure 7.2e and f).

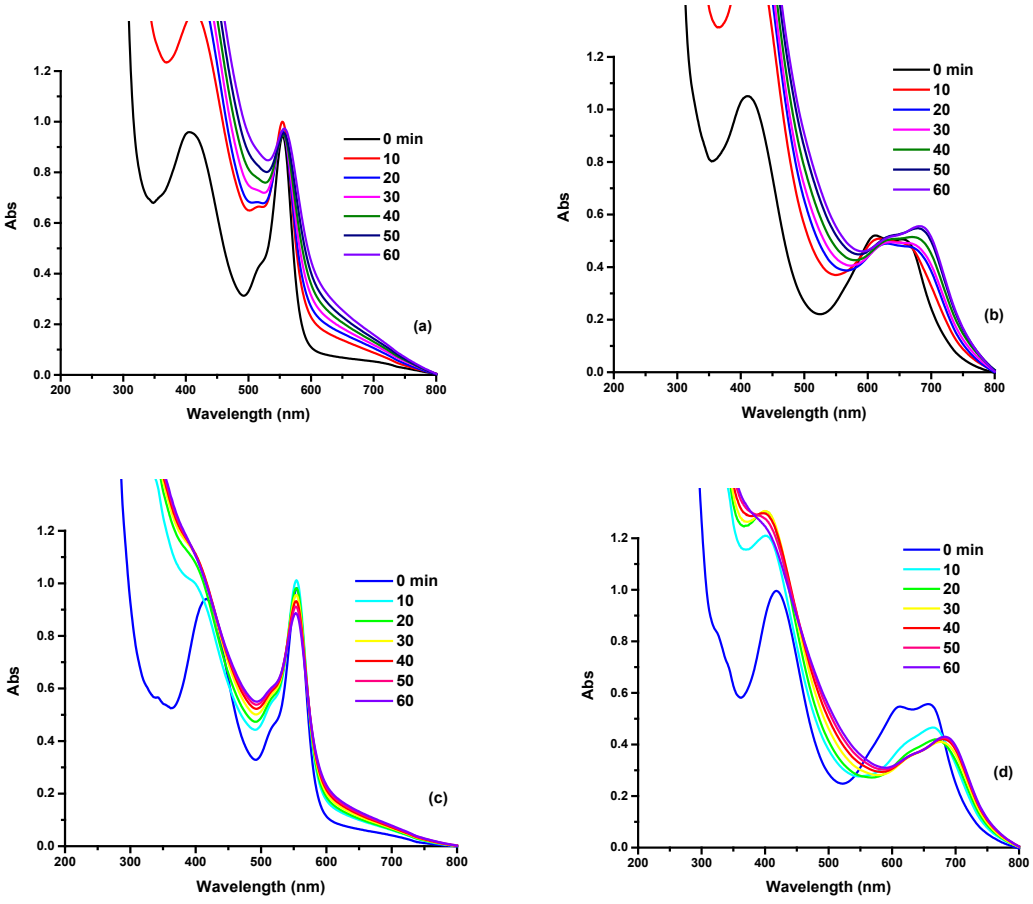

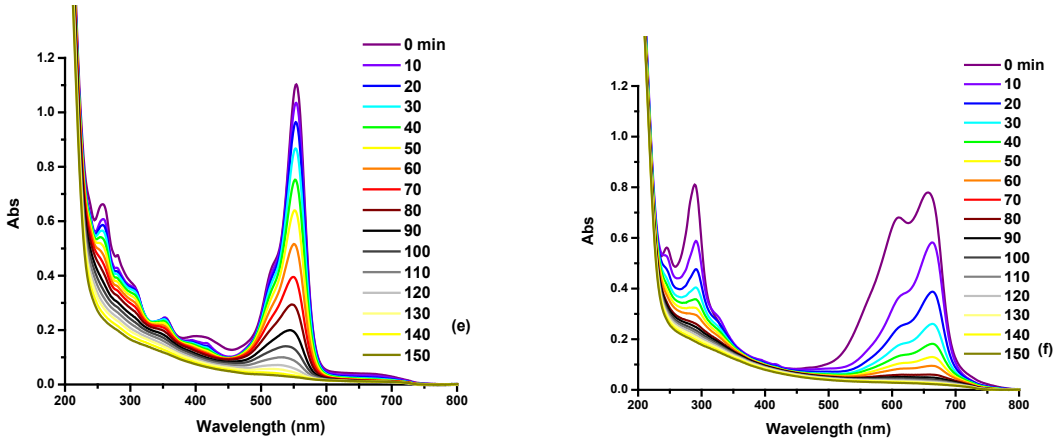


**Figure 7.2** The photocatalytic degradation of RhB and MB induced by fraction 1, 2 and 3 of CDs. The UV/vis absorption spectra of RhB (a) and MB (b) in the presence of fraction 1 at various time points; the UV/vis absorption spectra of RhB (c) and MB (d) in the presence of fraction 2 at various time points; the UV/vis absorption spectra of RhB (e) and MB (f) in the fraction 3 at various time points. The concentration of each fraction is 0.75 mg/mL.

The band gap of fraction 2 and 3 will be measured using diffuse reflectance spectroscopy. The mechanism of the dye degradation will be analyzed using various charge-carrier scavengers from the viewpoint of generation of superoxide and hydroxide radicals. The stability test will be conducted to reveal the effectiveness of CDs in the long term of dye degradation. The CDs will be employed in the photocatalytic degradation of, p-nitrophenol (PNP), one of the most hazardous refractory pollutants with high stability and solubility in water,[159] to demonstrate their application for various environmental contaminates.

### 7.2 Conjugation between Black and Orange Carbon Dots

To the best of my knowledge, many CDs species have been synthesized and some of them exhibit excellent and unique properties. For example, black CDs can specifically target bones of zebrafish and so far, it is the only CDs species that have been reported to exhibit such property. However, the fluorescence QY of black CDs is as low as 1%. Meanwhile, even though orange CDs don't have high fluorescence QY either, they have high PL

intensity. The low fluorescence QY was due to the high absorbance caused by the aggregation of orange CDs regarding the low zeta potential. However, when zebrafish was soaked into the aqueous dispersion of orange CDs, zebrafish exhibited yellow PL all over the body including the skin, blood and CNS. Therefore, each CDs species has two edges of a sword. If they can conjugate with each other by covalent bonds, they may benefit from each other's properties. Therefore, as one of my ongoing and future work, I will try to conjugate black and orange CDs with full characterizations. Figure 7.3a shows the UV/vis absorption spectrum of the conjugate. The peaks at 278 nm originates from black CDs while the peak at 469 nm is obtained from orange CDs, which might result from $NO_2$ absorption.[30] Fluorescence emission spectrum and its normalized spectrum in Figure 7.3b and c reveals that such conjugate has the maximum excitation and emission wavelengths at 400 and 504 nm. FTIR spectrum in Figure 7.3d indicates the addition of -$NH_2$ (1591 $cm^{-1}$) to black CDs due to the presence of orange CDs.

The conjugate of black and orange CDs was injected into the heart of 6-day post-fertilization wild-type zebrafish. The confocal images were taken under the excitation of 405 nm (Figure 7.4) with 6 zebrafish to reproduce the result. Figure 7.4 reveals black CDs carry orange CDs to the bones of zebrafish while orange CDs successfully delivered black CDs across the BBB to reach the central canal of spinal cord of zebrafish considering the inability of black CDs to overcome the BBB. Therefore, the future work is related to the permeation ability of orange CDs. Instead of injection, black CDs might be able to enter the body of zebrafish to target the bones by soaking zebrafish in CDs aqueous dispersion. Also, the size increase resulting from the conjugation is expected to restrict the movement of orange CDs to a certain tissue or organ of zebrafish.

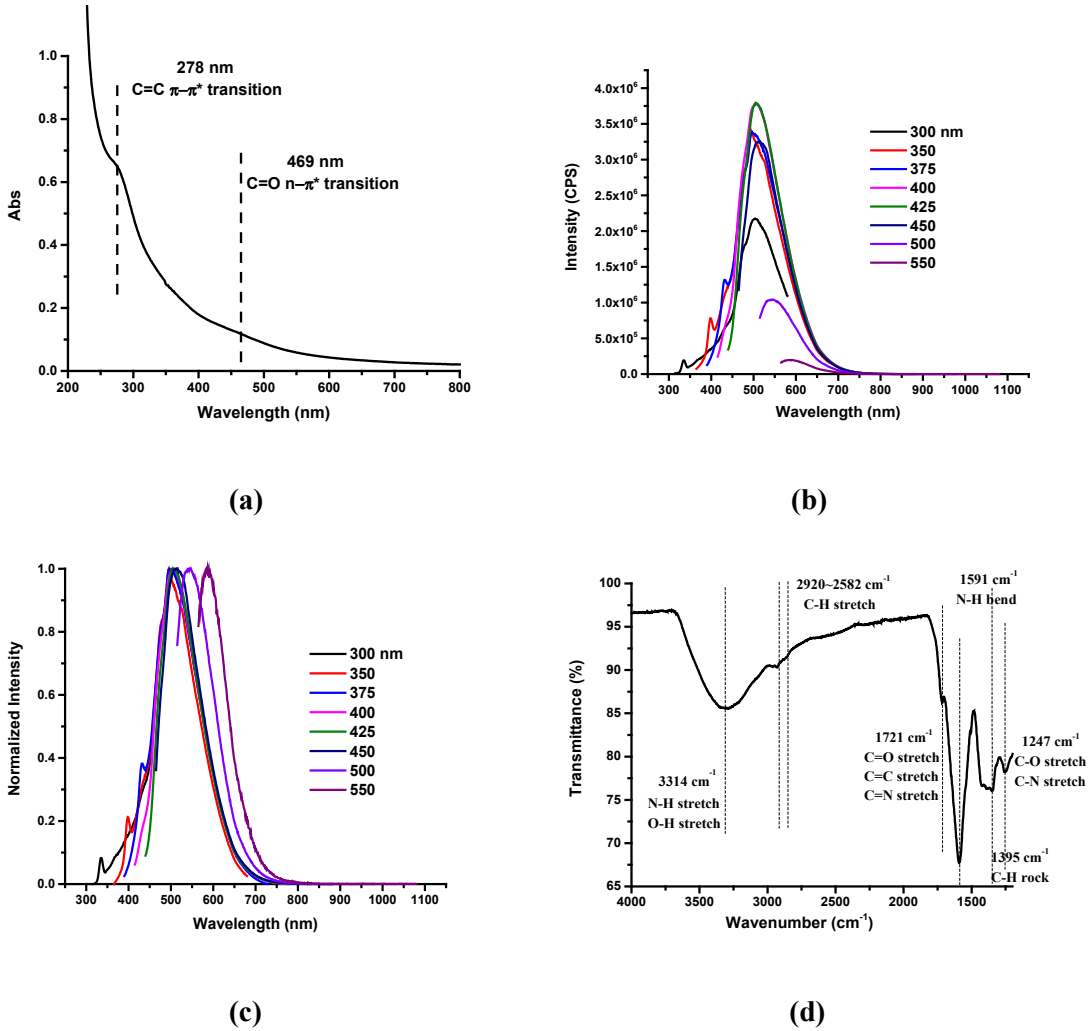


**Figure 7.3** The UV/vis absorption (a), fluorescence emission (b) and normalized spectra (c) (0.01 mg/mL) and FTIR spectrum (d) of the black and orange CDs conjugate with air background.

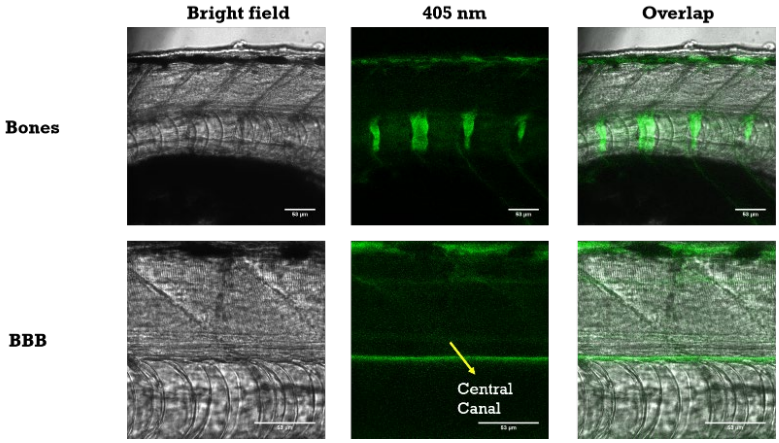


**Figure 7.4** Confocal images of 6-day post-fertilization wild-type zebrafish injected with the conjugate of orange and back CDs.

## References


1. Danilenko, V. V. *Phys. Solid State* **2004,** *46*, 595-599.

2. Monthioux, M.; Kuznetsov, V. L. *Carbon* **2006,** *44*, 1621-1623.

3. Ugarte, D. *Nature* **1992,** *359*, 707-709.

4. Bethune, D. S.; Kiang, C. H.; de Vries, M. S.; Gorman, G.; Savoy, R.; Vazquez, J.; Beyers, R. *Nature* **1993,** *363*, 605-607.

5. Ge, M.; Sattler, K. *Chem. Phys. Lett.* **1994,** *220*, 192-196.

6. Iijima, S.; Yudasaka, M.; Yamada, R.; Bandow, S.; Suenaga, K.; Kokai, F.; Takahashi, K. *Chem. Phys. Lett.* **1999,** *309*, 165-170.

7. Xu, X.; Ray, R.; Gu, Y.; Ploehn, H. J.; Gearheart, L.; Raker, K.; Scrivens, W. A. *J. Am. Chem. Soc.* **2004,** *126*, 12736-12737.

8. Zhou, Y.; Sharma, S. K.; Peng, Z.; Leblanc, R. M. *Polymers* **2017,** *9*, 67-85.

9. Zhang, T.; Zhao, F.; Li, L.; Qi, B.; Zhu, D.; Lü, J.; Lü, C. *ACS Appl. Mater. Interfaces* **2018,** *10*, 19796-19805.

10. Ding, H.; Yu, S.-B.; Wei, J.-S.; Xiong, H.-M. *ACS Nano* **2016,** *10*, 484-491.

11. Wang, H.; Sun, C.; Chen, X.; Zhang, Y.; Colvin, V. L.; Rice, Q.; Seo, J.; Feng, S.; Wang, S.; Yu, W. W. *Nanoscale* **2017,** *9*, 1909-1915.

12. Xu, Q.; Pu, P.; Zhao, J.; Dong, C.; Gao, C.; Chen, Y.; Chen, J.; Liu, Y.; Zhou, H. *J. Mater. Chem. A* **2015,** *3*, 542-546.

13. Shi, D.; Yan, F.; Zheng, T.; Wang, Y.; Zhou, X.; Chen, L. *RSC Adv.* **2015,** *5*, 98492-98499.

14. Qian, Z.; Shan, X.; Chai, L.; Ma, J.; Chen, J.; Feng, H. *ACS Appl. Mater. Interfaces* **2014,** *6*, 6797-6805.

15. Fei, H.; Ye, R.; Ye, G.; Gong, Y.; Peng, Z.; Fan, X.; Samuel, E. L. G.; Ajayan, P. M.; Tour, J. M. *ACS Nano* **2014,** *8*, 10837-10843.

16. Howes, P.; Green, M.; Johnston, C.; Crossley, A. *J. Mater. Chem.* **2008,** *18*, 3474-3480.

17. Hou, B.; Cho, Y.; Kim, B.-S.; Ahn, D.; Lee, S.; Park, J. B.; Lee, Y.-W.; Hong, J.; Im, H.; Morris, S. M.; Sohn, J. I.; Cha, S.; Kim, J. M. *J. Mater. Chem. C* **2017,** *5*, 3692-3698.

18. Zhu, J.; Zhao, Z.-J.; Li, J.-J.; Zhao, J.-W. *Spectrochim. Acta A* **2017,** *177*, 140-146.

19. Li, S.; Wang, L.; Chusuei, C. C.; Suarez, V. M.; Blackwelder, P. L.; Micic, M.; Orbulescu, J.; Leblanc, R. M. *Chem. Mater.* **2015,** *27*, 1764-1771.

20. Peng, Z.; Miyanji, E. H.; Zhou, Y.; Pardo, J.; Hettiarachchi, S. D.; Li, S.; Blackwelder, P. L.; Skromne, I.; Leblanc, R. M. *Nanoscale* **2017,** *9*, 17533-17543.

21. Mintz, K. J.; Mercado, G.; Zhou, Y.; Ji, Y.; Hettiarachchi, S. D.; Liyanage, P. Y.; Pandey, R. R.; Chusuei, C. C.; Dallman, J.; Leblanc, R. M. *Colloids Surf. B* **2019,** *176*, 488-493.

22. Zhu, S.; Meng, Q.; Wang, L.; Zhang, J.; Song, Y.; Jin, H.; Zhang, K.; Sun, H.; Wang, H.; Yang, B. *Angew. Chem. Int. Ed.* **2013,** *52*, 3953-3957.

23. Chen, D.; Gao, H.; Chen, X.; Fang, G.; Yuan, S.; Yuan, Y. *ACS Photonics* **2017,** *4*, 2352-2358.

24. Zhu, J.; Bai, X.; Chen, X.; Xie, Z.; Zhu, Y.; Pan, G.; Zhai, Y.; Zhang, H.; Dong, B.; Song, H. *Dalton Trans.* **2018,** *47*, 3811-3818.

25. Zheng, C.; An, X.; Gong, J. *RSC Adv.* **2015,** *5*, 32319-32322.

26. Essner, J. B.; Laber, C. H.; Ravula, S.; Polo-Parada, L.; Baker, G. A. *Green Chem.* **2016,** *18*, 243-250.

27. Wang, Z.; Yuan, F.; Li, X.; Li, Y.; Zhong, H.; Fan, L.; Yang, S. *Adv. Mater.* **2017,** *29*, 1702910.

28. Cao, L.; Wang, X.; Meziani, M. J.; Lu, F.; Wang, H.; Luo, P. G.; Lin, Y.; Harruff, B. A.; Veca, L. M.; Murray, D.; Xie, S.-Y.; Sun, Y.-P. *J. Am. Chem. Soc.* **2007,** *129*, 11318-11319.

29. Hsu, P.-C.; Chang, H.-T. *ChemComm* **2012,** *48*, 3984-3986.

30. Zhou, Y.; Mintz, K. J.; Oztan, C. Y.; Hettiarachchi, S. D.; Peng, Z.; Seven, E. S.; Liyanage, P. Y.; De La Torre, S.; Celik, E.; Leblanc, R. M. *Polymers* **2018,** *10*, 921-932.

31. Zhang, Z.; Zheng, T.; Li, X.; Xu, J.; Zeng, H. *Part. Part. Syst. Char.* **2016,** *33*, 457-472.

32. Li, Y.; Zhang, Z.-Y.; Yang, H.-F.; Shao, G.; Gan, F. *RSC Adv.* **2018,** *8*, 3982-3988.

33. Omer, K. M.; Tofiq, D. I.; Hassan, A. Q. *Microchim. Acta* **2018,** *185*, 466-473.

34. Mutuyimana, F. P.; Liu, J.; Na, M.; Nsanzamahoro, S.; Rao, Z.; Chen, H.; Chen, X. *Microchim. Acta* **2018,** *185*, 518-527.

35. Zhou, Y.; Desserre, A.; Sharma, S. K.; Li, S.; Marksberry, M. H.; Chusuei, C. C.; Blackwelder, P. L.; Leblanc, R. M. *ChemPhysChem* **2017,** *18*, 890-897.

36. Wang, Y.; Chang, X.; Jing, N.; Zhang, Y. *Anal. Methods* **2018,** *10*, 2775-2784.

37. Liu, Q.; Zhang, N.; Shi, H.; Ji, W.; Guo, X.; Yuan, W.; Hu, Q. *New J. Chem.* **2018,** *42*, 3097-3101.

38. Dang, H.; Huang, L.-K.; Zhang, Y.; Wang, C.-F.; Chen, S. *Ind. Eng. Chem. Res.* **2016,** *55*, 5335-5341.

39. Chae, A.; Choi, Y.; Jo, S.; Nur'aeni; Paoprasert, P.; Park, S. Y.; In, I. *RSC Adv.* **2017,** *7*, 12663-12669.

40. Wang, S.; Wang, H.; Zhang, R.; Zhao, L.; Wu, X.; Xie, H.; Zhang, J.; Sun, H. *J. Alloys Compd.* **2018,** *746*, 567-575.

41. Su, R.; Wang, D.; Liu, M.; Yan, J.; Wang, J.-X.; Zhan, Q.; Pu, Y.; Foster, N. R.; Chen, J.-F. *ACS Omega* **2018,** *3*, 13211-13218.

42. Sahu, S.; Behera, B.; Maiti, T. K.; Mohapatra, S. *ChemComm* **2012,** *48*, 8835-8837.

43. Chen, K.; Qing, W.; Hu, W.; Lu, M.; Wang, Y.; Liu, X. *Spectrochim. Acta A* **2019,** *213*, 228-234.

44. Jiang, C.; Wu, H.; Song, X.; Ma, X.; Wang, J.; Tan, M. *Talanta* **2014,** *127*, 68-74.

45. Fernando, K. A. S.; Sahu, S.; Liu, Y.; Lewis, W. K.; Guliants, E. A.; Jafariyan, A.; Wang, P.; Bunker, C. E.; Sun, Y.-P. *ACS Appl. Mater. Interfaces* **2015,** *7*, 8363-8376.

46. Mandani, S.; Dey, D.; Sharma, B.; Sarma, T. K. *Carbon* **2017,** *119*, 569-572.

47. Lu, S.; Guo, S.; Xu, P.; Li, X.; Zhao, Y.; Gu, W.; Xue, M. *Int. J. Nanomed.* **2016,** *11*, 6325-6336.

48. Zhou, Y.; Liyanage, P. Y.; Geleroff, D. L.; Peng, Z.; Mintz, K. J.; Hettiarachchi, S. D.; Pandey, R. R.; Chusuei, C. C.; Blackwelder, P. L.; Leblanc, R. M. *ChemPhysChem* **2018,** *19*, 2589-2597.

49. Vinci, J. C.; Ferrer, I. M.; Seedhouse, S. J.; Bourdon, A. K.; Reynard, J. M.; Foster, B. A.; Bright, F. V.; Colón, L. A. *J. Phys. Chem. Lett.* **2013,** *4*, 239-243.

50. Zhou, Y.; Zahran, E. M.; Quiroga, B. A.; Perez, J.; Mintz, K. J.; Peng, Z.; Liyanage, P. Y.; Pandey, R. R.; Chusuei, C. C.; Leblanc, R. M. *Appl. Catal., B* **2019,** *248*, 157-166.

51. Yu, Y.; Fan, G.; Fermi, A.; Mazzaro, R.; Morandi, V.; Ceroni, P.; Smilgies, D.-M.; Korgel, B. A. *J. Phys. Chem. C* **2017,** *121*, 23240-23248.

52. Zhu, S.; Song, Y.; Zhao, X.; Shao, J.; Zhang, J.; Yang, B. *Nano Res.* **2015,** *8*, 355-381.

53. Krysmann, M. J.; Kelarakis, A.; Dallas, P.; Giannelis, E. P. *J. Am. Chem. Soc.* **2012,** *134*, 747-750.

54. Chien, C.-T.; Li, S.-S.; Lai, W.-J.; Yeh, Y.-C.; Chen, H.-A.; Chen, I.-S.; Chen, L.-C.; Chen, K.-H.; Nemoto, T.; Isoda, S.; Chen, M.; Fujita, T.; Eda, G.; Yamaguchi, H.; Chhowalla, M.; Chen, C.-W. *Angew. Chem. Int. Ed.* **2012,** *51*, 6662-6666.

55. Nguyen, V.; Yan, L.; Si, J.; Hou, X. *Opt. Mater. Express* **2016,** *6*, 312-320.

56. Mintz, K. J.; Zhou, Y.; Leblanc, R. M. *Nanoscale* **2019,** DOI: 10.1039/c8nr10059d.

57. Yang, Z.; Xu, M.; Liu, Y.; He, F.; Gao, F.; Su, Y.; Wei, H.; Zhang, Y. *Nanoscale* **2014,** *6*, 1890-1895.

58. Sarkar, S.; Sudolská, M.; Dubecký, M.; Reckmeier, C. J.; Rogach, A. L.; Zbořil, R.; Otyepka, M. *J. Phys. Chem. C* **2016,** *120*, 1303-1308.

59. Sun, Y.-P.; Zhou, B.; Lin, Y.; Wang, W.; Fernando, K. A. S.; Pathak, P.; Meziani, M. J.; Harruff, B. A.; Wang, X.; Wang, H.; Luo, P. G.; Yang, H.; Kose, M. E.; Chen, B.; Veca, L. M.; Xie, S.-Y. *J. Am. Chem. Soc.* **2006,** *128*, 7756-7757.

60. Wang, X.; Cao, L.; Yang, S.-T.; Lu, F.; Meziani, M. J.; Tian, L.; Sun, K. W.; Bloodgood, M. A.; Sun, Y.-P. *Angew. Chem. Int. Ed.* **2010,** *49*, 5310-5314.

61. Williams, A. T. R.; Winfield, S. A.; Miller, J. N. *Analyst* **1983,** *108*, 1067-1071.

62. Mintz, K. J.; Guerrero, B.; Leblanc, R. M. *J. Phys. Chem. C* **2018,** *122*, 29507-29515.

63. Liu, H.; Li, Z.; Sun, Y.; Geng, X.; Hu, Y.; Meng, H.; Ge, J.; Qu, L. *Sci. Rep.* **2018,** *8*, 1086-1093.

64. Wang, H.-J.; He, X.; Luo, T.-Y.; Zhang, J.; Liu, Y.-H.; Yu, X.-Q. *Nanoscale* **2017,** *9*, 5935-5947.

65. Lin, Y.; Wang, C.; Li, L.; Wang, H.; Liu, K.; Wang, K.; Li, B. *ACS Appl. Mater. Interfaces* **2015,** *7*, 27262-27270.

66. Liyanage, P. Y.; Graham, R. M.; Pandey, R. R.; Chusuei, C. C.; Mintz, K. J.; Zhou, Y.; Harper, J. K.; Wu, W.; Wikramanayake, A. H.; Vanni, S.; Leblanc, R. M. *Bioconjugate Chem.* **2018,** *30*, 111-123.

67. Mintz, K.; Waidely, E.; Zhou, Y.; Peng, Z.; Al-Youbi, A. O.; Bashammakh, A. S.; El-Shahawi, M. S.; Leblanc, R. M. *Anal. Chim. Acta* **2018,** *1041*, 114-121.

68. Li, S.; Skromne, I.; Peng, Z.; Dallman, J.; Al-Youbi, A. O.; Bashammakh, A. S.; El-Shahawi, M. S.; Leblanc, R. M. *J. Mater. Chem. B* **2016,** *4*, 7398-7405.

69. Clarke, B. *Clin. J. Am. Soc. Nephrol.* **2008,** *3*, S131-S139.

70. Mackie, E. J.; Ahmed, Y. A.; Tatarczuch, L.; Chen, K. S.; Mirams, M. *Int. J. Biochem. Cell Biol.* **2008,** *40*, 46-62.

71. Peng, Z.; Li, S.; Han, X.; Al-Youbi, A. O.; Bashammakh, A. S.; El-Shahawi, M. S.; Leblanc, R. M. *Anal. Chim. Acta* **2016,** *937*, 113-118.

72. Wang, R.-L.; Bencic, D. C.; Garcia-Reyero, N.; Perkins, E. J.; Villeneuve, D. L.; Ankley, G. T.; Biales, A. D. *PLOS ONE* **2014,** *9*, e114178-e114201.

73. Henning, P.; Conaway, H. H.; Lerner, U. H. *Front. Endocrinol.* **2015,** *6*, 31-43.

74. Vogler, A. *Inorg. Chem. Commun.* **2015,** *57*, 69-71.

75. Mayer, F.; Mayer, N.; Chinn, L.; Pinsonneault, R. L.; Kroetz, D.; Bainton, R. J. *J. Neurosci.* **2009,** *29*, 3538-3550.

76. Cserr, H. F.; Bundgaard, M. *Am. J. Physiol.* **1984,** *246*, R277-R288.

77. Harati, R.; Villégier, A.-S.; Banks, W. A.; Mabondzo, A. *J. Neuroinflammation* **2012,** *9*, 273-288.

78. Luissint, A.-C.; Artus, C.; Glacial, F.; Ganeshamoorthy, K.; Couraud, P.-O. *Fluids Barriers CNS* **2012,** *9*, 23-34.

79. Begley, D. J. *Pharmacol. Ther.* **2004,** *104*, 29-45.

80. Sandoval, K. E.; Witt, K. A. *Neurobiol. Dis.* **2008,** *32*, 200-219.

81. Grabrucker, A. M.; Chhabra, R.; Belletti, D.; Forni, F.; Vandelli, M. A.; Ruozi, B.; Tosi, G. In *The Blood Brain Barrier (BBB)*, Fricker, G.; Ott, M.; Mahringer, A., Eds. Springer Berlin Heidelberg: Berlin, Heidelberg, 2014; pp 71-89.

82. Zheng, W.; Aschner, M.; Ghersi-Egea, J.-F. *Toxicol. Appl. Pharmacol.* **2003,** *192*, 1-11.

83. Cummings, J. L.; Cole, G. *JAMA* **2002,** *287*, 2335-2338.

84. Alavijeh, M. S.; Chishty, M.; Qaiser, M. Z.; Palmer, A. M. *NeuroRx* **2005,** *2*, 554-571.

85. Wohlfart, S.; Gelperina, S.; Kreuter, J. *J. Control. Release* **2012,** *161*, 264-273.

86. Spindler, K. R.; Hsu, T.-H. *Trends Microbiol.* **2012,** *20*, 282-290.

87. Koo, Y.-E. L.; Reddy, G. R.; Bhojani, M.; Schneider, R.; Philbert, M. A.; Rehemtulla, A.; Ross, B. D.; Kopelman, R. *Adv. Drug Deliv. Rev.* **2006,** *58*, 1556-1577.

88. Gumerlock, M. K.; Belshe, B. D.; Madsen, R.; Watts, C. *J. Neuro-Oncol.* **1992,** *12*, 33-46.

89. Wu, S.-K.; Chu, P.-C.; Chai, W.-Y.; Kang, S.-T.; Tsai, C.-H.; Fan, C.-H.; Yeh, C.-K.; Liu, H.-L. *Sci. Rep.* **2017,** *7*, 46689-46699.

90. Chu, P.-C.; Chai, W.-Y.; Tsai, C.-H.; Kang, S.-T.; Yeh, C.-K.; Liu, H.-L. *Sci. Rep.* **2016,** *6*, 33264-33276.

91. Upadhyay, R. K. *BioMed Res. Int.* **2014,** *2014*, 869269-869306.

92. Kreuter, J. *Adv. Drug Deliv. Rev.* **2001,** *47*, 65-81.

93. Loureiro, J. A.; Gomes, B.; Fricker, G.; Coelho, M. A. N.; Rocha, S.; Pereira, M. C. *Colloids Surf. B* **2016,** *145*, 8-13.

94. Peluffo, H.; Unzueta, U.; Negro-Demontel, M. L.; Xu, Z.; Váquez, E.; Ferrer-Miralles, N.; Villaverde, A. *Biotechnol. Adv.* **2015,** *33*, 277-287.

95. Koffie, R. M.; Farrar, C. T.; Saidi, L.-J.; William, C. M.; Hyman, B. T.; Spires-Jones, T. L. *Proc. Natl. Acad. Sci.* **2011,** *108*, 18837-18842.

96. Supriya, D. M.; Indrajit, R.; GaiXia, X.; Ken-Tye, Y.; Hong, D.; Ravikumar, A.; Jessica, L. R.; Donald, E. S.; Bindukumar, B. N.; Elaine, Y. L.; Paras, N. P.; Stanley, A. S. *Curr. HIV Res.* **2010,** *8*, 396-404.

97. Reimold, I.; Domke, D.; Bender, J.; Seyfried, C. A.; Radunz, H.-E.; Fricker, G. *Eur. J. Pharm. Biopharm.* **2008,** *70*, 627-632.

98. Nance, E.; Timbie, K.; Miller, G. W.; Song, J.; Louttit, C.; Klibanov, A. L.; Shih, T.-Y.; Swaminathan, G.; Tamargo, R. J.; Woodworth, G. F.; Hanes, J.; Price, R. J. *J. Control. Release* **2014,** *189*, 123-132.

99. Zhang, T.-T.; Li, W.; Meng, G.; Wang, P.; Liao, W. *Biomater. Sci.* **2016,** *4*, 219-229.

100. Vergoni, A. V.; Tosi, G.; Tacchi, R.; Vandelli, M. A.; Bertolini, A.; Costantino, L. *Nanomedicine* **2009,** *5*, 369-377.

101. Spuch, C.; Navarro, C. *J. Drug Deliv.* **2011,** *2011*, 12-24.

102. Cheng, Y.; Dai, Q.; Morshed, R. A.; Fan, X.; Wegscheid, M. L.; Wainwright, D. A.; Han, Y.; Zhang, L.; Auffinger, B.; Tobias, A. L.; Rincón, E.; Thaci, B.; Ahmed, A. U.; Warnke, P. C.; He, C.; Lesniak, M. S. *Small* **2014,** *10*, 5137-5150.

103. Trickler, W. J.; Lantz, S. M.; Murdock, R. C.; Schrand, A. M.; Robinson, B. L.; Newport, G. D.; Schlager, J. J.; Oldenburg, S. J.; Paule, M. G.; Slikker, W., Jr; Hussain, S. M.; Ali, S. F. *Toxicol. Sci.* **2010,** *118*, 160-170.

104. Andreas, M. G.; Magali, R.; Craig, C. G. *Drug Deliv. Lett.* **2011,** *1*, 13-23.

105. Xu, G.; Mahajan, S.; Roy, I.; Yong, K.-T. *Front. Pharmacol.* **2013,** *4*, 140-147.

106. Zheng, M.; Ruan, S.; Liu, S.; Sun, T.; Qu, D.; Zhao, H.; Xie, Z.; Gao, H.; Jing, X.; Sun, Z. *ACS Nano* **2015,** *9*, 11455-11461.

107. Peng, Z.; Han, X.; Li, S.; Al-Youbi, A. O.; Bashammakh, A. S.; El-Shahawi, M. S.; Leblanc, R. M. *Coord. Chem. Rev.* **2017,** *343*, 256-277.

108. Bhaskar, S.; Tian, F.; Stoeger, T.; Kreyling, W.; de la Fuente, J. M.; Grazú, V.; Borm, P.; Estrada, G.; Ntziachristos, V.; Razansky, D. *Part Fibre Toxicol.* **2010,** *7*, 3-27.

109. Mikitsh, J. L.; Chacko, A.-M. *Perspect. Medicin. Chem.* **2014,** *6*, PMC.S13384-13397.

110. Maeda, H.; Wu, J.; Sawa, T.; Matsumura, Y.; Hori, K. *J. Control. Release* **2000,** *65*, 271-284.

111. Grabrucker, A.M.; Ruozi, B.; Belletti, D.; Pederzoli, F.; Forni, F.; Vandelli, M. A.; Tosi, G. *Tissue Barriers* **2016,** *4*, e1153568-e1153586.

112. Pulicherla, K. K.; Verma, M. K. *AAPS PharmSciTech* **2015,** *16*, 223-233.

113. Hervé, F.; Ghinea, N.; Scherrmann, J.-M. *AAPS J.* **2008,** *10*, 455-472.

114. Jones, A. R.; Shusta, E. V. *Pharm. Res.* **2007,** *24*, 1759-1771.

115. Bhunia, S. K.; Saha, A.; Maity, A. R.; Ray, S. C.; Jana, N. R. *Sci. Rep.* **2013,** *3*, 1473-1479.

116. Pardridge, W. M. *NeuroRX* **2005,** *2*, 3-14.

117. Wang, F.; Xie, Z.; Zhang, B.; Liu, Y.; Yang, W.; Liu, C.-y. *Nanoscale* **2014,** *6*, 3818-3823.

118. Wang, C.-F.; Cheng, R.; Ji, W.-Q.; Ma, K.; Ling, L.; Chen, S. *ACS Appl. Mater. Interfaces* **2018,** *10*, 39205-39213.

119. Zhang, Y.; Feng, J.; He, M.; Jiang, J.; Xu, T.; Zhou, L.; Chen, W.; Xiang, W.; Liang, X. *RSC Adv.* **2017,** *7*, 49542-49547.

120. Parvin, N.; Mandal, T. K. *RSC Adv.* **2016,** *6*, 18134-18140.

121. Wang, J.; Wang, C.-F.; Chen, S. *Angew. Chem. Int. Ed.* **2012,** *51*, 9297-9301.

122. Li, M.; Yao, W.; Liu, J.; Tian, Q.; Liu, L.; Ding, J.; Xue, Q.; Lu, Q.; Wu, W. *J. Mater. Chem. C* **2017,** *5*, 6512-6520.

123. Sodhi, G. S.; Kaur, J. *Forensic Sci. Int.* **2001,** *120*, 172-176.

124. Milenkovic, I.; Algarra, M.; Alcoholado, C.; Cifuentes, M.; Lázaro-Martínez, J. M.; Rodríguez-Castellón, E.; Mutavdžić, D.; Radotić, K.; Bandosz, T. J. *Carbon* **2019,** *144*, 791-797.

125. Fernandes, D.; Krysmann, M. J.; Kelarakis, A. *ChemComm* **2015,** *51*, 4902-4905.

126. Zhao, D.; Ma, W.; Xiao, X. *Nanomaterials* **2018,** *8*, 612-621.

127. Chen, J.; Wei, J.-S.; Zhang, P.; Niu, X.-Q.; Zhao, W.; Zhu, Z.-Y.; Ding, H.; Xiong, H.-M. *ACS Appl. Mater. Interfaces* **2017,** *9*, 18429-18433.

128. Jiang, B.-P.; Yu, Y.-X.; Guo, X.-L.; Ding, Z.-Y.; Zhou, B.; Liang, H.; Shen, X.-C. *Carbon* **2018,** *128*, 12-20.

129. Luo, C.; Zhou, L.; Chiou, K.; Huang, J. *Chem* **2018,** *4*, 784-794.

130. Martins, N. C. T.; Ângelo, J.; Girão, A. V.; Trindade, T.; Andrade, L.; Mendes, A. *Appl. Catal., B* **2016,** *193*, 67-74.

131. Marco, V.; Evgenia, K.; A., D. I.; P., J. M.; George, B.; Andreas, S.-O.; A., S. W. *ChemNanoMat* **2016,** *2*, 739-747.

132. Rajamanickam, D.; Shanthi, M. *Arabian J. Chem.* **2016,** *9*, S1858-S1868.

133. Fujishima, A.; Honda, K. *Nature* **1972,** *238*, 37-38.

134. Haro, M.; Abargues, R.; Herraiz-Cardona, I.; Martínez-Pastor, J.; Giménez, S. *Electrochim. Acta* **2014,** *144*, 64-70.

135. Hung, W.-H.; Chien, T.-M.; Tseng, C.-M. *J. Phys. Chem. C* **2014,** *118*, 12676-12681.

136. Chen, X.; Wu, Z.; Liu, D.; Gao, Z. *Nanoscale Res. Lett.* **2017,** *12*, 143-152.

137. Wang, J.; Lim, Y.-F.; Wei Ho, G. *Nanoscale* **2014,** *6*, 9673-9680.

138. Saison, T.; Chemin, N.; Chanéac, C.; Durupthy, O.; Mariey, L.; Maugé, F.; Brezová, V.; Jolivet, J.-P. *J. Phys. Chem. C* **2015,** *119*, 12967-12977.

139. Li, G.-S.; Zhang, D.-Q.; Yu, J. C. *Environ. Sci. Technol.* **2009,** *43*, 7079-7085.

140. Naseri, A.; Samadi, M.; Pourjavadi, A.; Moshfegh, A. Z.; Ramakrishna, S. *J. Mater. Chem. A* **2017,** *5*, 23406-23433.

141. Sachsenhauser, M.; Walczak, K.; Hampel, P. A.; Stutzmann, M.; Sharp, I. D.; Garrido, J. A. *Langmuir* **2016,** *32*, 1637-1644.

142. Jafari, T.; Moharreri, E.; Amin, A.; Miao, R.; Song, W.; Suib, S. *Molecules* **2016,** *21*, 900-928.

143. Yuan, F.; Wang, Z.; Li, X.; Li, Y.; Tan, Z. a.; Fan, L.; Yang, S. *Adv. Mater.* **2017,** *29*, 1604436-1604441.

144. Reza Gholipour, M.; Dinh, C.-T.; Beland, F.; Do, T.-O. *Nanoscale* **2015,** *7*, 8187-8208.

145. Zheng, D.-W.; Li, B.; Li, C.-X.; Fan, J.-X.; Lei, Q.; Li, C.; Xu, Z.; Zhang, X.-Z. *ACS Nano* **2016,** *10*, 8715-8722.

146. Ni, M.; Leung, M. K. H.; Leung, D. Y. C.; Sumathy, K. *Renew. Sust. Energ. Rev.* **2007,** *11*, 401-425.

147. Wang, X.; Maeda, K.; Thomas, A.; Takanabe, K.; Xin, G.; Carlsson, J. M.; Domen, K.; Antonietti, M. *Nat. Mater.* **2008,** *8*, 76-80.

148. Wang, R.; Lu, K.-Q.; Zhang, F.; Tang, Z.-R.; Xu, Y.-J. *Appl. Catal., B* **2018,** *233*, 11-18.

149. Zhang, N.; Yang, M.-Q.; Liu, S.; Sun, Y.; Xu, Y.-J. *Chem. Rev.* **2015,** *115*, 10307-10377.

150. Lu, K.-Q.; Quan, Q.; Zhang, N.; Xu, Y.-J. *J. Energ. Chem.* **2016,** *25*, 927-935.

151. Wang, R.; Lu, K.-Q.; Tang, Z.-R.; Xu, Y.-J. *J. Mater. Chem. A* **2017,** *5*, 3717-3734.

152. Zhang, H.; Ming, H.; Lian, S.; Huang, H.; Li, H.; Zhang, L.; Liu, Y.; Kang, Z.; Lee, S.-T. *Dalton Trans.* **2011,** *40*, 10822-10825.

153. Yu, H.; Zhao, Y.; Zhou, C.; Shang, L.; Peng, Y.; Cao, Y.; Wu, L.-Z.; Tung, C.-H.; Zhang, T. *J. Mater. Chem. A* **2014,** *2*, 3344-3351.

154. Muthulingam, S.; Bae, K. B.; Khan, R.; Lee, I.-H.; Uthirakumar, P. *J. Environ. Chem. Eng.* **2016,** *4*, 1148-1155.

155. Cheng, Z.; Wang, F.; Shifa, T. A.; Liu, K.; Huang, Y.; Liu, Q.; Jiang, C.; He, J. *Appl. Phys. Lett.* **2016,** *109*, 053905-053909.

156. Zhang, Y.; Park, M.; Kim, H. Y.; Ding, B.; Park, S.-J. *Sci. Rep.* **2017,** *7*, 45086-45097.

157. Yang, P.; Zhao, J.; Zhang, L.; Li, L.; Zhu, Z. *Chem. Eur. J* **2015,** *21*, 8561-8568.

158. Haitao, L.; Xiaodie, H.; Zhenhui, K.; Hui, H.; Yang, L.; Jinglin, L.; Suoyuan, L.; A., T. C. H.; Xiaobao, Y.; Shuit-Tong, L. *Angew. Chem. Int. Ed.* **2010,** *49*, 4430-4434.

159. Chen, Y.; Sun, F.; Huang, Z.; Chen, H.; Zhuang, Z.; Pan, Z.; Long, J.; Gu, F. *Appl. Catal., B* **2017,** *215*, 8-17.